INFORMATION TO USERS

This manuscript has been reproduced from the microfilm master. UMI films the text directly from the original or copy submitted. Thus, some thesis and dissertation copies are in typewriter face, while others may be from any type of computer printer.

The quality of this reproduction is dependent upon the quality of the copy submitted. Broken or indistinct print, colored or poor quality illustrations and photographs, print bleedthrough, substandard margins, and improper alignment can adversely affect reproduction.

In the unlikely event that the author did not send UMI a complete manuscript and there are missing pages, these will be noted. Also, if unauthorized copyright material had to be removed, a note will indicate the deletion.

Oversize materials (e.g., maps, drawings, charts) are reproduced by sectioning the original, beginning at the upper left-hand corner and continuing from left to right in equal sections with small overlaps.

Photographs included in the original manuscript have been reproduced xerographically in this copy. Higher quality 6" x 9" black and white photographic prints are available for any photographs or illustrations appearing in this copy for an additional charge. Contact UMI directly to order.

Bell & Howell Information and Learning
300 North Zeeb Road, Ann Arbor, MI 48106-1346 USA
800-521-0600

UNIVERSITY OF CALIFORNIA

Los Angeles

Nonlinear Model-Based Control of Particulate Processes

A dissertation submitted in partial satisfaction of the

requirements for the degree Doctor of Philosophy

in Chemical Engineering

by

Timothy Yeechung Chiu

2000

UMI Number: 9993027

UMI Microform 9993027

Bell & Howell Information and Learning Company
300 North Zeeb Road
P.O. Box 1346
Ann Arbor, MI 48106-1346

The dissertation of Timothy Yeechung Chiu is approved.

Jane P. Chang

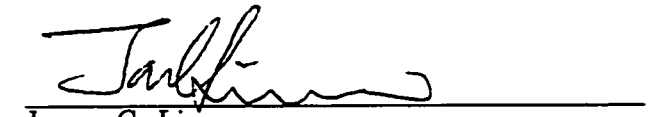

James C. Liao

Fernando Paganini

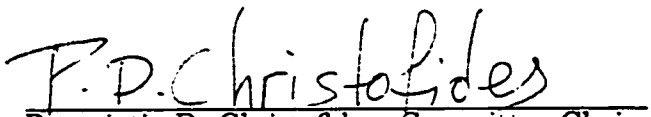

Panagiotis D. Christofides, Committee Chair

University of California, Los Angeles

2000

Contents

List of Figures

List of Tables

ACKNOWLEDGMENTS

I am grateful to my advisor, Professor Panagiotis D. Christofides, for his guidance, support, encouragement and confidence in me throughout the course of the project.

I would also like to thank Professor Jane P. Chang and Professor James C. Liao of the Department of Chemical Engineering, and Professor Fernando Paganini of the Department of Electrical Engineering to participate in my examination committee.

The friendship of the many wonderful graduate students of Professor Christofides is much appreciated. This includes Antonios Armaou, Harris Antoniades, Nael El-Farra, James Baker, Eugene Bendersky, and Ashish Kalani.

I would like to thank my parents. Their support were absolutely indispensable and I am indebted to them for all my accomplishments. My sister and brother had also given me a great deal of support and I thank them deeply for their encouragement.

VITA

September 13, 1975	Born, Hong Kong
1996	Summer Internship as Environmental Scientist United States Environmental Protection Agency Region 9 San Francisco, California
1997	Summer Internship as Process Engineer Mobil Oil Corporation Torrance, California
1997	Bachelor of Science, Chemical Engineering University of California, Los Angeles
1998-99	Teaching Assistant Department of Chemical Eningeering University of California, Los Angeles
1998-99	Teaching Assistant Department of Chemistry and Biochemistry University of California, Los Angeles
1998	Outstanding Teaching Assistant Award Department of Chemical Engineering University of California, Los Angeles
1999	Master of Science, Chemical Engineering University of California, Los Angeles
1999	Outstanding Master of Science Award Department of Chemical Engineering University of California, Los Angeles
1999-2000	Process Engineer FCI Electronics Cypress, California
2000	AIChE Article Journal of the Month, February 2000 American Institute of Chemical Engineers

PUBLICATIONS AND PRESENTATIONS

Christofides, P. D. and T. Chiu, "Nonlinear Control of Particulate Processes", AIChE Annual Meeting, paper 196a, Los Angeles, California, 1997.

Christofides, P. D. and T. Chiu, "Nonlinear Control of Particulate Processes", *Preprints of 1997 AIChE Proceedings on Fluidisation and Fluid-Particle Systems*, AIChE Annual Meeting, 277-282, Los Angeles, California, 1997.

Chiu, T. and P. D. Christofides, "Control of Particulate Processes Based on Uncertain Population Balance Models", AIChE Annual Meeting, paper 246g, Miami Beach, Florida, 1998.

Chiu, T. and P. D. Christofides, "Nonlinear Control of Particulate Processes", *AIChE J.*, **45**, 1279-1297, 1999.

Chiu, T. and P. D. Christofides, "Robust Nonlinear Control of a Continuous Crystallizer", *Comp. & Chem. Eng.*, **23**(s), 249-252, 1999.

Chiu, T. and P. D. Christofides, "Dynamics and Control of Constrained Particulate Processes", AIChE Annual Meeting, paper 146b, Dallas, Texas, 1999.

Chiu, T. Y. and P. D. Christofides, "Robust Nonlinear Control of Particulate Processes", *AIChE J.*, **46**, 266-280, 2000.

Chiu, T., N. El-Farra and P. D. Christofides, "Nonlinear Control of Particulate Processes with Input Constraints", *Proceedings of American Control Conference*, 1752-1759, Chicago, Illinois, 2000.

Chiu, T. and P. D. Christofides, "Parameter Estimation for Control of Particulate Processes Using Nonlinear Order Reduction", AIChE Annual Meeting, paper 17h, Los Angeles, California, 2000.

ABSTRACT OF THE DISSERTATION

Nonlinear Model-Based Control of Particulate Processes

by

Timothy Yeechung Chiu

Doctor of Philosophy in Chemical Engineering

University of California, Los Angeles, 2000

Professor Panagiotis D. Christofides, Chair

Particulate processes are characterized by the co-presence of a continuous phase and a dispersed (particulate) phase, and are widely used in industry for the manufacturing of many high-value products. Examples include the crystallization of proteins for pharmaceutical applications, the emulsion polymerization reactors for the production of latex and the titania powder aerosol reactors used in the production of white pigments. It is now well understood that the physico-chemical and mechanical properties of materials made with particulates depend heavily on the characteristics of the corresponding particle size distribution (PSD).

Population balances have provided a natural framework for mathematical modeling of PSDs and typically lead to systems of nonlinear partial integro-differential equations that describe the rate of change of the PSD. The complex nature of population balance models has motivated extensive research efforts on the development of efficient numerical methods for the computation of their solutions. However, research on population balance model-based control of particulate processes has been very

limited. The need to control the shape of PSDs in industrial applications, together with recent advancements in technology for real-time PSD measurements, motivates the synthesis and implementation of high performance model-based feedback control systems on particulate processes.

This thesis presents a general and practical framework for the synthesis of nonlinear practically-implementable feedback controllers for particulate processes using population balances. A model reduction procedure based on combination of the method of weighted residuals and the concept of approximate inertial manifold is proposed for the construction of low-order ODE systems that accurately reproduce the dominant dynamics of the particulate process. These ODE systems are subsequently used for the synthesis of nonlinear low-order output feedback controllers that enforce exponential stability in the closed-loop system and achieve a particle size distribution with desired characteristics. The important practical issues of robust controller design using uncertain population balances and nonlinear controller design in the presence of control actuator constraints are also studied. The proposed control algorithms are successfully applied to continuous and batch crystallization systems and are shown to outperform conventional control schemes.

Chapter 1

Introduction

Particulate processes (also known as dispersed-phase processes) are characterized by material domains that are comprised of a continuous phase and a dispersed phase and are essential in making many high-value industrial products. Examples include the crystallization of proteins for pharmaceutical applications, the emulsion polymerization reactors for the production of latex, and the titania powder aerosol reactors used in the production of white pigments. It is now well understood that the physico chemical and mechanical properties of materials made with particulates depend heavily on the characteristics of the corresponding particle-size distribution (PSD) (for example, a nearly monodisperse PSD is required for titania pigments to obtain the maximum hiding powder per unit mass). Therefore, the problem of synthesizing and implementing high-performance model-based feedback control systems on particulate processes to achieve PSDs with desired characteristics has significant industrial value. On the other hand, recent developments in measurement technology allow the accurate and fast on-line measurement of key process variables including PSDs (see the article by Rawlings [66] for an excellent review of the available measurement technology), which can then be used for feedback control purposes.

Population balances have provided a natural framework for the mathematical modeling of PSDs (see, for example, the tutorial article by Hulburt and Katz [38] and the review article by Ramkrishna [62]), and have been successfully used to describe PSDs in emulsion polymerization reactors [24], crystallizers [66], and aerosol reactors [31, 79]. Application of population balances to particulate processes typically leads to systems of nonlinear partial integro-differential equations that describe the rate of change of the PSD. The population balances are coupled with the material and energy balances that describe the rate of change of the state variables of the continuous phase (these are usually systems of nonlinear differential equations, which include integrals over the entire particle-size spectrum), leading to complete particulate process models.

The nonlinear (owing to complex growth, nucleation, agglomeration and breakage mechanisms, and their Arrhenius dependence on temperature) and distributed nature of population balances has motivated extensive research on the development of efficient numerical methods for the accurate computation of their solution. Examples of solution methods for continuous population balances include the method of self-preserving distributions [31], the method of weighted residuals [62, 33], the sectional method [34, 55], and discretization via fixed/moving pivot techniques [51, 52], while methods for the solution of discretized population balances have been proposed by Hounslow [37] and Hill and Ng [35]. An excellent review of results in this area can be found in the article by Ramkrishna [62]. The ability to accurately solve population balance models motivated numerous research studies on the dynamics of particulate processes. These studies confirmed the existence of a wide range of complex static and dynamic phenomena including multiple steady-states and sustained oscillations (see, for example, the article by Lei et al. [56], Jerauld et al. [40] and Rawlings

and Ray [67, 68] for a theoretical analysis of oscillatory behavior in crystallizers and emulsion polymerization reactors, respectively), which had been previously observed in experimental studies (see the classic book by Randolph and Larson [64] for results and references). The highly nonlinear and oscillatory behavior of many particulate processes implies the need to implement nonlinear model-based feedback controllers in order to ensure a stable and efficient operation.

In spite of the rich literature on population balance modeling, numerical solution, and dynamical analysis of particulate processes, research on model-based control of such processes has been very limited. Specifically, previous efforts have mainly focused on the understanding of fundamental control-theoretic properties (controllability and observability) of population balance models [72] and the application of conventional control schemes (such as proportional-integral and proportional-integral-derivative control, self-tuning control) to crystallizers and emulsion polymerization processes (see, for example, the articles by Semino and Ray [73], Rohani and Bourne [69], Dimitratos et al. [24], and the references therein). Notable exceptions on model-based control of particulate processes include an optimization-based control method which was developed by Eaton and Rawlings [25], and successfully applied to a batch crystallization process, as well as nonlinear state feedback control of a cell culture by Kurtz et al. [54]. The main difficulty in synthesizing nonlinear model-based feedback controllers for particulate processes is the distributed parameter nature of the population balance models which does not allow their direct use for the synthesis of low-order (and therefore, practically implementable) output feedback controllers. Furthermore, a direct application of the aforementioned solution methods to derive finite dimensional approximations of the population balance models may lead to ODE systems of very high order, which are inappropriate for the synthesis of low-order

controllers.

In addition to being highly nonlinear and infinite dimensional, the population balance models of most particulate processes are uncertain. Typical sources of model uncertainty include unknown or partially known $time-varying$ process parameters, exogenous disturbances and unmodeled dynamics. It is well-known that the presence of uncertain variables and unmodeled dynamics, if not taken into account in the controller design, may lead to severe deterioration of the nominal closed-loop performance or even to closed-loop instability. Research on robust control of nonlinear distributed chemical processes with uncertainty has mainly focused on transport-reaction processes described by nonlinear partial differential equations (PDEs). In this area, important contributions include the development of Lyapunov-based robust control methods for hyperbolic [19] and parabolic PDEs [81, 80, 14]; the reader may refer to the book [15] for detailed results and references in this area. An alternative approach for the design of controllers for PDE systems with time-invariant uncertain variables involves the use of adaptive control methods (e.g., [6, 78, 23, 4]). Despite this progress, at this stage, there is no general framework for the synthesis of practically-implementable nonlinear feedback controllers for particulate processes that allow attaining desired particle size distributions in the presence of significant model uncertainty.

Another unresolved issue on control of particulate processes is the ability of the controller to deal with constraints in the capacity of the control actuators. This is an important limitation of these methods, especially in view of the fact that the capacity of control actuators used to regulate particulate processes is almost always limited. Such limitations may arise naturally due to the finite capacity of control actuators (e.g., bounds on magnitude of the opening of valves) or may be imposed on the ma-

nipulated input to insure safe process operation, meet environmental regulations, or maintain desired product quality specifications. Input constraints restrict our ability to freely modify the dynamic behavior of particulate processes; and the ill-effects due to actuator constraints manifest themselves, for example, in the form of sluggishness of response and loss of stability. Additional problems that arise in the case of dynamic controllers include undesired oscillations and overshoots, a phenomenon usually referred to as "windup".

Recognition of the detrimental effects of input constraints on the stability and performance of chemical processes in general has motivated many recent studies on the dynamics and control of chemical processes subject to input constraints. Notable contributions in this regard include controller design and stability analysis within the model predictive control framework [53, 65, 71, 70], constrained quadratic-optimal control [13], the design of "anti-windup" schemes in order to prevent excessive performance deterioration of an already designed controller when the input saturates [49, 46, 58, 77, 44], the study of the nonlinear bounded control problem for a class of two and three state chemical reactors [2, 1], and some general results on the dynamics of constrained nonlinear systems [45]. While the control of nonlinear finite-dimensional systems with input constraints has received significant attention, there are no results on model-based control of particulate processes with input constraints.

Motivated by the lack of population balance-based control methods for particulate processes that can deal with the practical issues of nonlinear behavior, model uncertainty and actuator saturation, and the need to achieve tight size distribution control in many particulate processes, the objectives of the present thesis are:

- to present general nonlinear, robust and constrained control methods for particulate processes based on population balance models, and

- to illustrate the application of the proposed methods to size distribution control in batch and continuous crystallization processes and document their effectiveness and advantages with respect to conventional control methods.

The rest of the thesis is structured as follows.

Chapter 2 proposes a general method for the synthesis of practically implementable nonlinear model-based feedback controllers that enforce the desired stability and performance specifications (such as PSDs with desired total mass and mean particle size) in the closed-loop system. A a model reduction procedure based on a combination of the method of weighted residuals and the concept of approximate inertial manifold is proposed and used for the construction of low-order ODE systems that accurately reproduce the dominant dynamics of the particulate process. These ODE systems are subsequently used for the synthesis of nonlinear low-order output feedback controllers that enforce exponential stability in the closed-loop system and achieve a desired particle size distribution. Precise closed-loop stability conditions are given and controller implementation issues are addressed.

Chapter 3 shows two applications of the nonlinear control method proposed in Chapter 2 to a batch and a continuous crystallization systems. Low-dimensional approximations of the population balances are derived and used for nonlinear control design. The performance of the nonlinear controllers is successfully tested through simulations using the detailed population balance models and is shown to be superior to the one of linear control schemes.

Chapter 4 proposed a general method for the synthesis of practically-implementable robust nonlinear controllers that explicitly handle time-varying uncertain variables (e.g., unknown process parameters and disturbances) and unmodeled dynamics (e.g., fast actuator and sensor dynamics not included in the process model). The robust

nonlinear controllers are were synthesized via Lyapunov's direct method and are shown to enforce stability in the closed-loop system and attenuation of the effect of uncertain variables on the outputs, and achieve particle size distributions with desired characteristics. The method is successfully applied to a continuous crystallizer with fines trap and is shown to outperform a nonlinear controller design which does not account for the effect of time-varying uncertainty.

Chapter 5 presents a general methodology for the analysis and control of constrained particulate processes modeled by population balance equations. Using finite-dimensional ODE approximations of the population balances, we characterize the limitations imposed by input constraints on our ability to modify the dynamics of the particulate process and provide an explicit characterization of the set of admissible set-points that can be achieved in the presence of constraints. This information together with the derived ODE systems is then used as the basis for the synthesis of practically-implementable nonlinear bounded output feedback controllers that enforce exponential stability in the closed-loop system and achieve particle size distributions with desired characteristics in the presence of active input constraints. The approach is used to control a continuous crystallizer with actuator saturation.

Finally, Chapter 6 presents the main conclusions of this thesis. The proofs of all the results are given in the appendices.

Chapter 2

Nonlinear Model Reduction and Control of Particulate Processes

2.1 Introduction

This chapter focuses on nonlinear feedback control of spatially-homogeneous particulate processes modeled by a class of nonlinear partial integro-differential equation systems. The objective is to develop a general and rigorous method for the synthesis of practically implementable nonlinear model-based feedback controllers that enforce the desired stability and performance specifications (such as PSDs with desired total mass and mean particle size) in the closed-loop system.

This chapter is structured as follows: Section 2.2 presents a general class of nonlinear partial integro-differential equation systems which describes the majority of spatially-homogeneous particulate processes and uses a crystallizer example to motivate the proposed approach for control of particulate processes. Section 2.3 proposes a model reduction procedure based on a combination of the method of weighted residuals and the concept of approximate inertial manifold for the construction of low-order ODE systems that accurately reproduce the dominant dynamics of the particulate

process. These ODE systems are subsequently used for the synthesis of nonlinear low-order output feedback controllers that enforce exponential stability in the closed-loop system and achieve a desired particle size distribution. Precise closed-loop stability conditions are given and controller implementation issues are addressed. In Chapter 3, the performance and robustness of the proposed control method are successfully tested through simulations on a continuous crystallizer and are shown to be superior to the ones of a proportional-integral control scheme. The results of this chapter were first presented in [7, 16].

2.2 Modeling and Dynamics of Particulate Processes

2.2.1 Particulate Process Model

We focus on spatially homogeneous (well-mixed) particulate processes with simultaneous particle growth, nucleation, agglomeration, and breakage and consider the case of a single internal particle coordinate which, for the sake of exposition, is assumed to be the particle-size. Applying a dynamic material balance on the number of particles of size r to $r + dr$ (population balance), we obtain the following general nonlinear partial integro-differential equation which describes the rate of change of the PSD, $n(r,t)$:

$$\frac{\partial n}{\partial t} = -\frac{\partial (G(x,r)n)}{\partial r} + w(n,x,r) \tag{2.1}$$

where $n(r,t) \in L_2[0,r_{max})$ ($L_2[0,r_{max})$ is the Hilbert space of continuous functions defined on the interval $[0,r_{max})$), $r \in [0,r_{max}]$ is the particle size, and r_{max} is the maximum particle size (which may be infinity), t is the time and $x \in \mathbb{R}^n$ is the vector of state variables which describe properties of the continuous phase (for example solute concentration, temperature, and pH in a crystallizer); see Eq.2.2 below for the system that describes the dynamics of x. $G(x,r)$ and $w(n,x,r)$ are nonlinear scalar functions

whose physical meaning can be explained as follows: $G(x,r)$ accounts for particle growth through condensation and is usually referred to as growth rate. It usually depends on the concentrations of the various species present in the continuous phase, the temperature of the process, and the particle size. On the other hand, $w(n,x,r)$ represents the net rate of introduction of new particles into the system. It includes all the means by which particles appear or disappear within the system including particle agglomeration (merging of two particles into one), breakage (division of one particle to two), as well as, nucleation of particles of size $r \geq 0$ and particle feed and removal.

The rate of change of the continuous-phase variables x can be derived by a direct application of mass and energy balances to the continuous phase and is given by a nonlinear integro-differential equation system of the general form:

$$\dot{x} = f(x) + g(x)u(t) + A\int_0^{r_{max}} a(n,r,x)dr \tag{2.2}$$

where $f(x), a(n,r,x)$ are nonlinear vector functions, $g(x)$ is a nonlinear matrix function, A is a constant matrix and $u(t) = [u_1\ u_2\ \cdots\ u_m] \in \mathbb{R}^m$ is the vector of manipulated inputs. The term $A\int_0^{r_{max}} a(n,r,x)dr$ accounts for mass and heat transfer from the continuous phase to all the particles in the population.

We define a vector of controlled outputs to express the various control objectives (such as regulation of total number of particles, mean particle size, temperature, pH, and so on) as:

$$y_i(t) = h_i(\int_0^{r_{max}} c_\kappa(r)n(r,t)dr, x),\ \ i = 1,\ldots,m,\ \ \kappa = 1,\ldots,l \tag{2.3}$$

where $y_i(t)$ is the ith controlled output, $h_i(\int_0^{r_{max}} c_\kappa(r)n(r,t)dr, x)$ is a nonlinear smooth scalar function of its arguments, and $c_\kappa(r)$ is a known smooth function of r which depends on the desired performance specifications. To simplify the notation

of the theoretical development, we will not consider measured outputs separately from controlled outputs, which means that we need to assume the availability of on-line measurements of the controlled outputs $y_i(t)$.

Throughout the thesis, we will use the inner product and norm in $L_2[0, r_{max})$, which are defined, respectively, as:

$$(\phi_1, \phi_2) = \int_0^{r_{max}} \phi_1(z)\phi_2(z)dz, \quad ||\phi_1||_2 = (\phi_1, \phi_1)^{\frac{1}{2}} \tag{2.4}$$

where ϕ_1, ϕ_2 are two elements of $L_2[0, r_{max})$. Furthermore, the order of magnitude and Lie derivative notations will be needed in our development. In particular, $\delta(\epsilon) = O(\epsilon)$ if there exist positive real numbers k_1 and k_2 such that $|\delta(\epsilon)| \leq k_1|\epsilon|$, $\forall\ |\epsilon| < k_2$, and $L_f\bar{h}$ denotes the standard Lie derivative of a scalar function $\bar{h}(x)$ with respect to the vector function $f(x)$, $L_f^k\bar{h}$ denotes the k-th order Lie derivative and $L_gL_f^{k-1}\bar{h}$ denotes the mixed Lie derivative where $g(x)$ is a vector function.

Remark 2.1: Referring to the general mathematical model of Eqs.2.1-2.2, the following remarks are in order: a) the particle-size distribution function $n(r,t)$ is assumed to be a sufficiently smooth function of its arguments (that is, $n(r,t)$ and its partial derivatives with respect to r and t, up to a desired order, are continuous functions); this is a reasonable assumption for large size distributions, even though particles are discrete and their number is integer-valued, b) a single internal coordinate (particle size) is considered; this is motivated by the majority of industrial particulate process control problems where the central objective is to produce particulates with a desired particle size distribution, c) the particles are assumed to be small enough so that the environment in which they are dispersed can be adequately described by a local value of its state vector, d) the vector of manipulated inputs $u(t)$ is a lumped variable (that is, it only depends on time; for example, the inlet concentration of solute in a crystallizer) and the controlled outputs $y_i(t)$ are taken to be nonlinear functions of x

and appropriate weighted averages of n (examples of controlled outputs included in this formulation are total mass of particles, mean particle size, solute concentration, process temperature, and pH); both choices are typical in most practical applications as illustrated by the crystallization process studied in Chapter 3.

Remark 2.2: The nonlinear model reduction and controller synthesis results that will be presented in this thesis can be generalized to particulate processes, which include manipulated inputs in the population balance (such as manipulation of fines destruction rate; see [56, 63], and Remark 2.6 below) with the following state-space description:

$$\begin{aligned} \frac{\partial n}{\partial t} &= -\frac{\partial(G(x,r)n)}{\partial r} + w(n,x,r) + g_1(n,x,r)u(t) \\ \dot{x} &= f(x) + g_2(x, \int_0^{r_{max}} a_1(n,r,x)dr)u(t) + g_3(x, \int_0^{r_{max}} a_2(n,r,x)dr) \\ y_i(t) &= h_i(\int_0^{r_{max}} c_\kappa(r)n(r,t)dr, x), \quad i = 1,\ldots,m, \quad \kappa = 1,\ldots,l \end{aligned} \tag{2.5}$$

where $g_1(n,x,r), g_3(x, \int_0^{r_{max}} a_2(n,r,x)dr), a_1(n,r,x), a_2(n,r,x)$ are nonlinear vector functions and $g_2(x, \int_0^{r_{max}} a_1(n,r,x)dr)$ is a nonlinear matrix function.

2.2.2 Dynamics of Particulate Processes: a Continuous Crystallizer

Crystallization is a particulate process which is widely used in industry for the production of many products including fertilizers, proteins, and pesticides. The fact that the shape of the crystal-size distribution influences significantly the necessary liquid-solid separation, as well as the properties of the product, implies that crystallization requires a population balance in order to be accurately described, analyzed, and controlled. Crystallizers typically exhibit highly oscillatory behavior which suggests the use of feedback control to ensure stable operation and attain a crystal-size distribution with desired characteristics.

A continuous crystallizer (Figure 2.1), which exhibits highly oscillatory behavior,

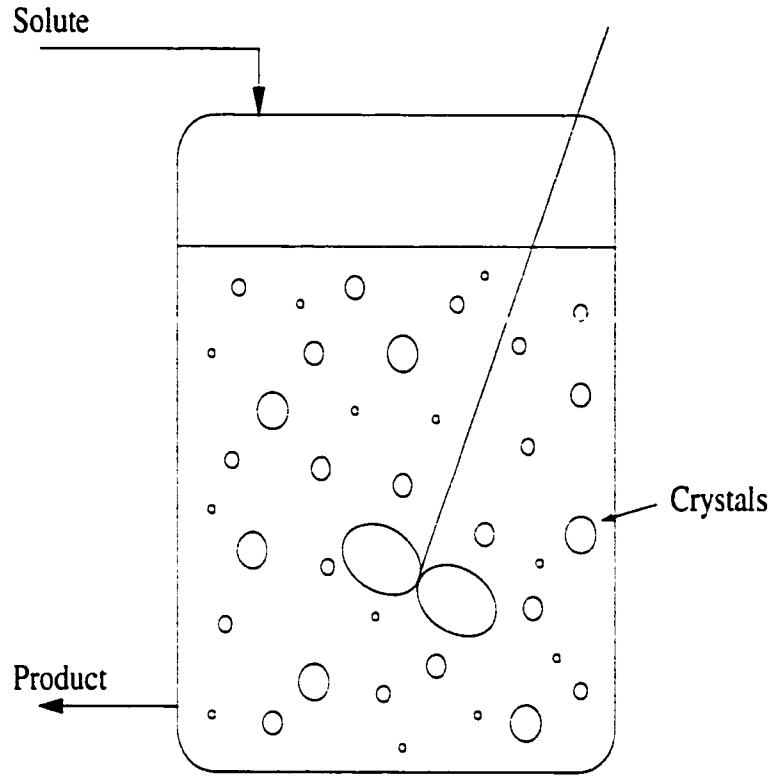

Figure 2.1: A continuous crystallizer.

is considered, and it will be shown that its dominant dynamics can be accurately described by a small set of ODEs; this finding implies that the dominant dynamics of the process are characterized by a small number of degrees of freedom (low-dimensional) and motivates the proposed approach for nonlinear model-based feedback control of particulate processes. Under the assumptions of isothermal operation, constant volume, mixed suspension, nucleation of crystals of infinitesimal size and mixed product removal, a dynamic model for the crystallizer can be derived from a population balance for the particle phase and a mass balance for the solute concentration, and it is

of the form [56, 40]:

$$\begin{aligned} \frac{\partial n}{\partial \bar{t}} &= -\frac{\partial (R(\bar{t})n)}{\partial r} - \frac{n}{\tau} + \delta(r-0)Q(\bar{t}) \\ \frac{dc}{d\bar{t}} &= \frac{(c_0-\rho)}{\bar{\epsilon}\tau} + \frac{(\rho-c)}{\tau} + \frac{(\rho-c)}{\bar{\epsilon}}\frac{d\bar{\epsilon}}{d\bar{t}} \end{aligned} \tag{2.6}$$

where $n(r,\bar{t})$ is the number of crystals of radius $r \in [0,\infty)$ at time $\bar{t}$ per unit volume of suspension, τ is the residence time, c is the solute concentration in the crystallizer, c_0 is the solute concentration in the feed, and $\bar{\epsilon} = 1 - \int_0^\infty n(r,\bar{t})\frac{4}{3}\pi r^3 dr$ is the volume of liquid per unit volume of suspension. $R(\bar{t})$ is the growth rate, $\delta(r-0)$ is the standard Dirac function and $Q(\bar{t})$ is the nucleation rate. The term $\delta(r-0)Q(\bar{t})$ accounts for the production of crystals of infinitesimal (zero) size via nucleation. $R(\bar{t})$ and $Q(\bar{t})$ are assumed to follow McCabe's law and Volmer's nucleation law, respectively:

$$R(\bar{t}) = k_1(c-c_s), \quad Q(\bar{t}) = \bar{\epsilon}k_2 e^{-\frac{k_3}{\left(\frac{c}{c_s}-1\right)^2}} \tag{2.7}$$

where k_1,k_2,and k_3 are constants and c_s is the concentration of solute at saturation. Using the expressions for $Q(\bar{t})$ and $R(\bar{t})$, the system of Eq.2.6 can be equivalently written as:

$$\begin{aligned} \frac{\partial n}{\partial \bar{t}} &= -k_1(c-c_s)\frac{\partial n}{\partial r} - \frac{n}{\tau} + \delta(r-0)\bar{\epsilon}k_2 e^{-\frac{k_3}{\left(\frac{c}{c_s}-1\right)^2}} \\ \frac{dc}{d\bar{t}} &= \frac{(c_0-\rho)}{\bar{\epsilon}\tau} + \frac{(\rho-c)}{\tau} + \frac{(\rho-c)}{\bar{\epsilon}}\frac{d\bar{\epsilon}}{d\bar{t}} \end{aligned} \tag{2.8}$$

To study the dynamic behavior of the crystallizer in question, a second-order accurate finite difference scheme with 1,000 discretization points was used to obtain the solution of the system of Eq.2.6 (the values of the process parameters used in the simulations are given in Tables 2.1 and 2.2). Figure 2.2 shows the open-loop oscillatory profiles of the total crystal concentration and total crystal size, respectively. It is clear that the crystallizer exhibits highly oscillatory behavior, which is the result of the interplay between growth and nucleation caused by the relative nonlinearity of the nucleation

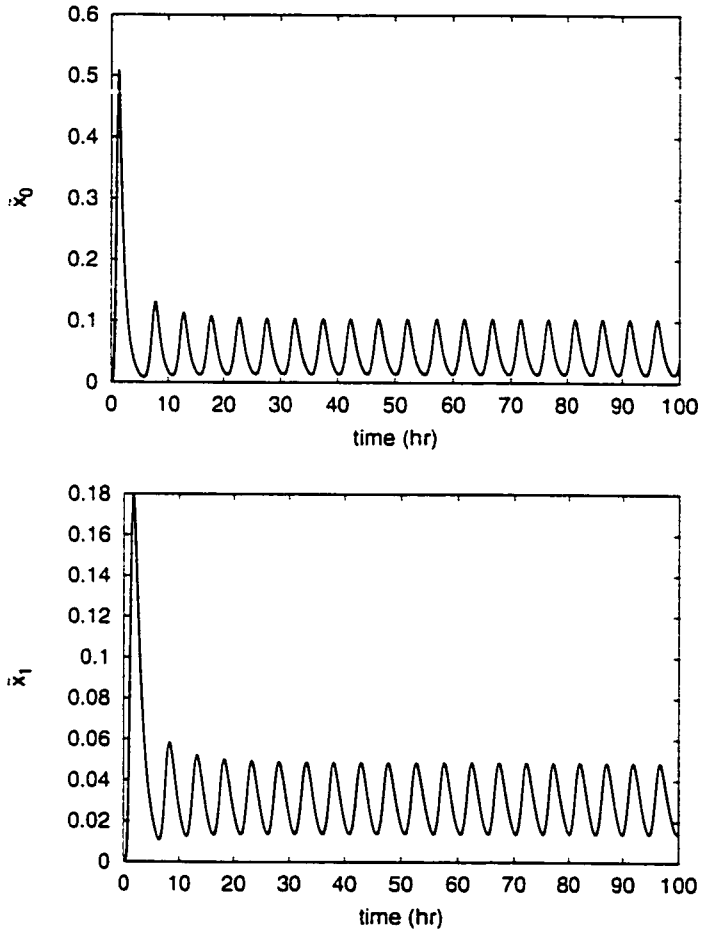

Figure 2.2: Open-loop profiles of crystal concentration (top) and total crystal size (bottom); distributed parameter model.

c_0	=	1000.0	$kg\ m^{-3}$
c_s	=	980.2	$kg\ m^{-3}$
ρ	=	1770.0	$kg\ m^{-3}$
τ	=	1.0	hr
k_1	=	5.065×10^{-2}	$mm\ m^3\ kg^{-1}\ hr^{-1}$
k_2	=	7.958	$mm^{-3}\ hr^{-1}$
k_3	=	1.217×10^{-3}	

Table 2.1: Process parameters

σ	=	$k_1\tau(c_0 - c_s)$	=	1.0	mm
Da	=	$8\pi\sigma^3 k_2 \tau$	=	200.0	
F	=	$k_3 c_s^2/(c_0 - c_s)^2$	=	3.0	
α	=	$(\rho - c_s)/(c_0 - c_s)$	=	40.0	

Table 2.2: Dimensionless parameters

rate as compared to growth rate (compare the nonlinear dependence of $Q(\bar{t})$ and $R(\bar{t})$ on c in Eq.2.7). To establish that the dynamics of the crystallizer are characterized by a small number of degrees of freedom, the method of moments is applied to the system of Eq.2.6 to derive an approximate ODE model. This is possible because the nucleation and growth rates are assumed to be independent of particle size which allows closure of the moment equations (see Eq.2.12 below). It is noted that the method of moments has been extensively used in the past to analyze the dynamics of particulate processes (see, for example, the articles by Hulburt and Katz [38] and Pratsinis [61]).

Defining the νth moment of $n(r, \bar{t})$ as:

$$\mu_\nu = \int_0^\infty r^\nu n(r, \bar{t}) dr, \quad \nu = 0, \ldots, \tag{2.9}$$

multiplying the population balance in Eq.2.8 by r^ν, and integrating over all particle sizes, the following system of infinite ordinary differential equations, which describes the rate of change of the moments of the particle size distribution and the solute

concentration, is obtained:

$$\begin{aligned}
\frac{d\mu_0}{d\bar{t}} &= -\frac{\mu_0}{\tau} + \left(1 - \frac{4}{3}\pi\mu_3\right) k_2 e^{-\frac{k_3}{\left(\frac{c}{c_s} - 1\right)^2}} \\
\frac{d\mu_\nu}{d\bar{t}} &= -\frac{\mu_\nu}{\tau} + \nu k_1 (c - c_s)\mu_{\nu-1}, \quad \nu = 1, 2, 3, \ldots, \\
\frac{dc}{d\bar{t}} &= \frac{c_0 - c - 4\pi\tau(c - c_s)\mu_2(\rho - c)}{\tau\left(1 - \frac{4}{3}\pi\mu_3\right)}
\end{aligned} \tag{2.10}$$

Introducing the following set of dimensionless variables and parameters:

$$t = \frac{\bar{t}}{\tau},\ \tilde{x}_0 = 8\pi\sigma^3\mu_0,\ \tilde{x}_1 = 8\pi\sigma^2\mu_1,\ \tilde{x}_2 = 4\pi\sigma\mu_2,\ \tilde{x}_3 = \frac{4}{3}\pi\mu_3,\ \ldots,$$

$$\sigma = k_1\tau(c_0 - c_s),\ Da = 8\pi\sigma^3 k_2\tau,\ F = \frac{k_3 c_s^2}{(c_0 - c_s)^2},\ \alpha = \frac{(\rho - c_s)}{(c_0 - c_s)},\ \tilde{y} = \frac{(c - c_s)}{(c_0 - c_s)} \tag{2.11}$$

the following dimensionless system is obtained:

$$\begin{aligned}
\frac{d\tilde{x}_0}{dt} &= -\tilde{x}_0 + (1 - \tilde{x}_3) Da\, e^{\frac{-F}{\tilde{y}^2}} \\
\frac{d\tilde{x}_1}{dt} &= -\tilde{x}_1 + \tilde{y}\tilde{x}_0 \\
\frac{d\tilde{x}_2}{dt} &= -\tilde{x}_2 + \tilde{y}\tilde{x}_1 \\
\frac{d\tilde{x}_3}{dt} &= -\tilde{x}_3 + \tilde{y}\tilde{x}_2 \\
\frac{d\tilde{x}_\nu}{dt} &= -\tilde{x}_\nu + \tilde{y}\tilde{x}_{\nu-1},\ \nu = 4, \ldots, \\
\frac{d\tilde{y}}{dt} &= \frac{1 - \tilde{y} - (\alpha - \tilde{y})\tilde{y}\tilde{x}_2}{1 - \tilde{x}_3}
\end{aligned} \tag{2.12}$$

On the basis of the system of Eq.2.12, it is clear that the moments of order four and higher do not affect those of order three and lower, and moreover, the state of the infinite dimensional system:

$$\frac{d\tilde{x}_\nu}{dt} = -\tilde{x}_\nu + \tilde{y}\tilde{x}_{\nu-1},\ \nu = 4, \ldots, \tag{2.13}$$

is bounded when x_3 and y are bounded, and it converges to a globally exponentially stable equilibrium point when $\lim_{t\to\infty} x_3 = c_1$ and $\lim_{t\to\infty} \tilde{y} = c_2$, where c_1, c_2 are constants.

This implies that the dominant dynamics (that is, dynamics associated with eigenvalues that are close to the imaginary axis) of the process of Eq.2.8 can be adequately captured by the following fifth-order moment model:

$$\begin{aligned}
\frac{d\tilde{x}_0}{dt} &= -\tilde{x}_0 + (1-\tilde{x}_3)Dae^{\frac{-F}{\tilde{y}^2}} \\
\frac{d\tilde{x}_1}{dt} &= -\tilde{x}_1 + \tilde{y}\tilde{x}_0 \\
\frac{d\tilde{x}_2}{dt} &= -\tilde{x}_2 + \tilde{y}\tilde{x}_1 \\
\frac{d\tilde{x}_3}{dt} &= -\tilde{x}_3 + \tilde{y}\tilde{x}_2 \\
\frac{d\tilde{y}}{dt} &= \frac{1-\tilde{y}-(\alpha-\tilde{y})\tilde{y}\tilde{x}_2}{1-\tilde{x}_3}
\end{aligned} \tag{2.14}$$

The ability of the above fifth-order moment model to reproduce the dynamics, and to some extent the solutions, of the distributed model of Eq.2.6 is shown in Figure 2.3, where the profiles of the total particle concentration generated by the two models are compared (both models start from the same initial conditions). Even though the discrepancy of the total particle concentration profiles predicted by the two models increases with time (this is expected due to the open-loop instability of the process; see Remark 2.7 below), it is clear that the fifth-order moment model of Eq.2.14 provides a very good approximation of the distributed model of Eq.2.6, thereby establishing that the dominant dynamics of the system of Eq.2.8 are low-dimensional and motivating the use of the moment model for nonlinear controller design (see Chapter 3 for the design and implementation of a nonlinear controller based on the fifth-order model of Eq.2.14).

Remark 2.3: The stability properties of the fifth-order model of Eq.2.14 have been thoroughly studied by Jerauld et al. [40] (see also [56]), where it has been shown that the global phase space of this model consists of a unique unstable steady-state surrounded by a stable periodic orbit, and that the linearization of the system of Eq.2.6

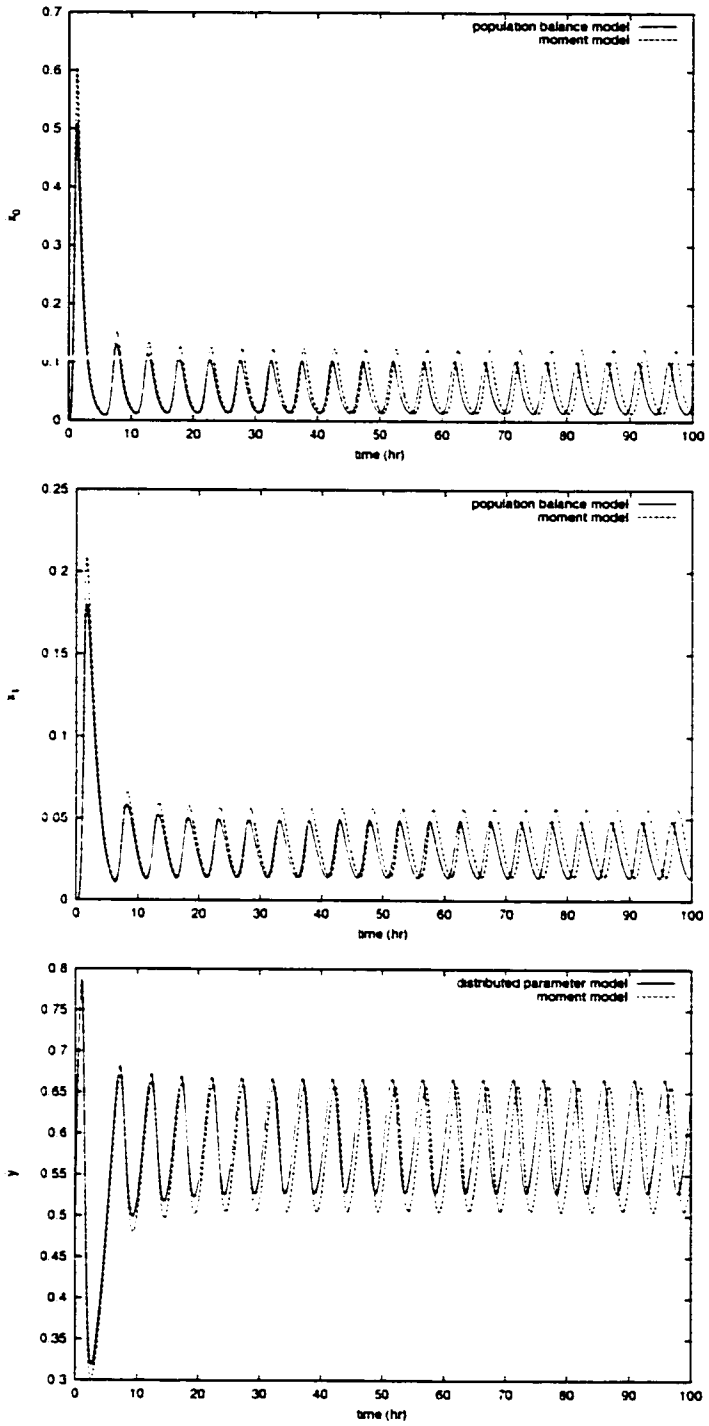

Figure 2.3: Comparison of open-loop profiles of crystal concentration (top), total crystal size (middle) and solute concentration (bottom) obtained from the distributed parameter model and the moment model.

around the unstable steady-state includes two isolated complex conjugate eigenvalues with a positive real part. For the dimensionless parameters of Table 2.2, the unique unstable steady-state is $\tilde{x}_0 = 0.047$, $\tilde{x}_1 = 0.028$, $\tilde{x}_2 = 0.017$, $\tilde{x}_3 = 0.01$, $\tilde{y} = 0.5996$.

Remark 2.4: We note that even though the number of discretization points, 1,000, used to solve the system of Eq.2.6 is very large (owing to the poor convergence properties of the finite difference scheme), the computation of an accurate (that is, independent of the discretization) solution is critical for the thorough evaluation of the performance of a nonlinear feedback controller synthesized on the basis of a low-order approximation of the distributed parameter system of Eq.2.6 (see Chapter 3 for closed-loop system simulations under nonlinear low-order output feedback control). The adequacy of 1,000 discretization points to yield an accurate solution is established in Figure 2.4, where the profiles of the total crystal concentration and total crystal size for 800 and 1,000 discretization points are compared and are shown to be almost identical.

Remark 2.5: Despite the fact that the model of Eq.2.6 consists of a first-order hyperbolic PDE (population balance) coupled with a nonlinear integro-differential equation (solute mass balance), it is evident from the above dynamical analysis, and the results of the simulation study, that its open-loop dynamic behavior is completely different than the one usually exhibited by systems of first-order hyperbolic PDEs (which arise in the modeling of convection-reaction processes). More specifically, the dominant dynamic behavior of the system of Eq.2.6 is characterized by a small number of degrees of freedom (and thus, it can be described by low-order ODE systems). On the other hand, first-order hyperbolic PDE systems involve spatial differential operators whose eigenvalues cluster along vertical, or nearly vertical, asymptotes in the complex plane, and therefore, they do not exhibit low-dimensional dynamic be-

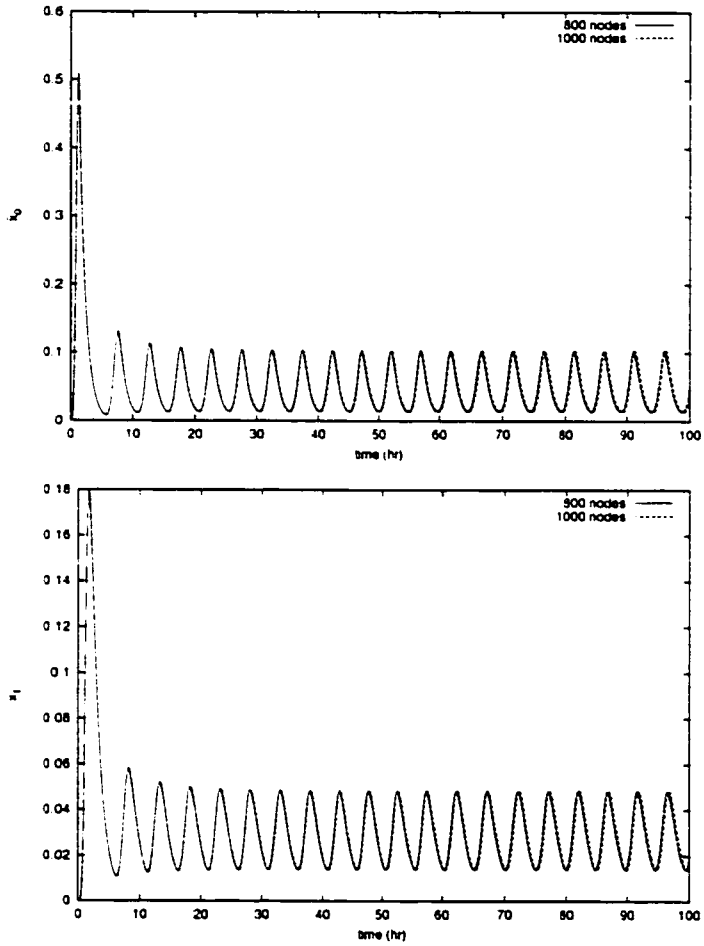

Figure 2.4: Effect of the number of discretization points on crystal concentration (top) and total crystal size (bottom); distributed parameter model.

havior. This fundamental difference on the nature of the dynamic behavior between first-order hyperbolic PDE systems and particulate process models motivates employing fundamentally different approaches for designing controllers for such systems. In particular, for first-order hyperbolic PDEs, the controller design problem is addressed directly on the basis of the PDE system (see [17] for results on nonlinear control), while for systems of Eqs.2.1-2.2, the controller design problem will be addressed on the basis of low-order approximations that capture the dominant dynamics, as outlined in section 2.3.1 in the next section.

Remark 2.6: When a fines trap is used to remove fines, small crystals, from the crystal magma (refer to [56, 63] for a detailed description of crystallizer with fines trap), the model of the crystallizer takes the following form [56]:

$$\begin{aligned} \frac{\partial n}{\partial \bar{t}} &= -k_1(c-c_s)\frac{\partial n}{\partial r} - \frac{n}{\tau} - \bar{h}(r)\frac{n}{\bar{\tau}} + \delta(r-0)\bar{\epsilon}k_2 e^{-\frac{k_3}{\left(\frac{c}{c_s}-1\right)^2}} \\ \frac{dc}{d\bar{t}} &= \frac{(c_0-\rho)}{\bar{\epsilon}\tau} + \frac{(\rho-c)}{\tau} + \frac{(\rho-c)}{\bar{\epsilon}}\frac{d\bar{\epsilon}}{d\bar{t}} \end{aligned} \tag{2.15}$$

where $1/\bar{\tau} = F_0/V$ is the rate at which crystals are circulated through the fines trap (F_0 is the fines recirculation rate and V is the active volume of the crystallizer), and $\bar{h}(r)$ expresses the desired selection curve for fines destruction (classification function). For example, if we desire to remove crystals of size r_m and smaller, then $\bar{h}(r)$ has the form:

$$\bar{h}(r) = \left[\begin{array}{ll} 1, & for \;\; r \leq r_m \\ 0, & for \;\; r > r_m \end{array} \right] \tag{2.16}$$

For the distributed parameter model of Eq.2.15 with the above expression for $\bar{h}(r)$, one can easily show that a direct application of the method of moments leads to an unclosed set of moments equations, thereby implying the need of using a general model reduction procedure for particulate processes (see section 2.3.2).

2.3 Nonlinear Model Reduction and Control of Particulate Processes

2.3.1 Methodological Framework for Control of Particulate Processes

Owing to its distributed parameter nature, the system of Eqs.2.1-2.2 cannot be directly used as the basis for the synthesis of low-order nonlinear controllers that can be implemented. This fact, together with the realization that the dominant dynamics of particulate processes are characterized by a small number of degrees of freedom, motivates employing the following methodology for the synthesis of low-order nonlinear output feedback controllers for systems of the form of Eqs.2.1-2.2:

1. Initially, the method of weighted residuals is used to derive a nonlinear, possibly high-order, ODE system that accurately reproduces the solutions and dynamics of the system of Eqs.2.1-2.2. Then, a procedure based on the concept of approximate inertial manifold is employed for the construction of low-order ODE systems that accurately reproduce the dominant dynamics of the large-scale ODE system obtained by the method of weighted residuals. The asymptotic validity of the ODE approximations is established by using results from the perturbation theory.

2. Then, the low-order ODE approximation of the system of Eqs.2.1-2.2 is used as the basis for the synthesis, via geometric control methods, of nonlinear output feedback controllers that stabilize the closed-loop ODE system and enforce set-point tracking.

3. Finally, the resulting closed-loop system (particulate process model of Eqs.2.1-2.2 and controller) is analyzed to derive conditions that guarantee that the desired stability and set-point tracking properties are enforced in the infinite dimensional

closed-loop system.

2.3.2 Nonlinear Model Reduction of Particulate Process Models

In this section, we introduce a general methodology for deriving low-order ODE systems that accurately reproduce the dominant dynamics of the nonlinear integro-differential equation system of Eqs.2.1-2.2. The proposed model reduction methodology exploits the low-dimensional behavior of the dominant dynamics of the system of Eqs.2.1-2.2 and is based on a combination of the method of weighted residuals with the concept of approximate inertial manifold.

2.3.3 Method of Weighted Residuals

We initially use the method of weighted residuals to construct a nonlinear, possibly high-order, ODE system that accurately reproduces the solutions and dynamics of the distributed parameter system of Eqs.2.1-2.2. The central idea of the method of weighted residuals (see [62] for a comprehensive review of results on the use of this method for solving population balance equations) is to approximate the exact solution of $n(r,t)$ by an infinite series of orthogonal basis functions defined on the interval $[0, r_{max})$ with time-varying coefficients, substitute the series expansion into Eq.2.1 to form the residual, and then force the residual to be orthogonal to a complete set of weighted functions (that is, the inner product of the residual with a complete set of weighting functions in $L_2[0, r_{max})$ is set equal to zero) to compute a set of ODEs which describe the rate of change of the time-varying coefficients of the series expansion of the solution.

Specifically, we consider an orthogonal set of basis functions $\phi_k(r)$, where $r \in [0, r_{max})$, $k = 1, \ldots, \infty$, and expand the particle size distribution function $n(r,t)$ in

an infinite series in terms of $\phi_k(r)$ as follows:

$$n(r,t) = \sum_{k=1}^{\infty} a_k(t)\phi_k(r) \tag{2.17}$$

where $a_k(t)$ are time-varying coefficients. Substituting Eq.2.17 into Eqs.2.1-2.2, we get:

$$\begin{aligned} \sum_{k=1}^{\infty}\phi_k(r)\frac{\partial a_k(t)}{\partial t} &= -\sum_{k=1}^{\infty}a_k(t)\frac{\partial(G(x,r)\phi_k(r))}{\partial r} + w(\sum_{k=1}^{\infty}a_k(t)\phi_k(r),x,r) \\ \dot{x} &= f(x)+g(x)u(t)+A\int_0^{r_{max}} a(\sum_{k=1}^{\infty}a_k(t)\phi_k(r),r,x)dr \end{aligned} \tag{2.18}$$

Multiplying the population balance with the weighting functions $\psi_\nu(r)$, and integrating over the entire particle size spectrum (that is, taking inner product in $L_2[0,r_{max})$ with the weighting functions), the following set of infinite ODEs is obtained:

$$\begin{aligned} \int_0^{r_{max}}\psi_\nu(r)\sum_{k=1}^{\infty}\phi_k(r)\frac{\partial a_k(t)}{\partial t}dr &= -\sum_{k=1}^{\infty}a_k(t)\int_0^{r_{max}}\psi_\nu(r)\frac{\partial(G(x,r)\phi_k(r))}{\partial r}dr \\ &\quad +\int_0^{r_{max}}\psi_\nu(r)w(\sum_{k=1}^{\infty}a_k(t)\phi_k(r),x,r)dr, \\ &\quad \nu=1,\ldots,\infty \\ \dot{x} &= f(x)+g(x)u(t)+A\int_0^{r_{max}}a(\sum_{k=1}^{\infty}a_k(t)\phi_k(r),r,x)dr \end{aligned} \tag{2.19}$$

Truncating the series expansion of $n(r,t)$ up to order N and keeping the first N equations (that is, $\nu=1,\ldots,N$), the infinite dimensional system of Eq.2.19 reduces

to the following finite set of ODEs:

$$\begin{aligned}
\int_0^{r_{max}} \psi_\nu(r) \sum_{k=1}^{N} \phi_k(r) \frac{\partial a_{kN}(t)}{\partial t} dr &= -\sum_{k=1}^{N} a_{kN}(t) \int_0^{r_{max}} \psi_\nu(r) \frac{\partial (G(x_N, r)\phi_k(r))}{\partial r} dr \\
&\quad + \int_0^{r_{max}} \psi_\nu(r) w(\sum_{k=1}^{N} a_{kN}(t)\phi_k(r), x_N, r) dr, \\
&\quad \nu = 1, \ldots, N \\
\dot{x}_N &= f(x_N) + g(x_N)u(t) \\
&\quad + A \int_0^{r_{max}} a(\sum_{k=1}^{N} a_{kN}(t)\phi_k(r), r, x_N) dr \\
y_i(t) &= h_i(\int_0^{r_{max}} c_\kappa \sum_{k=1}^{N} a_{kN}(t)\phi_k(r) dr, x_N), \\
&\quad i = 1, \ldots, m, \quad \kappa = 1, \ldots, l
\end{aligned} \tag{2.20}$$

where x_N and a_{kN} are the approximations of x and a_k obtained by an N-th order truncation. From Eq.2.20, it is clear that the form of the ODEs that describe the rate of change of $a_{kN}(t)$ depends on the choice of the basis and weighting functions, as well as on N. The basis and weighting functions determine the type of weighted residual method being used (see Remarks 2.8 and 2.9 below).

Proposition 2.1 that follows establishes a convergence property for the discrepancy between the solutions of the particulate process model of Eqs.2.1-2.2 and the approximation of Eq.2.20, for sufficiently large N.

Proposition 2.1: *Consider the system of Eqs.2.1-2.2 with $u(t) \equiv 0$ and assume that n and $\frac{\partial n}{\partial r}$ are continuous functions of r. Suppose also that the system of Eq.2.20 is locally exponentially stable, for any N. Then, there exists an N sufficiently large so that $\forall t \geq 0$:*

$$\begin{aligned}
n(r,t) &= n_N(r,t) + O(\epsilon(N)) \\
x(t) &= x_N(t) + O(\epsilon(N))
\end{aligned} \tag{2.21}$$

where $\epsilon(N)$ is a small positive real number that depends on N and satisfies $\lim_{N \to \infty} \epsilon(N)$

$= 0$, *and* $n_N(r,t) = \sum_{k=1}^{N} a_{kN}(t)\phi_k(r)$ *is the approximation of* $n(r,t)$ *which is obtained by solving Eq.2.20 with* $u(t) \equiv 0$.

Remark 2.7: The assumption that the system of Eq.2.20 (and thus, the system of Eqs.2.1-2.2) is locally exponentially stable is necessary in order to prove that the estimates of Eq.2.21 hold for all times. When the system of Eq.2.20 is not exponentially stable, one can only prove that the estimates of Eq.2.21 hold for $t \in [0, \tau]$ where τ is a positive real number of $O(1)$ (see simulation results in section 2.2.2 for a verification of this fact). Furthermore, the convergence result can be shown for the $L_2[0,\infty)$ norm of the difference between the solution of the population balance $n(r,t)$ and its approximation of Eq.2.17, that is, for all $t \in [0,\infty)$:

$$\lim_{N\to\infty} ||n(r,t) - \sum_{k=1}^{N} a_{kN}(t)\phi_k(r)||_2 = 0 \tag{2.22}$$

Remark 2.8: The method of weighted residuals reduces to the method of moments when the basis functions are chosen to be Laguerre polynomials and the weighting functions are chosen as $\psi_\nu = r^\nu$. The moments of the particle size distribution are defined as:

$$\mu_\nu = \int_0^\infty r^\nu n(r,t)dr, \quad \nu = 0,\ldots,\infty \tag{2.23}$$

and the moment equations can be directly generated from the population balance model by multiplying it by r^ν, $\nu = 0,\ldots,\infty$ and integrating from 0 to ∞. The procedure of forming moments of the population balance equation very often leads to terms that may not reduce to moments, terms that include fractional moments, or to an unclosed set of moment equations. To overcome this problem, the particle size distribution is expanded in terms of Laguerre polynomials defined in $L_2[0,\infty)$ and the series solution is used to close the set of moment equations (this procedure can be used for models of crystallizers with fines trap; see Eqs.2.15-2.16).

Remark 2.9: When the number of basis functions $\phi_k(r)$ required to obtain a good approximation (measured in a desired norm) of the solution of the population balance, is small, then the weighting functions are usually chosen [66] to be identical to the basis functions, in which case the method of weighted residuals reduces to Galerkin's method.

Remark 2.10: When a "good" (in the sense of leading to the derivation of a moderate order ODE system of desired accuracy) set of basis functions $\phi_k(r)$ cannot be found within the standard basis function sets, one can compute a set of empirical eigenfunctions by applying the Karhunen-Loeve expansion [32, 36, 75] (also known as proper orthogonal decomposition) on an appropriate ensemble of solutions of the particulate process model of Eqs.2.1-2.2, which are obtained from detailed finite difference discretizations.

2.3.4 Inertial Manifold / Approximate Inertial Manifold

The system of Eq.2.20 was obtained from a direct application of the method of weighted residuals (with arbitrary basis functions) to the system of Eqs.2.1-2.2, and thus, may be of very high order in order to provide an accurate description of the dominant dynamics of the particulate process model. High-dimensionality of the system of Eq.2.20 leads to complex controller design and high-order controllers, which cannot be readily implemented in practice. To circumvent these problems, we exploit the low-dimensional behavior of the dominant dynamics of particulate processes and use an approach based on the concept of inertial manifold to derive low-order ODE systems that accurately describe the dominant dynamics of the system of Eq.2.20. The concept of inertial manifold is an appropriate tool for model reduction because if the trajectories of the system of Eq.2.20 are on the manifold, then this system is

exactly described by a low-order system.

We begin with the definition of the concept of inertial manifold, and we continue with the concept of approximate inertial manifold. To this end, we exploit the orthogonality of the basis functions $\phi_k(r)$ to uniquely split:

$$n_N = \sum_{k=1}^{p} a_{kN}(t)\phi_k(r) + \sum_{k=p+1}^{N} a_{kN}(t)\phi_k(r) =: n_p + n_q \tag{2.24}$$

where the first p eigenmodes are associated with the dominant (possibly unstable) dynamics of the system of Eq.2.20, and the remaining q eigenmodes are associated with exponentially stable dynamics.

Introducing the vector notation $a_N = [a_{1N} \cdots a_{NN}]$ and defining the new vectors of state variables $\tilde{x} = [a_{sN}^T \; x_N^T]^T$, $a_{sN} = [a_{1N} \cdots a_{pN}]^T$ and $a_{fN} = [a_{(p+1)N} \cdots a_{NN}]^T$, the system of Eq.2.20 can be written as:

$$\begin{aligned} \dot{a}_{fN} &= \bar{f}_q(a_{fN}, \tilde{x}) \\ \dot{\tilde{x}} &= \tilde{f}(\tilde{x}, a_{fN}) + \tilde{g}(\tilde{x}, a_{fN})u \\ y_i &= \tilde{h}_i(\tilde{x}, a_{fN}), \quad i = 1, \ldots, m \end{aligned} \tag{2.25}$$

where the explicit expression of $\bar{f}_q(a_{fN}, \tilde{x}), \tilde{f}(\tilde{x}, a_{fN}), \tilde{g}(\tilde{x}, a_{fN}), \tilde{h}_i(\tilde{x}, a_{fN})$ can be obtained by comparing Eq.2.20 and Eq.2.25 and will be omitted for brevity. Assuming that $\bar{f}_q(a_{fN}, \tilde{x}) = \tilde{A}a_{fN} + \tilde{f}_q(a_{fN}, \tilde{x})$, where $\tilde{A}$ is a Hurwitz matrix and $\tilde{f}_q(a_{fN}, \tilde{x})$ is a nonlinear vector function which does not include linear terms (this assumption is made to simplify the development and can be readily relaxed), the system of Eq.2.25 can be written as:

$$\begin{aligned} \dot{a}_{fN} &= \tilde{A}a_{fN} + \tilde{f}_q(a_{fN}, \tilde{x}) \\ \dot{\tilde{x}} &= \tilde{f}(\tilde{x}, a_{fN}) + \tilde{g}(\tilde{x}, a_{fN})u \\ y_i &= \tilde{h}_i(\tilde{x}, a_{fN}), \quad i = 1, \ldots, m \end{aligned} \tag{2.26}$$

For the above system, an inertial manifold $\mathcal{M}$ is a subset of $\mathbb{R}^{N+n}$, which satisfies the following properties [76]:

i) $\mathcal{M}$ is a finite dimensional Lipschitz manifold,

ii) $\mathcal{M}$ is a graph of a Lipschitz function $\Sigma(\tilde{x})$ mapping $\mathbb{R}^{p+n}$ into $\mathbb{R}^q$ and for every solution $\tilde{x}(t), a_{fN}(t)$ of Eq.2.26 with $a_{fN}(0) = \Sigma(\tilde{x}(0))$, then

$$a_{fN}(t) = \Sigma(\tilde{x}(t)), \quad \forall\, t \geq 0 \tag{2.27}$$

iii) $\mathcal{M}$ attracts every trajectory exponentially.

The evolution of the state $a_{fN}(t)$ on $\mathcal{M}$ is given by Eq.2.27, while the evolution of the state $\tilde{x}$ is governed by the following $(p+n)$-order system:

$$\begin{aligned} \dot{\tilde{x}} &= \tilde{f}(\tilde{x}, \Sigma(\tilde{x})) + \tilde{g}(\tilde{x}, \Sigma(\tilde{x}))u \\ y_i &= \tilde{h}_i(\tilde{x}, \Sigma(\tilde{x})), \quad i = 1, \ldots, m \end{aligned} \tag{2.28}$$

Differentiating Eq.2.27 and utilizing Eq.2.26, $\Sigma(\tilde{x})$ can be computed as the solution of the following partial differential equation:

$$\frac{\partial \Sigma}{\partial \tilde{x}}[\tilde{f}(\tilde{x}, \Sigma(\tilde{x})) + \tilde{g}(\tilde{x}, \Sigma(\tilde{x}))u] = \tilde{A}\Sigma(\tilde{x}) + \tilde{f}_q(\Sigma(\tilde{x}), \tilde{x}) \tag{2.29}$$

which $\Sigma(\tilde{x})$ has to satisfy for all $\tilde{x} \in \mathbb{R}^{p+n}$. From the structure of Eq.2.29, it is obvious that the computation of the explicit form of $\Sigma(\tilde{x})$ is a very difficult (if not impossible) task in most practical applications. To overcome this problem, and since the dynamics of the a_{fN} modes are stable and faster than the ones of the $\tilde{x}$ modes (note that the number of unstable eigenvalues of the system of Eqs.2.1-2.2 is finite, and by assumption, all the unstable eigenvalues are included in the $\tilde{x}$ subsystem), we obtain $\Sigma(\tilde{x})$ by setting $\dot{a}_{fN} = \dfrac{\partial \Sigma}{\partial \tilde{x}}[\tilde{f}(\tilde{x}, \Sigma) + \tilde{g}(\tilde{x}, \Sigma)u] \equiv 0$ and solving the equation:

$$\tilde{A}\Sigma(\tilde{x}) + \tilde{f}_q(\Sigma(\tilde{x}), \tilde{x}) = 0 \tag{2.30}$$

using a standard successive approximation (fixed point) algorithm [29] (see also [75]):

$$\begin{aligned} \tilde{\Sigma}_{\kappa+1}(\tilde{x}) &= -\tilde{A}^{-1}\tilde{f}_q(\tilde{\Sigma}_\kappa(\tilde{x}), \tilde{x}), \quad \kappa = 0, \ldots, \bar{l}, \quad \tilde{\Sigma}_0(\tilde{x}) = 0 \\ \tilde{a}_{fN} &= \tilde{\Sigma}_{\bar{l}+1}(\tilde{x}) \end{aligned} \tag{2.31}$$

where $\tilde{\Sigma}_{\bar{l}+1}(\tilde{x})$ is an approximation of $\Sigma(\tilde{x})$ (called approximate inertial manifold) and $\tilde{a}_{fN}$ is the approximation of a_{fN}. Substituting $\tilde{\Sigma}_{\bar{l}+1}(\tilde{x})$ into the system of Eq.2.28, the

following $(p+n)$-order approximation of the particulate process model is obtained:

$$\begin{aligned} \dot{\tilde{x}} &= \tilde{f}(\tilde{x}, \tilde{\Sigma}_{\bar{l}+1}(\tilde{x})) + \tilde{g}(\tilde{x}, \tilde{\Sigma}_{\bar{l}+1}(\tilde{x}))u =: \tilde{f}(\tilde{x}) + \tilde{g}(\tilde{x})u \\ y_{s_i} &= \tilde{h}_i(\tilde{x}, \tilde{\Sigma}_{\bar{l}+1}(\tilde{x})) =: \tilde{h}_i(\tilde{x}), \quad i = 1, \ldots, m \end{aligned} \tag{2.32}$$

where the subscript s in the controlled output, y_{s_i}, denotes that this controlled output is associated with an approximate low-order ODE system (refer to Eq.2.3 for the formulation of y_i for the distributed parameter model).

Proposition 2.2 that follows establishes that the local stability properties and solutions, for large times, of the systems Eq.2.32 and Eq.2.20 are equivalent. The proof is given in the appendix.

Proposition 2.2: *Suppose that the sequence of Eq.2.31, for the construction of* $\tilde{\Sigma}_{\bar{l}+1}(\tilde{x})$, *converges for* $\bar{l}$ *sufficiently large (that is, for any* $\tilde{\epsilon}$, *there exists an* $\bar{l}^*$ *such that if* $\bar{l} \geq \bar{l}^*$, *then* $|\Sigma(\tilde{x}) - \tilde{\Sigma}_{\bar{l}+1}(\tilde{x})| \leq \tilde{\epsilon}$*). Suppose also that the* $(p+n)$*-order system of Eq.2.32 with* $u(t) \equiv 0$ *is locally exponentially stable. Then, the* $(N+n)$*-order system of Eq.2.20 with* $u(t) \equiv 0$ *is locally exponentially stable and* $\lim_{t\to\infty} ||n_N - \bar{n}_N||_2 = O(\tilde{\epsilon}(\bar{l}))$ *where* $\bar{n}_N = \sum_{k=1}^{p} \tilde{a}_{kN}(t)\phi_k(r) + \sum_{k=p+1}^{N} \tilde{\Sigma}_{\bar{l}+1}(\tilde{x})\phi_k(r)$ *(*$\tilde{a}_{kN}(t)$ *is the solution obtained from the system of Eq.2.32) and* $\tilde{\epsilon}(\bar{l})$ *is a small positive real number that depends on* $\bar{l}$ *and satisfies* $\lim_{\bar{l}\to\infty} \tilde{\epsilon}(\bar{l}) = 0$.

Remark 2.11: We note that even though many particulate processes exhibit low-dimensional dynamic behavior, the delicate mathematical question of rigorously establishing existence of inertial manifolds for particulate process models, at this stage, is unresolved. Such a question has been positively answered for certain classes of diffusion-reaction systems and the Kuramoto-Sivashinsky equation (see [76] for details).

Remark 2.12: The expression of the approximate inertial manifold $\tilde{\Sigma}_{\bar{l}+1}(\tilde{x})$ of Eq.2.31 (where $\bar{l}$ is chosen based on the desired degree of approximation) was orig-

inally proposed in [29] and is called the steady manifold. Also refer to [18, 75] for alternative expressions of $\tilde{\Sigma}(\tilde{x})$, as well as detailed computational studies that show that the use of approximate inertial manifolds leads to accurate low-order ODE approximations and low-order controllers for diffusion-reaction systems described by parabolic partial differential equations.

Remark 2.13: For $\Sigma(\tilde{x}) = 0$, we obtain the following order $(p + n)$ approximation of the particulate process model:

$$\begin{aligned} \dot{a}_{sN} &= \bar{f}_p(a_{sN}, 0, x_N) \\ \dot{x}_N &= f(x_N) + g(x_N)u(t) + A\int_0^{r_{max}} a(n_p, x_N, r)dr \end{aligned} \tag{2.33}$$

The above system is identical to the one obtained by a direct application of the method of weighted residuals to the particulate process model of Eqs.2.1-2.2 (Eq.2.20 with $N = p$).

2.3.5 Nonlinear Output Feedback Control of Particulate Processes

In this section, the system of Eq.2.32 is used to synthesize a nonlinear finite dimensional output feedback controller that guarantees stability and enforces output tracking in the closed-loop ODE system and to establish that the same controller exponentially stabilizes the closed-loop particulate process model. The output feedback controller is constructed through a standard combination of a state feedback controller with a state observer. The state feedback controller is synthesized via geometric control methods and the state observer is an extended Luenberger-type observer. This begins with some preliminaries, which will be used to state the controller synthesis result.

2.3.6 Preliminaries

Referring to the system of Eq.2.32, we define the relative order of the output y_{s_i} with respect to the vector of manipulated inputs u as the smallest integer r_i for which

$$\left[L_{\tilde{g}_1} L_{\tilde{f}}^{r_i-1} \tilde{h}_i(\tilde{x}) \ \cdots \ L_{\tilde{g}_m} L_{\tilde{f}}^{r_i-1} \tilde{h}_i(\tilde{x})\right] \not\equiv [0 \ \cdots \ 0] \tag{2.34}$$

where $\tilde{g}_i$ is the i-th vector of the matrix $\tilde{g}$, or $r_i = \infty$ if such an integer does not exist. We also define the characteristic matrix

$$C(\tilde{x}) \ = \ \begin{bmatrix} L_{\tilde{g}_1} L_{\tilde{f}}^{r_1-1} \tilde{h}_1(\tilde{x}) & \cdots & L_{\tilde{g}_m} L_{\tilde{f}}^{r_1-1} \tilde{h}_1(\tilde{x}) \\ L_{\tilde{g}_1} L_{\tilde{f}}^{r_2-1} \tilde{h}_2(\tilde{x}) & \cdots & L_{\tilde{g}_m} L_{\tilde{f}}^{r_2-1} \tilde{h}_2(\tilde{x}) \\ \vdots & \cdots & \vdots \\ L_{\tilde{g}_1} L_{\tilde{f}}^{r_m-1} \tilde{h}_m(\tilde{x}) & \cdots & L_{\tilde{g}_m} L_{\tilde{f}}^{r_m-1} \tilde{h}_m(\tilde{x}) \end{bmatrix} \tag{2.35}$$

Controller Synthesis

We use the nonlinear system of Eq.2.32 as a basis for the synthesis, via geometric control methods, of nonlinear state feedback controllers of the general form:

$$u \ = \ p(\tilde{x}) + Q(\tilde{x})v \tag{2.36}$$

where $p(\tilde{x})$ is a smooth vector function, $Q(\tilde{x})$ is a smooth matrix, and $v \in \mathbb{R}^m$ is the constant reference input vector. The controllers guarantee local exponential stability and enforce a linear input/output response in the system of Eq.2.32 (the details on controller synthesis can be found in [39] and will be omitted here for brevity).

Under the hypothesis that the system of Eq.2.32 is locally observable (that is, its linearization around the desired operating steady-state is observable), the practical implementation of a nonlinear state feedback controller of the form of Eq.2.36 will be achieved by employing the following nonlinear state observer:

$$\frac{d\omega}{dt} \ = \ \tilde{f}(\omega) + \tilde{g}(\omega)u + L(y - \tilde{h}(\omega)) \tag{2.37}$$

where ω denotes the observer state vector (the dimension of the vector ω is equal to the dimension of $\tilde{x}$ in the system of Eq.2.32), $y = [y_1\ y_2\ \cdots y_l]^T$ is the measured output vector, and L is a matrix chosen so that the eigenvalues of the matrix $C_L = \frac{\partial \tilde{f}}{\partial \omega}_{(\omega=\omega_s)} - L\frac{\partial \tilde{h}}{\partial \omega}_{(\omega=\omega_s)}$, where ω_s is the operating steady-state, lie in the open left-half of the complex plane. The state observer of Eq.2.37 consists of a replica of the system of Eq.2.32 plus a linear gain multiplying the discrepancy between the actual and the estimated value of the output, and therefore, it is an extended Luenberger-type observer.

The state feedback control law of Eq.2.36 and the state observer of Eq.2.37 can be combined to yield the following nonlinear output feedback control law:

$$\begin{aligned} \frac{d\omega}{dt} &= \tilde{f}(\omega) + \tilde{g}(\omega)(p(\omega) + Q(\omega)v) + L(y - \tilde{h}(\omega)) \\ u &= p(\omega) + Q(\omega)v \end{aligned} \tag{2.38}$$

Theorem 2.1 below provides an explicit synthesis formula of the above output feedback control law and conditions that guarantee closed-loop stability and asymptotic output tracking (the proof can be found in Appendix A).

Theorem 2.1: *Suppose that the sequence of Eq.2.31 converges for $\bar{l}$ is sufficiently large. Consider the system of Eq.2.32 and assume that:* 1) *it is locally observable in the sense that there exists a matrix L such that $C_L = \frac{1}{\mu}\bar{A}$ where μ is a small positive parameter and $\bar{A}$ is a Hurwitz matrix,* 2) *its characteristic matrix, $C(\tilde{x})$, is nonsingular $\forall\ \tilde{x} \in D \subset \mathbb{R}^{p+n}$, and* 3) *its unforced ($v \equiv 0$) zero dynamics are locally exponentially stable. Finally, consider the particulate process model of Eqs.2.1-2.2 under the nonlinear output feedback controller:*

$$\begin{aligned} \frac{d\omega}{dt} &= \tilde{f}(\omega) + \tilde{g}(\omega)\left\{[\beta_{1r_1}\cdots\beta_{mr_m}]C(\omega)\right\}^{-1}\left\{v - \sum_{i=1}^{m}\sum_{k=0}^{r_i}\beta_{ik}L_{\tilde{f}}^{k}\tilde{h}_i(\omega)\right\} + L(y - \tilde{h}(\omega)) \\ u &= \left\{[\beta_{1r_1}\cdots\beta_{mr_m}]C(\omega)\right\}^{-1}\left\{v - \sum_{i=1}^{m}\sum_{k=0}^{r_i}\beta_{ik}L_{\tilde{f}}^{k}\tilde{h}_i(\omega)\right\} \end{aligned} \tag{2.39}$$

where the parameters β_{ik} are chosen so that the roots of the equation $det(B(s)) = 0$ are in the open left-half of the complex plane ($B(s)$ is an $l \times l$ matrix, whose (i,j)-th element is of the form $\sum_{k=0}^{r_i} \beta_{jk}^{i} s^k$). Then, there exists a positive real number μ^* such that if $\mu \in (0, \mu^*]$, the closed-loop system (particulate process model and controller of Eq.2.39) is exponentially stable and $\lim_{t\to\infty} |y_i - v_i| = O(\hat{\epsilon}(N + \bar{l}))$, where v_i is the set-point for the ith controlled output and $\hat{\epsilon}(N+\bar{l})$ is a small positive real number that depends on $N, \bar{l}$ and satisfies $\lim_{N,\bar{l}\to\infty} \hat{\epsilon}(N + \bar{l}) = 0$.

Remark 2.14: Regarding the practical application of Theorem 2.1, one has to initially pick an $\bar{l}$ and construct the system of Eq.2.32, and then verify assumptions 1, 2, and 3 of the theorem on the basis of this system. If these assumptions are satisfied, the synthesis formula of Eq.2.39 can be directly used to derive the explicit form of the controller (see Chapter 3 for an application of this procedure to the crystallizer example).

Remark 2.15: The assumption that $\bar{l}$ is sufficiently large is needed to obtain the stability and closeness of solutions results of Proposition 2.2 for the appropriate approximations of the closed-loop system, while the assumption $C_L = \frac{1}{\mu}\bar{A}$, where μ is a small positive parameter and $\bar{A}$ is a Hurwitz matrix, is needed to ensure that the presence of closed-loop system states, which are not included in the model used for controller synthesis, in the state observer does not lead to closed-loop instability. Finally, the assumption that the characteristic matrix $C(\bar{x})$ is nonsingular is made to simplify the presentation of the controller synthesis results and can be relaxed (see [39] for details).

Remark 2.16: The exponential stability of the closed-loop system guarantees that in the presence of small initialization errors of the observer states (that is, $\omega(0) \neq$

$\tilde{x}(0)$), and uncertainty in the process parameters and disturbances, the states of the closed-loop system will be bounded. Furthermore, since the number of manipulated inputs and controlled outputs is finite, it is possible to implement a linear error feedback controller (for example, a proportional-integral (PI) controller for single-input single-output processes) around the $(y_i - v_i)$, $i = 1, \ldots, l$, loops to ensure asymptotic offsetless output tracking in the closed-loop system, in the presence of such uncertainty.

Remark 2.17: Theorem 2.1 establishes that a nonlinear output feedback controller which guarantees local exponential stability and output tracking in the finite dimensional closed-loop system (Eqs.2.32-2.39), continues to enforce the same properties in the infinite dimensional closed-loop system (Eqs.2.1-2.2-2.39). This result is intuitively expected because: a) the dynamics of the modes of the particulate process model which are not taken into account in the controller design (that is, not included in the ODE model of Eq.2.32), are locally exponentially stable, and b) the control action $u(t)$ does not influence the dynamics of the modes which are not taken into account in the controller design (note that $u(t)$ does not enter in the a_{fN}-subsystem of Eq.2.25).

Remark 2.18: The nonlinear controller of Eq.2.39 possesses a robustness property with respect to fast and asymptotically stable unmodeled dynamics (that is, the controller enforces exponential stability and output tracking in the closed-loop system despite the presence of additional dynamics in the process, as long as they are stable and sufficiently fast). This property of the controller of Eq.2.39 can be rigorously established by analyzing the closed-loop system with the unmodeled dynamics using singular perturbations and is of particular importance for many practical applications where unmodeled dynamics often occur due to actuator and sensor dynamics, fast

process dynamics, and so on.

2.4 Conclusions

In this chapter, we considered spatially-homogeneous particulate processes modeled by a class of nonlinear partial integro-differential equation systems and developed a general method for the synthesis of practically implementable nonlinear output feedback controllers. The controllers enforce stability and attain a particle size distribution with desired characteristics in the closed-loop system. Initially, a model reduction procedure based on a combination of the method of weighted residuals and the concept of approximate inertial manifold was presented for the construction of low-order ODE systems that accurately reproduce the dynamics of the particulate process. These ODE systems were then used for the synthesis of nonlinear low-order output feedback controllers that enforce exponential stability in the closed-loop system and achieve a desired particle size distribution. In the next chapter, the proposed control method is applied to continuous and batch crystallization systems and its performance and robustness properties are tested through simulations.

Chapter 3

Application to Continuous and Batch Crystallizers

In this chapter, we present two applications of the nonlinear control method proposed in Chapter 2 to a batch and a continuous crystallization systems. Low-dimensional approximations of the population balances are derived and used for nonlinear control design. The performance of the nonlinear controllers is successfully tested through simulations using the detailed population balance models and is shown to be superior to the one of linear control schemes.

3.1 Application to a Continuous Crystallizer

3.1.1 Controller Synthesis

In this section, the proposed nonlinear control method is used to stabilize the continuous crystallizer introduced in section 2.2.2. Motivated by the fact that the crystallizer with the crystal size distribution as controlled output and the solute feed concentration as manipulated input is an approximately controllable system (see [72] for a rigorous controllability analysis), we study two representative control problems: the

first one involves manipulating the solute feed concentration, $u(t) = c_0 - c_{0_s}$ where c_{0_s} is the steady-state solute feed concentration, to achieve a crystal size distribution with desired mass, that is, the controlled output is defined as:

$$y(\bar{t}) = 8\pi\sigma^3 \int_0^\infty n(r,\bar{t})dr = \tilde{x}_0; \tag{3.1}$$

and the second one involves manipulating the solute feed concentration to achieve a crystal size distribution with a desired total particle size, that is, the controlled output is defined as:

$$y(\bar{t}) = 8\pi\sigma^2 \int_0^\infty rn(r,\bar{t})dr = \tilde{x}_1 \tag{3.2}$$

Refer to [56, 63, 25, 66] for the use of other manipulated variables including fines destruction rate and crystallizer temperature for the stabilization of crystallizers (note that the proposed control method can be used for the synthesis of nonlinear controllers when such manipulated inputs are considered).

Including the above specifications for manipulated input and controlled outputs in the model of Eq.2.8, one can easily see that the resulting system is in the form of Eq.2.5. Applying the method of moments to this system, utilizing the dimensionless variables of Eq.2.11 and $\bar{u} = \dfrac{(c_0 - c_{0_s})}{(c_0 - c_s)}$ and neglecting the moments of order four and higher, one can derive a system of the form of Eq.2.25 with $\tilde{x} = [\tilde{x}_0\ \tilde{x}_1\ \tilde{x}_2\ \tilde{x}_3\ \tilde{y}]^T$ and:

$$\tilde{f}(\tilde{x}) = \begin{bmatrix} \dfrac{-F}{\tilde{y}^2} \\ -\tilde{x}_0 + (1-\tilde{x}_3)Dae \\ -\tilde{x}_1 + \tilde{y}\tilde{x}_0 \\ -\tilde{x}_2 + \tilde{y}\tilde{x}_1 \\ -\tilde{x}_3 + \tilde{y}\tilde{x}_2 \\ \dfrac{1-\tilde{y}-(\alpha-\tilde{y})\tilde{y}\tilde{x}_2}{1-\tilde{x}_3} \end{bmatrix}, \quad \tilde{g}(\tilde{x}) = \begin{bmatrix} 0 \\ 0 \\ 0 \\ 0 \\ 1 \\ \dfrac{}{1-\tilde{x}_3} \end{bmatrix}$$

On the basis of this system, one can easily verify that assumptions 1, 2 and 3 of theorem 2.1 are satisfied. A direct application of the synthesis formula of Eq.2.39

then yields the following nonlinear output feedback controllers:

$$
\begin{aligned}
\frac{d\omega_0}{dt} &= -\omega_0 + (1-\omega_3)Dae^{\frac{-F}{\omega_4^2}} + L_0(\tilde{h}(\tilde{x}) - \tilde{h}(\omega)) \\
\frac{d\omega_1}{dt} &= -\omega_1 + \omega_4\omega_0 + L_1(\tilde{h}(\tilde{x}) - \tilde{h}(\omega)) \\
\frac{d\omega_2}{dt} &= -\omega_2 + \omega_4\omega_1 + L_2(\tilde{h}(\tilde{x}) - \tilde{h}(\omega)) \\
\frac{d\omega_3}{dt} &= -\omega_3 + \omega_4\omega_2 + L_3(\tilde{h}(\tilde{x}) - \tilde{h}(\omega)) \\
\frac{d\omega_4}{dt} &= \frac{1-\omega_4-(\alpha-\omega_4)\omega_4\omega_2}{1-\omega_3} + L_4(\tilde{h}(\tilde{x}) - \tilde{h}(\omega)) \\
&\quad + \frac{[\beta_2 L_{\tilde{g}} L_{\tilde{f}}\tilde{h}(\omega)]^{-1}\left\{v - \beta_0\tilde{h}(\omega) - \beta_1 L_{\tilde{f}}\tilde{h}(\omega) - \beta_2 L_{\tilde{f}}^2\tilde{h}(\omega)\right\}}{1-\omega_3} \\
\bar{u}(t) &= [\beta_2 L_{\tilde{g}} L_{\tilde{f}}\tilde{h}(\omega)]^{-1}\left\{v - \beta_0\tilde{h}(\omega) - \beta_1 L_{\tilde{f}}\tilde{h}(\omega) - \beta_2 L_{\tilde{f}}^2\tilde{h}(\omega)\right\}
\end{aligned}
\tag{3.3}
$$

where v is the set-point, β_0, β_1, β_2 and $L = [L_0\ L_1\ L_2\ L_3\ L_4]^T$ are controller parameters and $\tilde{h}(\omega) = \omega_0$ or $\tilde{h}(\omega) = \omega_1$. The nonlinear controller of Eq.3.3 was also combined with a PI controller (that is, the term $v - \beta_0\tilde{h}(\omega)$ was substituted by $v - \beta_0\tilde{h}(\tilde{x}) + \frac{1}{\tau_i'}\xi$, where $\dot{\xi} = v - \tilde{h}(\tilde{x})$, $\xi(0) = 0$ and τ_i' is the integral time constant) to ensure offsetless tracking in the presence of constant uncertainty in process parameters. The practical implementation of the nonlinear controllers of Eq.3.3 requires on-line measurements of the controlled outputs $\tilde{x}_0$ or $\tilde{x}_1$; in practice, such measurements can be obtained by using, for example, light scattering [5, 66].

3.1.2 Description of the Proposed Process

A schematic diagram of the proposed process is shown in Figure 3.1. A mix of solutions of different concentrations, with relative flow rates controlled by a controller (either nonlinear controller Eq.3.3 or PI controller in this case) in order to attain a desired inlet solute concentration, enter the crystallizer at a constant flow rate. Crystals, together with the solution, flow out of the crystallizer with the measurements

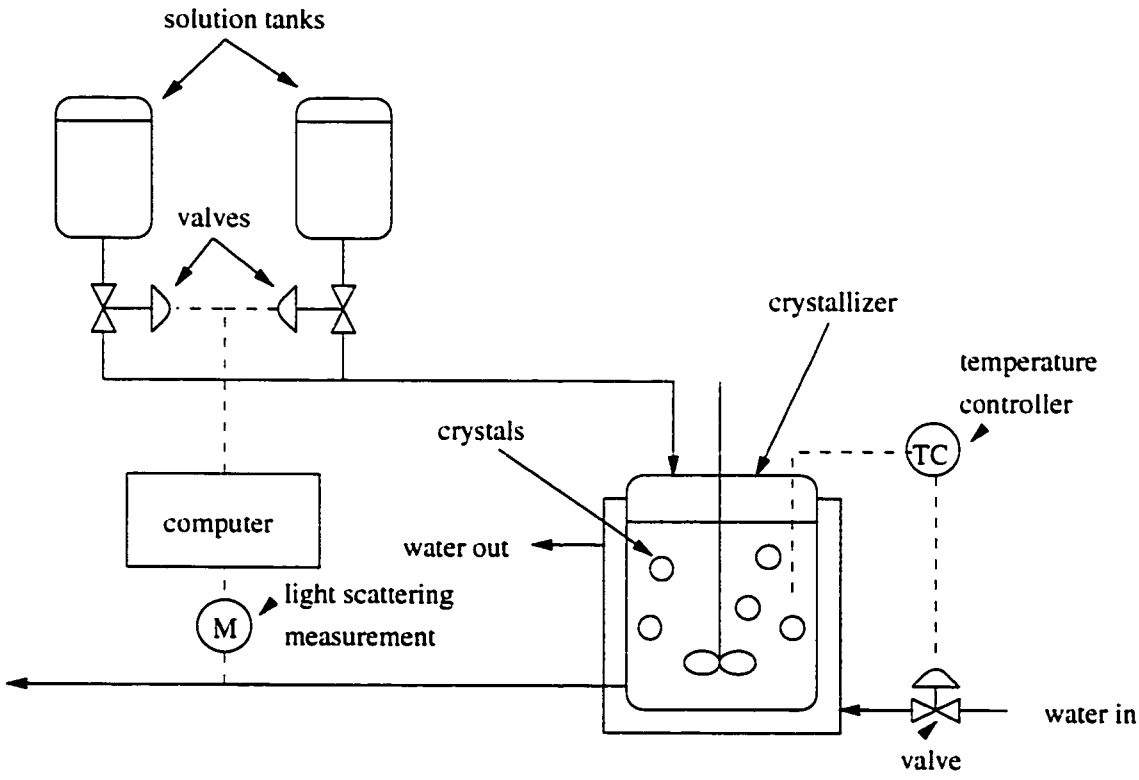

Figure 3.1: Schematic diagram for the proposed process.

of the values of the moments captured by a light scattering device [5, 66]. The control action required is generated by the computer and the signal is sent to the valves of the solution tanks in order to control the inlet solute concentration. The crystallizer is kept isothermal by the use of a conventional (for example, PI) controller, which manipulates temperature measurements obtained by a resistance thermal detector and send a signal to the valve to control the flow rate of cooling water.

3.1.3 Closed-loop Simulations

Several simulation runs were performed to evaluate the performance and robustness properties of the nonlinear controllers of Eq.3.3 and compare them with the ones of a PI controller. The values of the nonlinear controller parameters β_0, β_1, β_2 and L and the PI controller parameters K_c, τ_I, which were used in the simulations, are given in Tables 3.1 and 3.2 (K_c, τ_I were computed through extensive trial and error). In all

	without disturbance and delay	with disturbance	with delay
K_c	2.5	2.5	2.5
τ_i	0.5	0.5	1.0
L	$[1.0\ 0.0\ 0.0\ 0.0\ 1.0]^T$	$[1.0\ 0.0\ 0.0\ 0.0\ 1.0]^T$	$[1.0\ 0.0\ 0.0\ 0.0\ 1.0]^T$
β_0	1.0	1.0	1.0
β_1	2/3	2/3	2/3
β_2	1/9	1/9	1/9
τ_i'	20.0	20.0	20.0

Table 3.1: Controller parameters with $\tilde{x}_0$ as controlled output.

the simulation runs, the initial condition:

$$n(r,0) = 0.0,\ c(0) = 990.0\ kg/m^3$$

was used for the process model of Eq.2.8 and the finite difference method with 1,000 discretization points was used for its simulation. The initial conditions for the dynamic system included in the controller of Eq.3.3 were set to be: $\omega_0 = 0.047$,

	without disturbance and delay	with disturbance	with delay
K_c	2.5	2.5	2.0
τ_i	0.5	0.5	0.5
L	$[1.0\ 0.0\ 0.0\ 0.0\ 1.0]^T$	$[1.0\ 0.0\ 0.0\ 0.0\ 1.0]^T$	$[1.0\ 0.0\ 0.0\ 0.0\ 1.0]^T$
β_0	1.0	1.0	1.0
β_1	2.0	2.0	2.0
β_2	1.0	1.0	1.0
τ_i'	20.0	20.0	20.0

Table 3.2: Controller parameters with $\tilde{x}_1$ as controlled output.

$\omega_1 = 0.028$, $\omega_2 = 0.017$, $\omega_3 = 0.01$, and $\omega_4 = 0.5996$ (note that they do not correspond to the initial conditions used for the distributed parameter model in order to study the performance of the controller in the presence of significant initialization errors).

In the first set of simulation runs, $\tilde{x}_0$ was considered to be the controlled output. Initially, the set-point tracking capability of the nonlinear controller was evaluated under nominal conditions for a 0.5 increase in the value of the set-point ($v = 0.5$). Figure 3.2 shows the closed-loop output (top plot) and manipulated input (bottom plot) profiles obtained by using the nonlinear controller (solid lines) of Eq.3.3. For the sake of comparison, the corresponding profiles under PI control are also included (dashed lines). Clearly, the nonlinear controller drives the controlled output to its new set-point value in a significantly shorter time than the one required by the PI controller (note that both controlled outputs exhibit the same overshoot). For the same simulation run, the evolution of the closed-loop profile and the final steady-state profile of the crystal size distribution are shown in Figure 3.3. An exponentially-decaying crystal size distribution is obtained at the steady-state. Next, the robustness properties of the nonlinear controller in the presence of parametric uncertainties, unmodeled dynamics, and measurement sensor dead-time were investigated for a 0.5 increase in the value of the set-point. Figures 3.4 and 3.5 show the closed-loop output

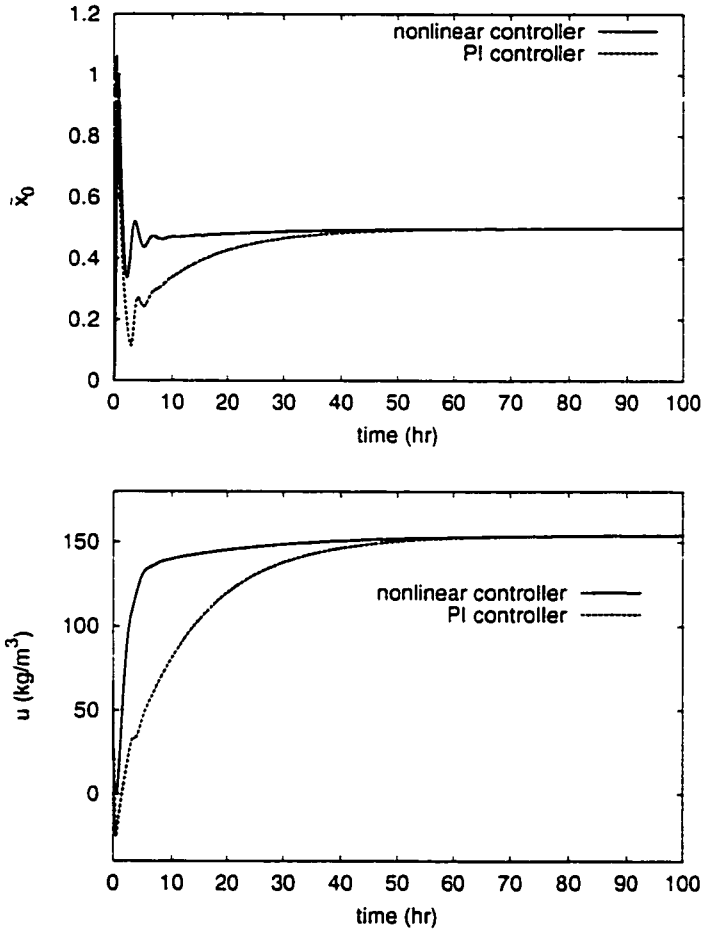

Figure 3.2: Closed-loop output (top) and manipulated input (bottom) profiles under nonlinear and PI control, for a 0.5 increase in the set-point ($\tilde{x}_0$ is the controlled output).

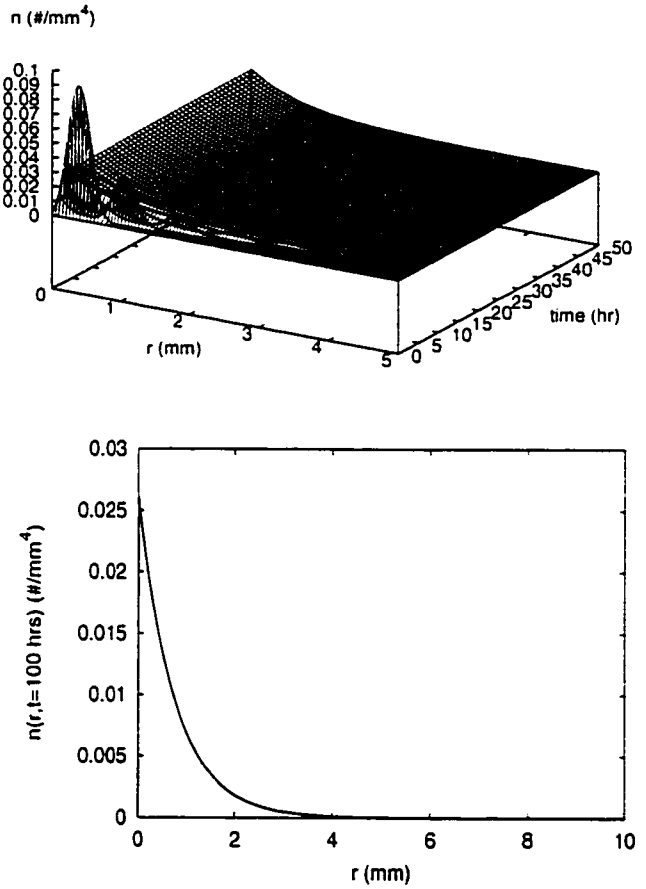

Figure 3.3: Profile of evolution of crystal size distribution (top) and final steady-state crystal size distribution (bottom) under nonlinear control ($\tilde{x}_0$ is the controlled output).

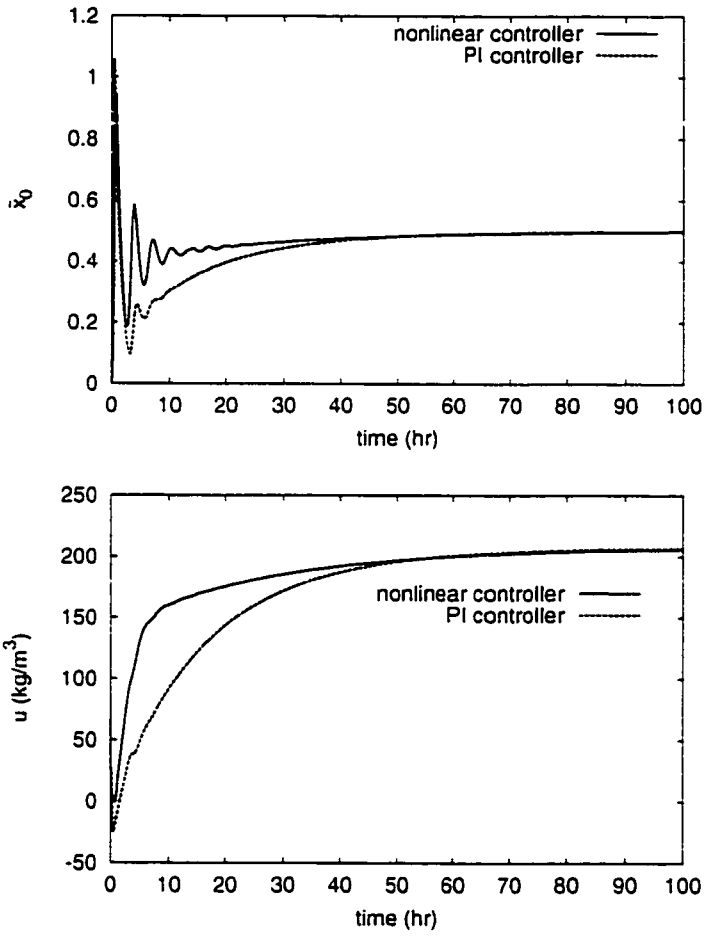

Figure 3.4: Closed-loop output (top) and manipulated input (bottom) profiles under nonlinear and PI control, for a 0.5 increase in the set-point in the presence of a 5% modeling error in both F and τ ($\tilde{x}_0$ is the controlled output).

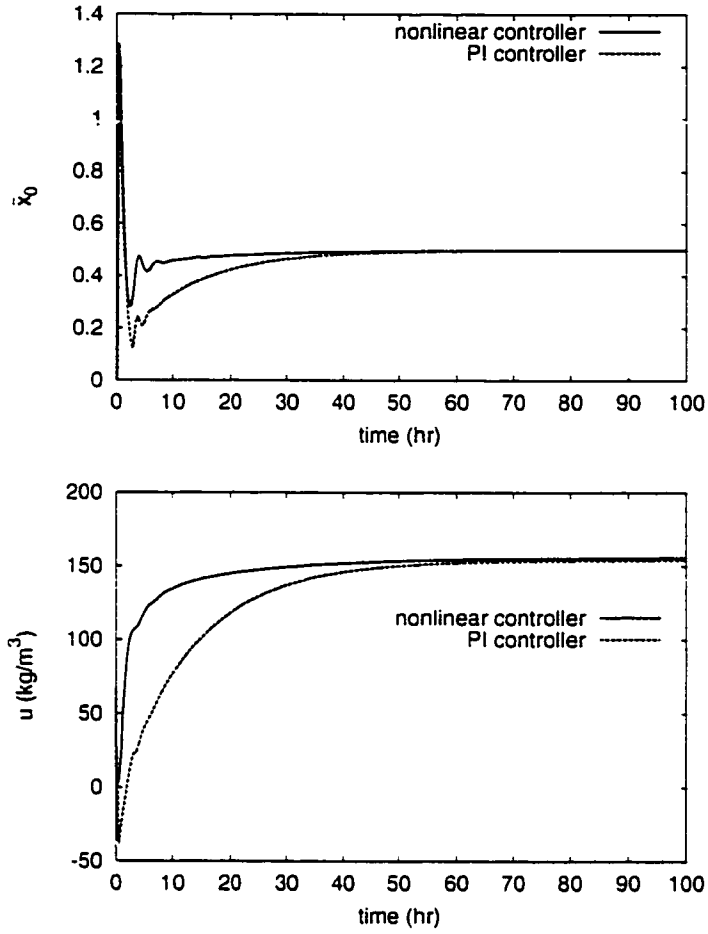

Figure 3.5: Closed-loop output (top) and manipulated input (bottom plot) profiles under nonlinear and PI control, for a 0.5 increase in the set-point in the presence of unmodeled actuator dynamics ($\tilde{x}_0$ is the controlled output).

(top plot) and manipulated input (bottom plot) profiles under the nonlinear controller (solid lines) in the presence of 5% error in both F and τ, and in the presence of fast actuator dynamics. To account for the actuator dynamics, the process model of Eq.2.6 was augmented with the dynamical system $\epsilon_z \dot{z}_1 = -z_1 + z_2$, $\epsilon_z \dot{z}_2 = -z_2 + u$, where $z_1, z_2 \in \mathbb{R}$ are the actuator states, z_1 is the actuator output and ϵ_z is a small parameter characterizing how fast are the actuator dynamics. The corresponding output and input profiles under PI control are also included (dashed lines). In the case of parametric uncertainties, the nonlinear controller exhibits very good robustness properties, driving quickly the output to its new set-point. In the case of unmodeled actuator dynamics, the nonlinear controller was also found to be more robust since the maximum ϵ_z, for which a stable closed-loop system was obtained, under nonlinear control is $\epsilon_z = 0.04$, while under proportional-integral control $\epsilon_z = 0.02$. Finally, a 10.0-minute delay in the measurement sensor was considered and the nonlinear controller of Eq.3.3 was redesigned within a Smith-Predictor framework, according to the results in [3] (details are omitted for brevity), to account for the presence of the delay. Figure 3.6 shows the profiles of the controlled outputs (top plot) and manipulated inputs (bottom plot) under nonlinear (solid lines) and PI (dashed lines) control, for a 0.5 increase in the value of the set-point. Clearly, the presence of the measurement delay deteriorates significantly the output response under PI control (note the oscillations of the controlled output), while it affects very little the output response under nonlinear control.

In the second set of simulation runs, $\tilde{x}_1$ was considered to be the controlled output. Initially, the performance of the nonlinear controller for a 0.5 increase in the value of the set-points was tested under nominal conditions. Figure 3.7 shows the closed-loop output (top plot) and manipulated input (bottom plot) profiles under nonlinear

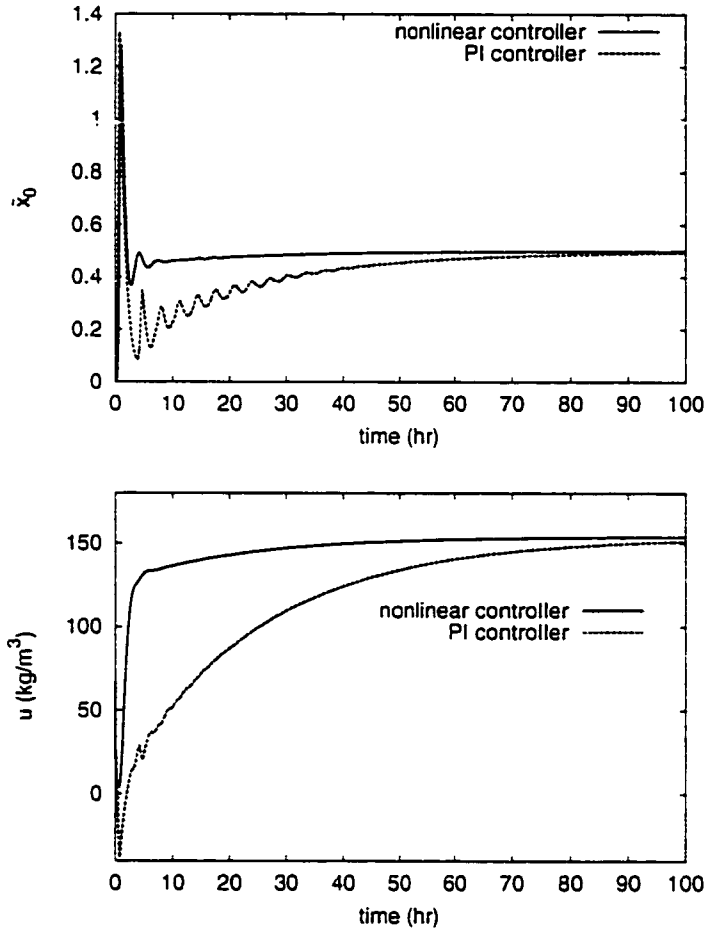

Figure 3.6: Closed-loop output (top) and manipulated input (bottom) profiles under nonlinear and PI control for a 0.5 increase in the set-point in the presence of a 10.0 minute delay in the output measurements ($\tilde{x}_0$ is the controlled output).

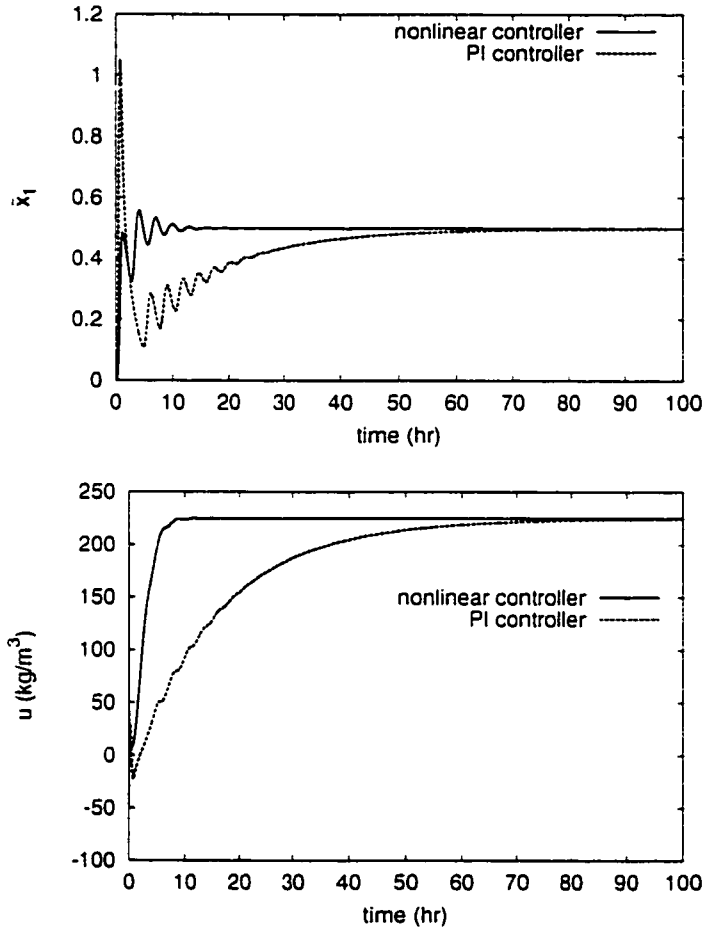

Figure 3.7: Closed-loop output (top) and manipulated input (bottom) profiles under nonlinear and PI control, for a 0.5 increase in the set-point ($\tilde{x}_1$ is the controlled output).

(solid lines) and PI (dashed lines) control. Again, the nonlinear controller drives the output to its new set-point much faster than the PI controller. The closed-loop profile of the evolution of the crystal size distribution is plotted in Figure 3.8 (top plot), along with the final steady-state profile of the crystal size distribution (middle plot) and the evolution of the mean crystal size (bottom plot). The stabilization of the crystal size distribution is quickly achieved and an exponentially-decaying crystal size distribution is obtained at steady state. Moreover, the final steady-state mean crystal size $\tilde{x}_1/\tilde{x}_0 = 0.77$ is about 28% higher than the mean crystal size of the open-loop unstable steady-state $\tilde{x}_1/\tilde{x}_0 = 0.60$, establishing that control of $\tilde{x}_1$ allows regulating the mean crystal size at a desired value. The robustness properties of the nonlinear controller in the presence of parametric uncertainties, unmodeled dynamics, and measurement sensor dead-time were also investigated. Initially, a 5% error in both F and τ, and unmodeled actuator dynamics, as described above, were separately considered. Figures 3.9 and 3.10 show the resulting closed-loop output (top plot) and manipulated input (bottom plot) profiles under nonlinear (solid lines) and PI (dashed lines) control. It is clear that the nonlinear controller possesses very good robustness properties with respect to parametric uncertainties, attenuating their effect on the output. Also, the nonlinear controller was found to be more robust with respect to unmodeled dynamics, $\epsilon_z = 0.02$, compared to the proportional-integral controller, $\epsilon_z = 0.01$. Finally, a delay of 10.0 minutes in the output measurement was considered (again, the nonlinear controller of Eq.3.3 was redesigned within a Smith-Predictor framework to account for the measurement delay). Figure 3.11 presents the output (top plot) and manipulated input (bottom plot) profiles under nonlinear (solid lines) and PI (dashed lines) control. Again, the superior performance of the nonlinear controller is evident.

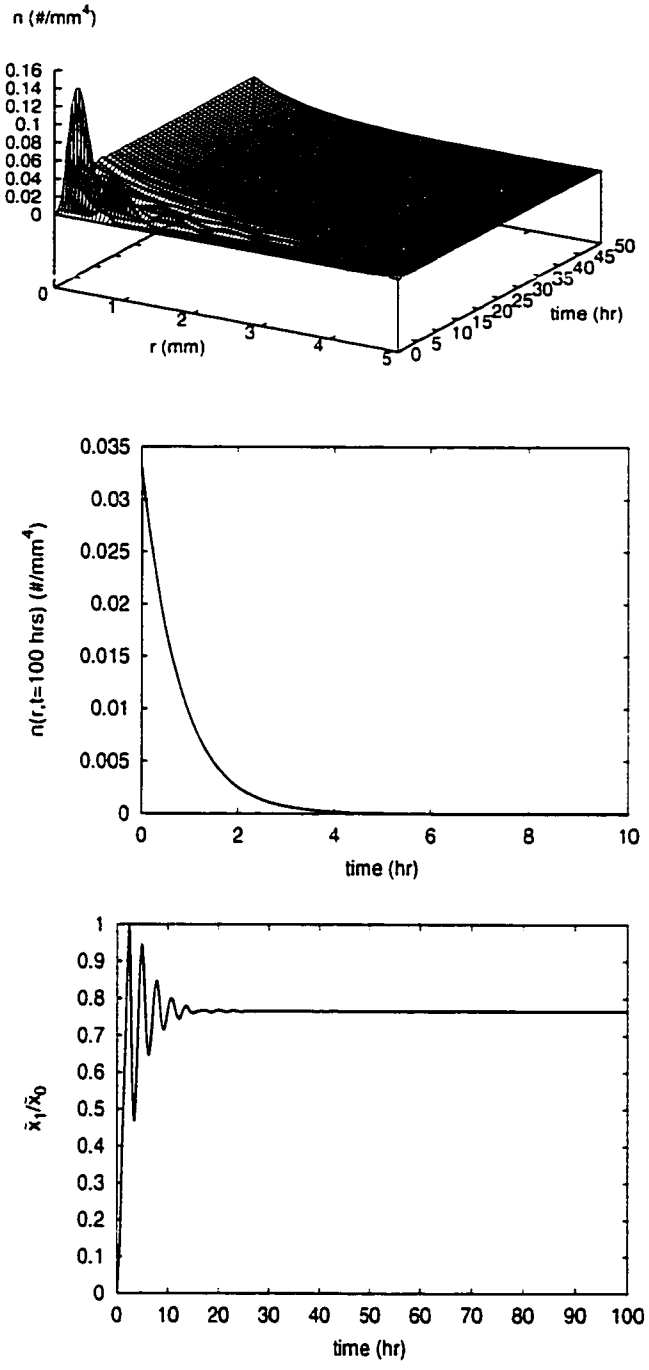

Figure 3.8: Profile of evolution of crystal size distribution (top), final steady-state crystal size distribution (middle) and evolution of mean crystal size (bottom) under nonlinear control ($\tilde{x}_1$ is the controlled output).

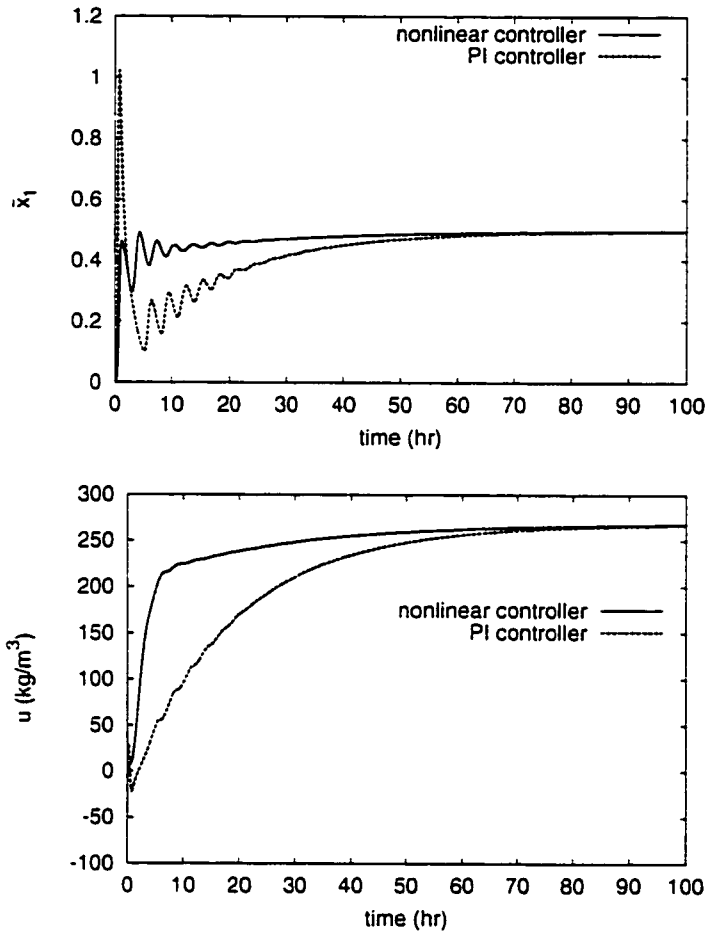

Figure 3.9: Closed-loop output (top) and manipulated input (bottom) profiles under nonlinear and PI control, for a 0.5 increase in the set-point in the presence of a 5% modeling error in both F and τ ($\tilde{x}_1$ is the controlled output).

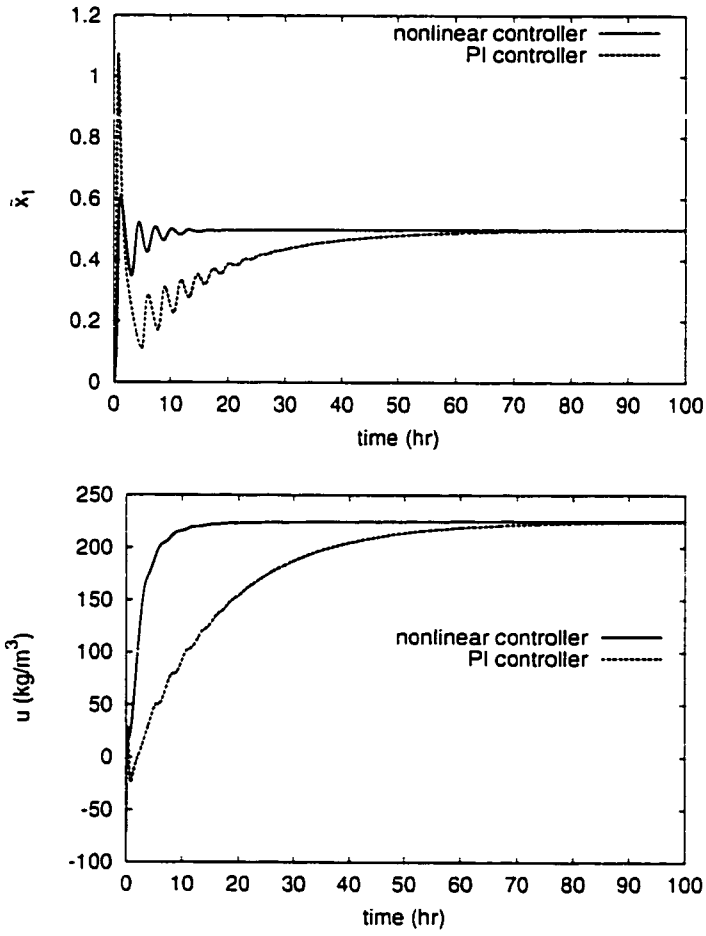

Figure 3.10: Closed-loop output (top) and manipulated input (bottom) profiles under nonlinear and PI control, for a 0.5 increase in the set-point in the presence of unmodeled actuator dynamics ($\tilde{x}_1$ is the controlled output).

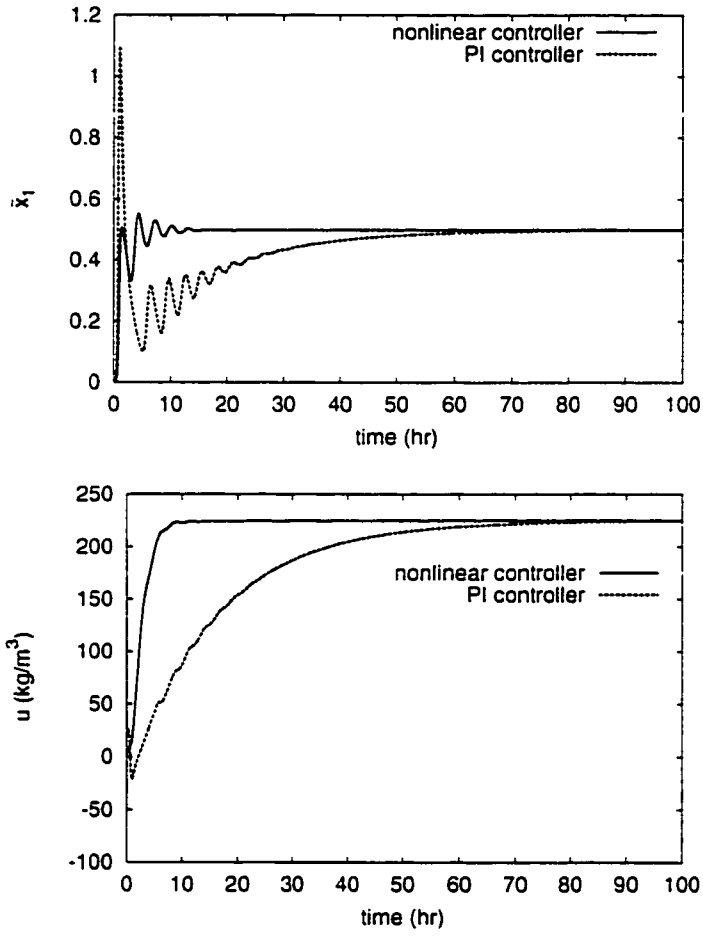

Figure 3.11: Closed-loop output (top) and manipulated input (bottom) profiles under nonlinear and PI control, for a 0.5 increase in the set-point in the presence of a 10.0-minute delay in the output measurements ($\tilde{x}_1$ is the controlled output).

Remark 3.1: We note that the fifth-order model of Eq.2.14, which was used for the design of the nonlinear output feedback controllers of Eq.3.3, was obtained by using the method of moments and no improvement of its accuracy was pursued by using approximate inertial manifolds. The reason is that the closed-loop performance and robustness properties of the controllers of Eq.3.3 are clearly excellent (see the closed-loop output profiles in Figures 3.2 and 3.7, respectively), thereby leaving no room for further improvement of the performance of the controller by using approximate inertial manifolds.

3.2 Application to a Batch Crystallizer

3.2.1 Introduction

A wide variety of high value products are produced through various classes of particulate processes, such as crystallization from solution. These processes are often carried out by batch cooling well-mixed crystallizers in the industry for low volume, high quality production.

Previous efforts on this subject have focused on open-loop optimal control of batch cooling crystallizers [41, 42, 57], and state feedback control of batch reactors [59, 60], but research on nonlinear feedback control of batch crystallizers has been very limited. The importance of controlling the shape of PSDs to ensure high quality production, together with recent advancements in technology for real-time PSD measurements, motivates the development of general nonlinear feedback control algorithms for batch crystallizers to enforce the desired set-point tracking properties in order to meet the necessary product specifications.

3.2.2 Process modeling - Control problem formulation

In this section, the control method proposed in Chapter 2 is applied to a non-isothermal batch crystallizer, shown in Figure 3.12. Using similar assumptions to

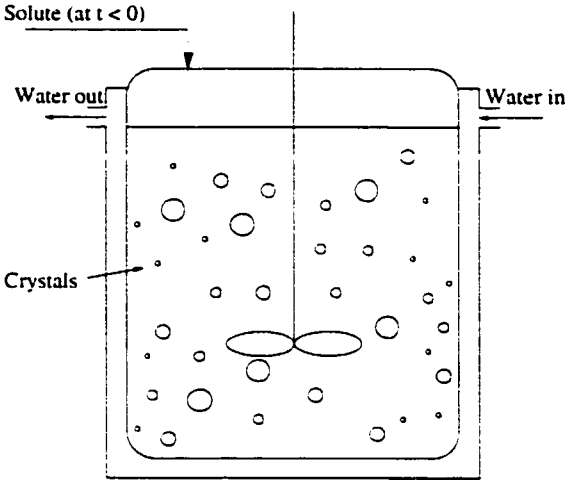

Figure 3.12: A Batch Cooling Crystallizer.

the one employed in the modeling of the continuous crystallizer in Chapter 2 (i.e., constant volume, mixed suspension, nucleation of crystals of infinitesimal size and mixed product removal), the model of the batch crystallization process takes the following form:

$$\begin{aligned} \frac{\partial n}{\partial t} &= -\frac{\partial(R(t)n)}{\partial r} + \delta(r-0)Q(t) \\ \frac{dc}{dt} &= \frac{(\rho - c)}{\bar{\epsilon}}\frac{d\bar{\epsilon}}{dt} \\ \frac{dT}{dt} &= \frac{\rho H_c}{\rho C_p}\frac{d\bar{\epsilon}}{dt} - \frac{U_c A_c}{\rho C_p V}(T - T_c) \end{aligned} \tag{3.4}$$

where $n(r,t)$ is the number of crystals of radius r at time t per unit volume of suspension, c is the solute concentration, c_0 is the solute concentration in the feed, $\bar{\epsilon} = 1 - \int_0^\infty n(r,t)\frac{4}{3}\pi r^3 dr$ is the volume of liquid per unit volume of suspension, T is the reactor temperature, H_c is the enthalpy of crystallization, C_p is the specific heat capacity, U_c is the heat transfer coefficient between the crystallizer and the cooling

water, A_c is the surface area of heat transfer between the crystallizer and the cooling water, V is the reactor volume, and T_c is the cooling water temperature. $R(t)$ is the growth rate, $\delta(r-0)$ is the standard Dirac function and $Q(t)$ is the nucleation rate. The term $\delta(r-0)Q(t)$ accounts for the production of crystals of infinitesimal (zero) size via nucleation. $R(t)$ and $Q(t)$ are goverened by the following relationships:

$$R(t) = k_1(c-c_s)e^{-\frac{E_g}{RT}}, \quad Q(t) = \bar{\epsilon}k_2 e^{-\frac{k_3}{\left(\frac{c}{c_s}-1\right)^2}} e^{-\frac{E_b}{RT}} \tag{3.5}$$

where k_1,k_2,and k_3 are constants, c_s is the concentration of solute at saturation, and E_g and E_b denote the activation energies for growth and nucleation, respectively. While k_1, k_2, k_3, E_g, E_b are taken to be constant (see Table 3.3 for their values), it is assumed that the saturation concentration, c_s, is a function of the crystallizer temperature and obeys the following relationship:

$$c_s = -3\bar{T}^2 + 38\bar{T} + 964.9 \tag{3.6}$$

where $\bar{T}$ is the dimensionless temperature defined as:

$$\bar{T} = \frac{T-273}{333-273} \tag{3.7}$$

Using the expressions of Eq.3.5, the system of Eq.3.4 can be equivalently written as:

$$\begin{aligned}
\frac{\partial n}{\partial t} &= -k_1(c-c_s)\frac{\partial n}{\partial r}e^{-\frac{E_g}{RT}} + \delta(r-0)\bar{\epsilon}k_2 e^{-\frac{k_3}{\left(\frac{c}{c_s}-1\right)^2}} e^{-\frac{E_b}{RT}} \\
\frac{dc}{dt} &= \frac{(\rho-c)}{\bar{\epsilon}}\frac{d\bar{\epsilon}}{dt} \\
\frac{dT}{dt} &= \frac{\rho H_c}{\rho C_p}\frac{d\bar{\epsilon}}{dt} - \frac{U_c A_c}{\rho C_p V}(T-T_c)
\end{aligned} \tag{3.8}$$

The control problem is formulated as the one of manipulating the deviation of the cooling water temperature ($u(t) = T_c - T_{c_s}$) to control the particle nucleation rate ($y(t) = Q$) such that a crystal size distribution with a larger average particle size

is obtained at the end of the batch run. The idea behind this particular choice of control problem is to manipulate the nucleation rate such that at the end of the batch run, the average crystal size is maximized. There are many situations in industrial applications where it is desirable to obtain large crystals for easier downstream processing. It will be shown in section 3.2.4 that by carefully controlling the nucleation rate, especially at the early stage of the batch run, it is possible to prevent an initial "burst" of infinitesimal size crystals, which results under a linear cooling input profile and dramatically reduces the average size of crystals at the end of the batch cycle.

3.2.3 Output Feedback Controller Design

In this section, we use the control method proposed in Chapter 2 to synthesize a nonlinear low-order controller for the batch crystallizer. The method of moments is initially used to derive a low-order ODE approximation of the population balance model of Eq.3.4, which will be used for controller design. Using the definition of moments in Eq.2.9, multiplying the population balance in Eq.3.4 by r^ν, and integrating over all particle sizes, the following system of infinite ODEs, which describes the rate of change of the moments of the particle size distribution, the solute concentration and temperature, is obtained:

$$\begin{aligned}
\frac{d\mu_0}{dt} &= \left(1-\frac{4}{3}\pi\mu_3\right) k_2 e^{-\frac{k_3}{\left(\frac{c}{c_s}-1\right)^2}} e^{-\frac{E_b}{RT}} \\
\frac{d\mu_\nu}{dt} &= \nu k_1 (c-c_s) e^{-\frac{E_g}{RT}} \mu_{\nu-1}, \quad \nu = 1,2,3,\ldots, \\
\frac{dc}{dt} &= \frac{-4\pi(c-c_s)\mu_2(\rho-c)}{\left(1-\frac{4}{3}\pi\mu_3\right)} \\
\frac{dT}{dt} &= -\frac{\rho_c \Delta H_c}{\rho C_p} 4\pi k_1 (c-c_s) e^{-\frac{E_g}{RT}} \mu_2 - \frac{UA_c}{\rho C_p V}(T-T_c)
\end{aligned} \tag{3.9}$$

On the basis of the system of Eq.3.9, it is clear that the moments of order four and higher do not affect those of order three and lower, which means that the dominant dynamics of the system of Eq.3.9 can be adequately captured by the following sixth-order model, which consists of the first four moment equations and the energy and solute mass balances:

$$\begin{aligned}
\frac{d\mu_0}{dt} &= \left(1-\frac{4}{3}\pi\mu_3\right) k_2 e^{-\frac{k_3}{\left(\frac{c}{c_s}-1\right)^2}} e^{-\frac{E_b}{RT}} \\
\frac{d\mu_1}{dt} &= k_1(c-c_s)e^{-\frac{E_g}{RT}}\mu_0 \\
\frac{d\mu_2}{dt} &= 2k_1(c-c_s)e^{-\frac{E_g}{RT}}\mu_1 \\
\frac{d\mu_3}{dt} &= 3k_1(c-c_s)e^{-\frac{E_g}{RT}}\mu_2 \\
\frac{dc}{dt} &= \frac{-4\pi(c-c_s)\mu_2(\rho-c)}{\left(1-\frac{4}{3}\pi\mu_3\right)} \\
\frac{dT}{dt} &= -\frac{\rho_c\Delta H_c}{\rho C_p}4\pi k_1(c-c_s)e^{-\frac{E_g}{RT}}\mu_2 - \frac{UA_c}{\rho C_p V}(T-T_c)
\end{aligned} \tag{3.10}$$

We will now employ the nonlinear control method proposed in Chapter 2 to design a nonlinear controller for the batch crystallizer. Including the specifications for the manipulated input and the controlled output in the model of Eq.3.10, one can derive

a system of the form of Eq.2.25 with $\tilde{x} = [\mu_0\ \mu_1\ \mu_2\ \mu_3\ c\ T]^T$ and:

$$\tilde{f}(\tilde{x}) = \begin{bmatrix} \left(1 - \frac{4}{3}\pi\mu_3\right) k_2 e^{-\frac{k_3}{\left(\frac{c}{c_s} - 1\right)^2}} e^{-\frac{E_b}{RT}} \\ k_1(c - c_s)e^{-\frac{E_g}{RT}}\mu_0 \\ 2k_1(c - c_s)e^{-\frac{E_g}{RT}}\mu_1 \\ 3k_1(c - c_s)e^{-\frac{E_g}{RT}}\mu_2 \\ \frac{-4\pi(c - c_s)\mu_2(\rho - c)}{\left(1 - \frac{4}{3}\pi\mu_3\right)} e^{-\frac{E_g}{RT}} \\ -\frac{\rho_c \Delta H_c}{\rho C_p} 4\pi k_1(c - c_s)e^{-\frac{E_g}{RT}}\mu_2 - \frac{UA_c}{\rho C_p V}(T - T_c) \end{bmatrix}, \quad \tilde{g}(\tilde{x}) = \begin{bmatrix} 0 \\ 0 \\ 0 \\ 0 \\ 0 \\ \frac{UA_c}{\rho C_p V} \end{bmatrix}$$

On the basis of this system, one can easily verify that assumptions 1, 2, and 3 of theorem 2.1 are satisfied. A direct application of the synthesis formula of Eq.2.39

then yields the following nonlinear output feedback controller:

$$
\begin{aligned}
\frac{d\omega_0}{dt} &= \left(1-\frac{4}{3}\pi\omega_3\right)k_2 e^{-\frac{k_3}{\left(\frac{\omega_4}{c_s}-1\right)^2}} e^{-\frac{E_b}{R\omega_5}} \\
\frac{d\omega_1}{dt} &= k_1(\omega_4-c_s)\omega_0 e^{-\frac{E_g}{R\omega_5}} + L_1(\tilde{h}(\tilde{x})-\tilde{h}(\omega)) \\
\frac{d\omega_2}{dt} &= 2k_1(\omega_4-c_s)\omega_1 e^{-\frac{E_g}{R\omega_5}} + L_2(\tilde{h}(\tilde{x})-\tilde{h}(\omega)) \\
\frac{d\omega_3}{dt} &= 3k_1(\omega_4-c_s)\omega_2 e^{-\frac{E_g}{R\omega_5}} + L_3(\tilde{h}(\tilde{x})-\tilde{h}(\omega)) \\
\frac{d\omega_4}{dt} &= \frac{-4\pi(\omega_4-c_s)\omega_2(\rho-\omega_4)}{\left(1-\frac{4}{3}\pi\omega_3\right)} e^{-\frac{E_g}{R\omega_5}} + L_4(\tilde{h}(\tilde{x})-\tilde{h}(\omega)) \\
\frac{d\omega_5}{dt} &= -\frac{\rho_c\Delta H_c}{\rho C_p}4\pi k_1(\omega_4-c_s)e^{-\frac{E_g}{R\omega_5}}\omega_2 - \frac{UA_c}{\rho C_p V}(\omega_5-T_c) + L_5(\tilde{h}(\tilde{x})-\tilde{h}(\omega)) \\
&\quad + \frac{[\beta_2 L_{\tilde{g}}L_{\tilde{f}}\tilde{h}(\omega)]^{-1}\left\{v-\beta_0\tilde{h}(\omega)-\beta_1 L_{\tilde{f}}\tilde{h}(\omega)-\beta_2 L_{\tilde{f}}^2\tilde{h}(\omega)\right\}}{1-\omega_3} \\
\bar{u}(t) &= [\beta_2 L_{\tilde{g}}L_{\tilde{f}}\tilde{h}(\omega)]^{-1}\left\{v+\beta_1\dot{v}+\beta_2\ddot{v}-\beta_0\tilde{h}(\omega)-\beta_1 L_{\tilde{f}}\tilde{h}(\omega)-\beta_2 L_{\tilde{f}}^2\tilde{h}(\omega)\right\}
\end{aligned}
\tag{3.11}
$$

where v is the set-point, β_0, β_1, β_2 and $L = [L_0\ L_1\ L_2\ L_3\ L_4]^T$ are controller parameters and $\tilde{h}(\omega) = Q(t)$.

3.2.4 Simulation Results

Several simulation runs were performed to evaluate the performance of the nonlinear controller of Eq.3.11 and compare with the ones of a linear input profile. The values of the controller parameters β_0, β_1, β_2, and L, which were used in the simulations, are given in Table 3.3. In all simulation runs, the following initial condition was used

V	=	0.01	m^3
k_1	=	5.064×10^{-2}	
k_2	=	7.957	
E_b	=	1×10^{-5}	$kJ\ mol^{-1}$
E_g	=	2200	$kJ\ mol^{-1}$
A_c	=	0.25	m^2
U	=	1800	$kJ\ m^{-2}\ hr^{-1}\ C^{-1}$
ρ_c	=	1770	$kg\ m^{-3}$
ρC_p	=	3000	$kJ\ m^{-3}\ C^{-1}$
ΔH	=	-50	$kJ\ kg^{-1}$
T_0	=	25	C
T_c	=	25	C

Table 3.3: Process parameters.

for the process model of Eq.3.4

$$n(r,0) = 0.0, c(0) = 990\ kg/m^3 \tag{3.12}$$

and the finite difference method with 1000 discretization points was used for the simulations. The initial conditions for the observer states were computed numerically by using the initial conditions of Eq.3.12. As discussed in the continuous crystallizer example, even though the number of discretization points, 1000, used to solve the system of Eq.3.4 is very large (owing to the poor convergence properties of the finite difference scheme), the computation of an accurate (that is, independent of the discretization) solution is critical for the thorough evaluation of the performance of a nonlinear feedback controller synthesized on the basis of a low-order approximation of the distributed parameter system of Eq.3.4. The adequacy of the 1000 discretization points to yield an accurate solution was established through extensive simulations of the open- and closed-loop systems.

The reference input tracking capabilities of the nonlinear controller were evaluated with a reference trajectory of the form $v(t) = 3.5623 \times 10^{-5} e^{-1.5018t}$. Figure 3.13 shows the closed-loop output (top plot) and manipulated input (bottom plot) profiles

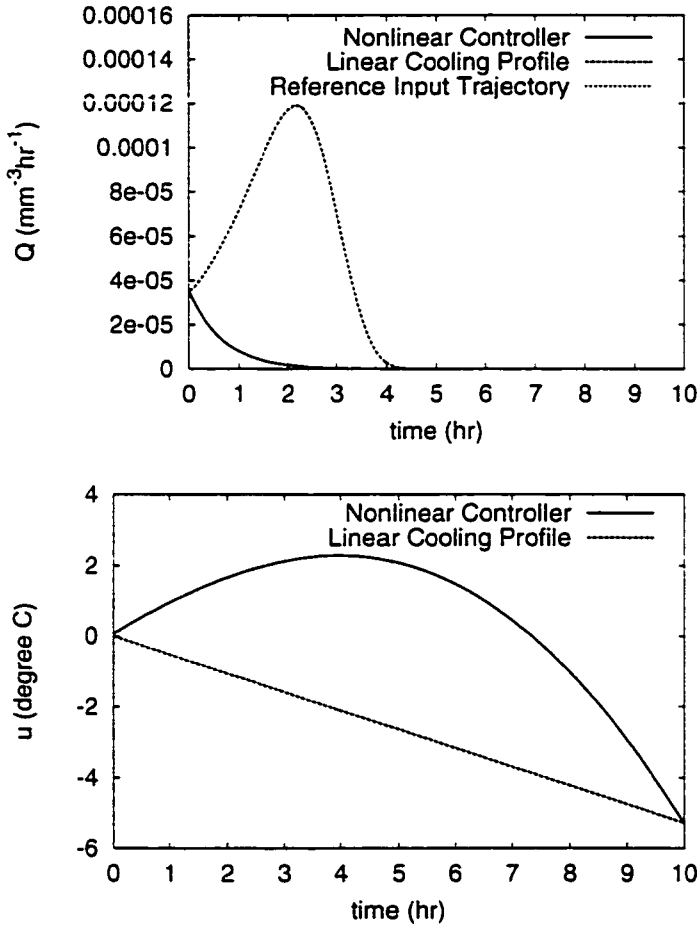

Figure 3.13: Closed-loop output (top) and manipulated input (botom) under nonlinear control and linear cooling profile.

obtained by using the nonlinear controller (solid lines) of Eq.3.11. The profiles of the nucleation rate and the reference input trajectory are shown to be almost identical. For the sake of comparison, the corresponding profiles under a linear cooling input profile of the form $u(t) = -0.528t$ are also shown in Figure 3.13. There is an initial "burst" of nucleated crystals as demonstrated by the high nucleation rate. This phenomenon affects the average particle size as can be seen in Figure 3.14. It is clear

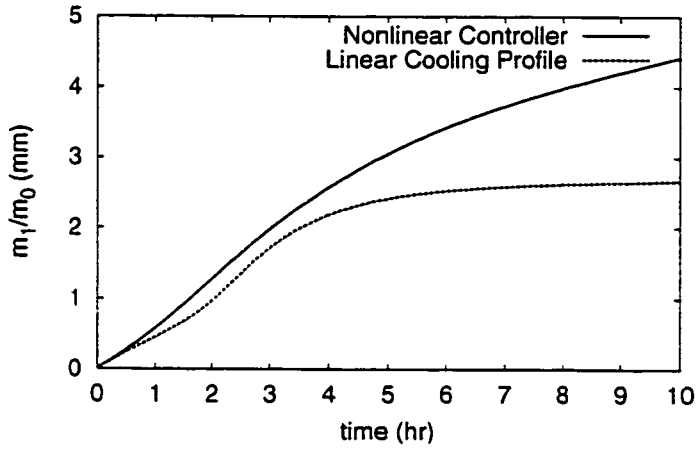

Figure 3.14: Closed-loop output under nonlinear control and linear cooling profile.

that under nonlinear control of the cooling water temperature, much larger crystals can be obtained compared to those obtained by using a linear profile for the cooling water temperature. At the end of the 10-hour run, the average crystal size under the nonlinear controller of Eq.3.11 is 4.42 mm, and under the linear cooling input profile the average crystal size is 2.67 mm. This reduction in crystal size can be attributed to the fact that high nucleation rate generates a large amount of crystals of infinitesimal size, which in turn causes a significant depletion of solute, thereby prohibiting the growth of crystals through condensation of solute molecules. Figure 3.15 shows the profile of the crystal size distribution under nonlinear control (top plot) and under the linear profile for the cooling water temperature, and the final steady-state profile

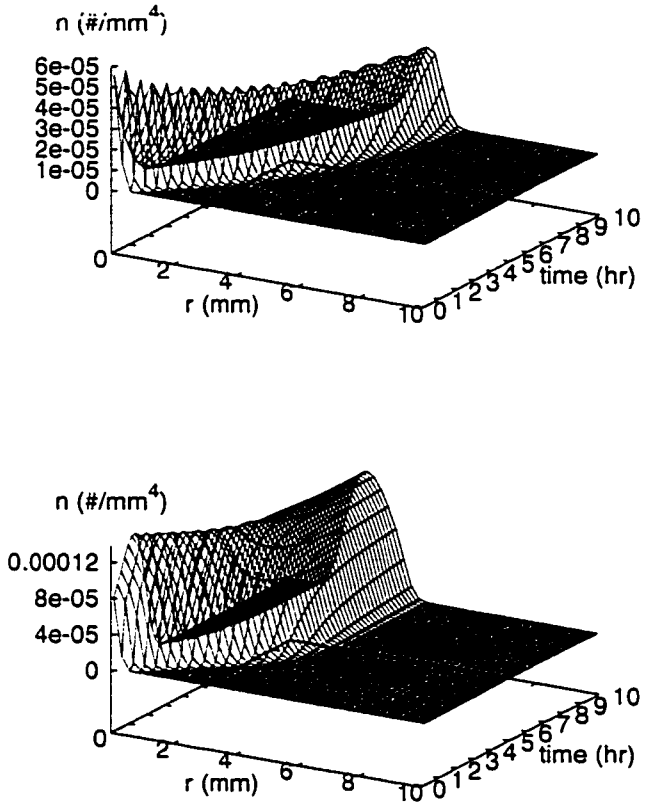

Figure 3.15: Profile of evolution of crystal size distribution under nonlinear control (top) and using a linear profile for the cooling water temperature (bottom).

profile of the crystal size distribution are shown in Figure 3.16. It is evident that

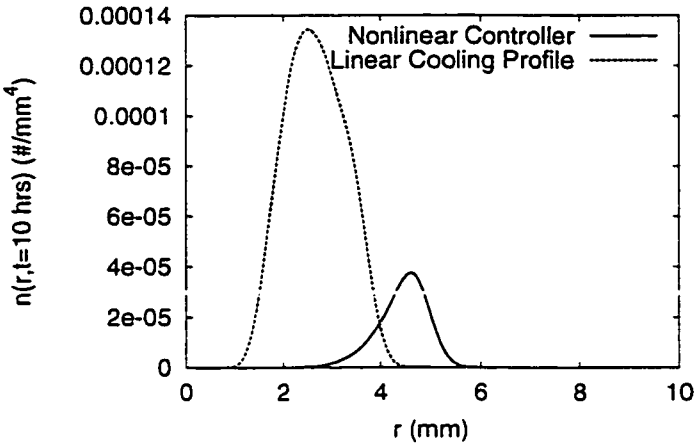

Figure 3.16: Final steady-state crystal size distribution under nonlinear control (solid line) and using a linear profile for the cooling water temperature (dashed line).

under nonlinear control, we obtain larger crystal size and smaller total number of crystals.

3.3 Conclusions

In this chapter, we applied the nonlinear control method proposed in Chapter 2 to continuous and batch crystallization systems. Low-dimensional approximations of the population balances were derived and used for nonlinear control design. The performance of the nonlinear controllers was successfully tested through simulations using the detailed population balance models and was shown to be superior to the one of linear control schemes.

Chapter 4

Robust Control of Particulate Processes using Uncertain Population Balances

4.1 Introduction

This chapter focuses on robust control of particulate processes described by uncertain population balances. The objective is to develop a general method for the synthesis of practically-implementable robust nonlinear controllers that explicitly handle time-varying uncertain variables (e.g., unknown process parameters and disturbances) and unmodeled dynamics (e.g., fast actuator and sensor dynamics not included in the process model). The robust nonlinear controllers enforce stability in the closed-loop system and attenuation of the effect of uncertain variables on the outputs, and achieve particle size distributions with desired characteristics (e.g., PSDs with desired total mass, mean particle size).

This chapter is structured as follows: After introducing the class of particulate process models considered in this work, the method of weighted residuals is used for

the construction of finite-dimensional systems that accurately reproduce the dominant dynamics of the particulate process. These ODE systems are subsequently used for the synthesis, via Lyapunov's direct method, of robust nonlinear controllers that enforce stability in the closed-loop system, attenuation of the effect of uncertain variables and achieve particle size distributions with desired characteristics. The problem of robustness with respect to unmodeled dynamics is addressed within the singular perturbation framework. It is established that the proposed robust controllers enforce the desired stability and performance specifications in the closed-loop system, provided that the unmodeled dynamics are stable and sufficiently fast. Finally, the proposed robust nonlinear control method is applied to a continuous crystallizer with fines trap, in which the nucleation rate and the crystal density change with time and the actuator and sensor dynamics are not included in the model used for the synthesis of the controller. The results of this chapter were first presented in [8, 9, 10].

4.2 Preliminaries

4.2.1 Particulate Process Model with Uncertainty

The mathematical models of particulate processes are typically obtained from an application of a population balance to the particle phase which accounts for particle growth, nucleation, agglomeration and breakage, as well as from the application of material and energy balances to the continuous phase. Uncertainty in particulate process models arises from two sources: uncertain variables (e.g., unknown process parameters and external disturbances) and unmodeled dynamics (e.g., fast actuator and sensor dynamics which are not taken into account in the process model). In order to develop a general control method for particulate processes with uncertain variables and unmodeled dynamics, we consider the following singularly perturbed system of

nonlinear partial integro-differential equations:

$$\begin{aligned}
\frac{\partial n}{\partial t} &= -\frac{\partial(G(x,r)n)}{\partial r} + \bar{w}(n,x,r,z,\theta(t)) + \bar{g}_1(n,x,r)u(t) \\
\dot{x} &= \bar{f}(x) + Q_1(x)z + \bar{g}_2(x)u(t) + \bar{g}_3(x,\theta(t),\int_0^{r_{max}} a_2(n,r,x)dr) \qquad (4.1) \\
\epsilon\dot{z} &= \tilde{f}(x) + Q_2(x)z + \tilde{g}_2(x)u(t) + \tilde{g}_3(x,\theta(t),\int_0^{r_{max}} a_2(n,r,x)dr)
\end{aligned}$$

where $n(r,t) \in L_2[0,r_{max})$ is the size distribution function, ($L_2[0,r_{max})$ is the Hilbert space of continuous functions defined on the interval $[0,r_{max})$), $r \in [0,r_{max}]$ is the particle size and r_{max} is the maximum particle size (which may be infinity), t is the time and $x \in \mathbb{R}^n$ is the vector of state variables which describe properties of the continuous phase (e.g., solute concentration, temperature and pH in a crystallizer), $u(t) = [u_1\ u_2\ \cdots\ u_m]^T \in \mathbb{R}^m$ is the vector of manipulated inputs, $\theta(t) = [\theta_1\ \theta_2\ \cdots\ \theta_q]^T \in \mathbb{R}^q$ denotes the vector of uncertain variables, $z \in \mathbb{R}^p$ is the vector of the fast (unmodeled) process dynamics, and ϵ is a small positive parameter which quantifies the speed ratio of the slow versus the fast dynamical phenomena of the process. $(G,\bar{w})$, $(\bar{g}_1,\bar{f},\bar{g}_3,\tilde{f},\tilde{g}_3,a_2)$, and $(Q_1,\bar{g}_2,Q_2,\tilde{g}_2)$ are nonlinear smooth scalar functions, vectors and matrices, respectively.

In Eq.4.1, the n-equation is the population balance where $G(x,r)$ is the growth rate and accounts for particle growth through condensation, and $w(n,x,r,z,\theta(t))$ is a term that accounts for the net rate of introduction of new particles into the system (it includes all the means by which particles appear or disappear within the system including particle agglomeration, breakage, nucleation, feed and removal). The x-subsystem of Eq.4.1 is derived by applying material and energy balances to the continuous phase, while the z-subsystem of Eq.4.1 represents the fast dynamics which are present in the process but are neglected in the model used for controller design. Finally, the terms $\bar{g}_3(x,\theta(t),\int_0^{r_{max}} a_2(n,r,x)dr)$ and $\tilde{g}_3(x,\theta(t),\int_0^{r_{max}} a_2(n,r,x)dr)$ account for mass and heat transfer from the continuous phase to all the particles in the

population.

We define a vector of controlled outputs to express the various control objectives (e.g. regulation of total number of particles, mean particle size, temperature, pH, etc.) as:

$$y_i(t) \;=\; h_i(\int_0^{r_{max}} c_\kappa(r)n(r,t)dr, x), \;\; i=1,\ldots,m, \;\; \kappa=1,\ldots,l \qquad (4.2)$$

where $y_i(t)$ is the ith controlled output, $h_i(\int_0^{r_{max}} c_\kappa(r)n(r,t)dr, x)$ is a nonlinear scalar smooth function of its arguments and $c_\kappa(r)$ is a known smooth function of r which depends on the desired performance specifications.

Throughout the paper, we will use the inner product and norm in $L_2[0, r_{max})$, which are defined, respectively, as:

$$(\phi_1, \phi_2) \;=\; \int_0^{r_{max}} \phi_1(z)\phi_2(z)dz, \quad ||\phi_1||_2 = (\phi_1, \phi_1)^{\frac{1}{2}} \qquad (4.3)$$

where ϕ_1, ϕ_2 are two elements of $L_2[0, r_{max})$. Furthermore, the order of magnitude and Lie derivative notations will be needed in our development. In particular, $\delta(\epsilon) = O(\epsilon)$ if there exist positive real numbers $\bar{k}_1$ and $\bar{k}_2$ such that: $|\delta(\epsilon)| \leq \bar{k}_1|\epsilon|$, $\forall\ |\epsilon| < \bar{k}_2$, and $L_f\bar{h}$ denotes the standard Lie derivative of a scalar function $\bar{h}(x)$ with respect to the vector function $f(x)$, $L_f^k\bar{h}$ denotes the k-th order Lie derivative and $L_gL_f^{k-1}\bar{h}$ denotes the mixed Lie derivative where $g(x)$ is a vector function.

Remark 4.1: Referring to the general mathematical model of Eq.4.1, the following remarks are in order: a) the particle size distribution function, $n(r,t)$, is assumed to be a sufficiently smooth function of its arguments (i.e., $n(r,t)$ and its partial derivatives with respect to r and t, up to a desired order, are continuous functions); this is a reasonable assumption for large size distributions even though particles are discrete and their number is integer-valued, b) a single internal particle coordinate (particle size) is considered; this is motivated by the majority of industrial particulate process

control problems where the central objective is to produce particulates with a desired particle size distribution, c) the particles are assumed to be small enough so that the environment, in which they are dispersed, can be adequately described by a local value of its state vector, d) we do not consider measured outputs separately from controlled outputs, and thus, we assume that measurements of the $y_i(t)$ are available, and e) the vector of uncertain variables, $\theta(t)$, and the vector of manipulated inputs, $u(t)$, appear in all the equations of the model.

Remark 4.2: The derivation of a singularly perturbed representation of a nonlinear process that exhibits two-time-scale behavior is, in general, a highly nontrivial task. The natural approach to address this problem involves defining the singular perturbation parameter ϵ, taking into account the physicochemical characteristics of the process, so that in the resulting singularly perturbed representation the separation of the fast and slow variables is consistent with the process dynamic behavior. This approach works for the majority of two-time-scale processes (see for example the applications considered in [48]). Whenever this approach does not work alternative approaches that utilize explicit coordinate changes (e.g., [48, 50]) may be employed to derive a singularly perturbed representation of a two-time-scale process. Referring to the specific singularly perturbed system of Eq.4.1, we note that the parameter ϵ appears only in the left-hand side (multiplying the time-derivative $\dot{z}$), while the fast variable z enters in an affine fashion. The first assumption is made for notational simplicity and can be readily relaxed, while the second assumption is consistent with the fact that in many physical and chemical processes the main nonlinearities are associated with the slow dynamics.

4.2.2 Two-time-scale Analysis

The central idea of the two-time-scale analysis is to infer the stability properties of and synthesize well-conditioned nonlinear controllers for the singularly perturbed system of Eq.4.1 based on ϵ-independent models that describe the slow and fast dynamics of this system in the slow and fast time-scale, respectively. Setting $\epsilon = 0$ in the system of Eq.4.1 and assuming that $Q_2(x,\theta)$ is invertible uniformly in $x \in \mathbb{R}^n$, $\theta \in \mathbb{R}^q$, the following system which describes the slow dynamics of the system of Eq.4.1 (called slow subsystem) is obtained:

$$\begin{aligned} \frac{\partial n}{\partial t} &= -\frac{\partial (G(x,r)n)}{\partial r} + w(n,x,r,\theta(t)) + g_1(n,x,r)u(t), \quad n(0,t) = b(x(t)) \\ \dot{x} &= f(x) + g_2(x)u(t) + g_3(x,\theta(t),\int_0^{r_{max}} a_2(n,r,x)dr) \end{aligned} \tag{4.4}$$

where f, a_2, g_1, g_3, g_2 are nonlinear functions whose explicit form is omitted for brevity. The system which describes the fast dynamics of the system of Eq.4.1 (called fast subsystem) can be obtained by defining the fast time-scale $\tau = \frac{t}{\epsilon}$, deriving the representation of the system of Eq.4.1 in the τ time scale and setting $\epsilon = 0$, and is of the form:

$$\frac{dz}{d\tau} = \tilde{f}(x) + Q_2(x)z + \tilde{g}_2(x)u(t) + \tilde{g}_3(x,\theta(t),\int_0^{r_{max}} a_2(n,r,x)dr) \tag{4.5}$$

where x and n can be considered equal to their initial values $x(0)$ and $n(r,0)$, and θ can be viewed as constant. To simplify the development of the theoretical results of the manuscript, we consider systems of the form of Eq.4.1, for which the corresponding fast subsystem of the form of Eq.4.5 is globally asymptotically stable (i.e., the eigenvalues of the matrix $Q_2(x)$ lie in the left half of the complex plane uniformly in $x \in \mathbb{R}^n$).

Remark 4.3: Whenever the open-loop fast subsystem of Eq.4.1 is unstable (i.e., one of the eigenvalues of the matrix $Q_2(x)$ lies in the right-half of the complex plane) and

the pair $[Q_2\ \tilde{g}_2]$ is stabilizable, a preliminary state feedback law of the form:

$$u = k^T(x)z + \tilde{u} \tag{4.6}$$

where $\tilde{u}$ is an auxiliary input, can be used to stabilize the fast dynamics, thereby yielding a two-time-scale system with stable fast dynamics. The design of the gain $k^T(x)$ can be performed by using standard optimal control methods [48].

4.3 Robust Nonlinear Control of Particulate Processes

The objective of this section is to synthesize robust nonlinear controllers for particulate processes of the form of Eq.4.4 that enforce stability and robust output tracking in the closed-loop system. Owing to the fact that the unmodeled dynamics in the model of Eq.4.1 are stable, the controllers will be synthesized on the basis of the model of Eq.4.4. Since this model is infinite-dimensional, we will initially use the method of weighted residuals to derive an ODE approximation of the system of Eq.4.4 which will be used for the synthesis of the robust nonlinear controllers.

4.3.1 Model Reduction

We initially use the method of weighted residuals to derive a nonlinear set of ODEs that accurately reproduces the solutions and the dominant dynamics of the distributed parameter system of Eq.4.4. The central idea of the method of weighted residuals is to approximate the exact solution of $n(r,t)$ by an infinite series of orthogonal basis functions defined in the interval $[0, r_{max})$ with time-varying coefficients, substitute the series expansion into Eq.4.4, and then take the inner product with respect to a complete set of weighted functions, to compute a set of ODEs which describes the rate of change of the time-varying coefficients of the series expansion of the solution.

Specifically, we expand the solution of $n(r,t)$ in an infinite series in terms of an orthogonal and complete set of basis functions, $\phi_k(r)$, where $r \in [0, r_{max})$, $k = 1, \ldots, \infty$, as follows:

$$n(r,t) = \sum_{k=1}^{\infty} a_k(t)\phi_k(r) \tag{4.7}$$

where $a_k(t)$ are time-varying coefficients. Substituting the above expansion into the particulate process model of Eq.4.4, we obtain:

$$\begin{aligned}
\sum_{k=1}^{\infty}\phi_k(r)\frac{\partial a_k(t)}{\partial t} &= -\sum_{k=1}^{\infty}a_k(t)\frac{\partial(G(x,r)\phi_k(r))}{\partial r} + w(\sum_{k=1}^{\infty}a_k(t)\phi_k(r), x, r, \theta(t)) \\
&\quad + g_1(\sum_{k=1}^{\infty}a_k(t)\phi_k(r), x, r)u(t) \\
\dot{x} &= f(x) + g_2(x)u(t) + g_3(x, \theta(t), \int_0^{r_{max}} a_2(\sum_{k=1}^{\infty}a_k(t)\phi_k(r), r, x)dr)
\end{aligned} \tag{4.8}$$

Multiplying the population balance with the weighting functions, $\psi_\nu(r)$, and integrating over the entire particle size spectrum (i.e., taking inner product in $L_2[0, r_{max})$ with the weighting functions), the following set of infinite ODEs is obtained:

$$\begin{aligned}
\int_0^{r_{max}}\psi_\nu(r)\sum_{k=1}^{\infty}\phi_k(r)\frac{\partial a_k(t)}{\partial t}dr &= -\sum_{k=1}^{\infty}a_k(t)\int_0^{r_{max}}\psi_\nu(r)\frac{\partial(G(x,r)\phi_k(r))}{\partial r}dr \\
&\quad + \int_0^{r_{max}}\psi_\nu(r)w(\sum_{k=1}^{\infty}a_k(t)\phi_k(r), x, r, \theta(t))dr \\
&\quad + \int_0^{r_{max}}\psi_\nu(r)g_1(\sum_{k=1}^{\infty}a_k(t)\phi_k(r), x, r)u(t)dr, \\
&\quad \nu = 1, \ldots, \infty \\
\dot{x} &= f(x) + g_2(x)u(t) \\
&\quad + g_3(x, \theta(t), \int_0^{r_{max}} a_2(\sum_{k=1}^{\infty}a_k(t)\phi_k(r), r, x)dr)
\end{aligned} \tag{4.9}$$

Eq.4.9 is an infinite set of ODEs which describe the rate of change of the time varying coefficients, $a_k(t)$, where $k = 1, \ldots, \infty$, of the series expansion of the solution. An

accurate approximation of Eq.4.9 is obtained by truncating the series expansion of $n(r,t)$ up to order N and keeping the first N equations (i.e., $\nu = 1,\ldots,N$). The infinite-dimensional system of Eq.4.9 reduces to the following finite set of ODEs:

$$\begin{aligned}
\int_0^{r_{max}} \psi_\nu(r) \sum_{k=1}^{N} \phi_k(r) \frac{\partial a_{kN}(t)}{\partial t} dr &= -\sum_{k=1}^{N} a_{kN}(t) \int_0^{r_{max}} \psi_\nu(r) \frac{\partial (G(x_N,r)\phi_k(r))}{\partial r} dr \\
&\quad + \int_0^{r_{max}} \psi_\nu(r) w(\sum_{k=1}^{N} a_{kN}(t)\phi_k(r), x_N, r, \theta(t)) dr \\
&\quad + \int_0^{r_{max}} \psi_\nu(r) g_1(\sum_{k=1}^{N} a_{kN}(t)\phi_k(r), x_N, r) u(t) dr, \\
&\quad \nu = 1,\ldots,N \\
\dot{x}_N &= f(x_N) + g_2(x_N)u(t) \\
&\quad + g_3(x_N, \theta(t), \int_0^{r_{max}} a_2(\sum_{k=1}^{N} a_{kN}(t)\phi_k(r), r, x_N) dr)
\end{aligned} \tag{4.10}$$

where x_N and a_{kN} are the approximations of x and a_k obtained by an N-th order truncation. Introducing the vector notation $a_N = [a_{1N} \cdots a_{NN}]$, and after some rearrangements, Eq.4.10 can be represented in the following general form:

$$\begin{aligned}
\dot{a}_N &= \bar{f}(a_N, x_N, \theta(t)) + \bar{g}(a_N, x_N) u(t) \\
\dot{x}_N &= f(x_N) + g_2(x_N)u(t) + g_3(x_N, a_N, \theta(t))
\end{aligned} \tag{4.11}$$

where the explicit expressions of $\bar{f}(a_N, x_N, \theta(t))$ and $\bar{g}(a_N, x_N)$ are omitted for brevity. Setting $\tilde{x} = [a_N^T \; x_N^T]^T$, we obtain the following system:

$$\begin{aligned}
\dot{\tilde{x}} &= \tilde{f}(\tilde{x}) + \sum_{i=1}^{m} \tilde{g}_i(\tilde{x}) u_i + \tilde{w}(\tilde{x}, \theta) \\
y_{si} &= \tilde{h}_i(\tilde{x}), \;\; i = 1,\ldots,m
\end{aligned} \tag{4.12}$$

where $\tilde{f}(\tilde{x}), \tilde{g}_i(\tilde{x}), \tilde{w}(\tilde{x}, \theta)$ are nonlinear vector functions whose explicit form is omitted brevity.

Remark 4.4: In the series expansion of Eq.4.7, the basis, $\{\phi_k\}$, $j = 1,\ldots,\infty$, of $L_2[0, r_{max})$ can be chosen from standard basis functions sets (for example, when

$r_{max} = \infty$, $\{\phi_k\}$ can be chosen to be Laguerre polynomials; see the crystallization example of section 4 for details on this issue), or it can be computed by applying Karhunen-Loève expansion on an appropriately chosen ensemble of solutions of the system of Eq.4.4 (see [36] for details on Karhunen-Loève expansion).

Remark 4.5: The method of weighted residuals reduces to the method of moments when the basis functions are chosen to be Laguerre polynomials and the weighting functions are chosen as $\psi_\nu = r^\nu$. The moments of the particle size distribution are defined as:

$$\mu_\nu = \int_0^\infty r^\nu n(r,t)dr, \quad \nu = 0, \ldots, \infty \tag{4.13}$$

and the moment equations can be directly generated from the population balance model by multiplying it by r^ν, $\nu = 0, \ldots, \infty$ and integrating from 0 to ∞. The procedure of forming moments of the population balance equation very often leads to terms that may not reduce to moments, terms that include fractional moments or to an unclosed set of moment equations. To overcome this problem, the particle size distribution is expanded in terms of Laguerre polynomials defined in $L_2[0, \infty)$ and the series solution is used to close the set of moment equations.

Remark 4.6: When an arbitrary set of basis functions is used in the expansion of Eq.4.7, the ODE system of Eq.4.11 may be of very high order in order to accurately describe the dominant dynamics of the system of Eq.4.4, and therefore, to be suitable for the synthesis of a high-performance nonlinear controller. Unfortunately, high dimensionality of the system of Eq.4.11 leads to complex design and high-order controllers, which cannot be readily implemented in practice. An approach to overcome this problem is to reduce the dimension of the system of Eq.4.11 utilizing the concept of approximate inertial manifold for particulate process models proposed in [7].

4.3.2 Robust Nonlinear Controller Design

The objective of this section is to use the ODE system of Eq.4.12 to synthesize robust state feedback controllers of the form:

$$u = p(\tilde{x}) + Q(\tilde{x})\bar{v} + r(\tilde{x}, t) \tag{4.14}$$

where $p(\tilde{x})$, $r(\tilde{x}, t)$ are vector functions, $Q(\tilde{x})$ is a matrix, and $\bar{v}$ is a vector of the form $\bar{v} = \mathcal{V}(v_i, v_i^{(1)}, \ldots, v_i^{(r_i)})$ where $\mathcal{V}(v_i, v_i^{(1)}, \ldots, v_i^{(r_i)})$ is a smooth vector function, $v_i^{(k)}$ is the k^{th} time derivative of the external reference input v_i (which is assumed to be a smooth function of time) and r_i is a positive integer, that enforce boundedness of the states and output tracking with arbitrary degree of asymptotic attenuation of the effect of the uncertainty on the output, in the closed-loop system, provided that ϵ is sufficiently small (i.e., the unmodeled dynamics are sufficiently fast). The control law of Eq.4.14 comprises of the component $p(\tilde{x}) + Q(\tilde{x})\bar{v}$, which is responsible for the output tracking and stabilization of the closed-loop slow system, and the component $r(\tilde{x}, t)$ which is responsible for the asymptotic attenuation of the effect of the uncertain variables on the outputs of the system of Eq.4.12. The control law of Eq.4.14 will be synthesized constructively using Lyapunov's direct method, and assuming the existence of known bounding functions that capture the magnitude of the uncertain terms and that certain structural conditions on the way the uncertain variables affect the output are satisfied. Finally, the reader may refer to remark 4.6 below for results on the implementation of a control law of the form of Eq.4.14 with a state observer, when measurements of the states of the system of Eq.4.1 are not available.

In order to develop a solution to the above robust control problem, we will need to impose the following three assumptions on the system of Eq.4.12. We initially assume that there exists a coordinate transformation that renders the system of Eq.4.12

partially linear. This assumption is motivated by the requirement of robust output tracking and is precisely formulated below:

Assumption 4.1 : *Referring to the system of Eq.4.12, there exist a set of integers* $(r_1, r_2, \ldots, r_m)$ *and a coordinate transformation* $(\zeta, \eta) = T(x_s, \theta)$ *such that the representation of the system, in the coordinates* (ζ, η)*, takes the form:*

$$
\begin{aligned}
\dot{\zeta}_1^{(1)} &= \zeta_2^{(1)} \\
&\vdots \\
\dot{\zeta}_{r_1-1}^{(1)} &= \zeta_{r_1}^{(1)} \\
\dot{\zeta}_{r_1}^{(1)} &= L_{\tilde{f}}^{r_1}\tilde{h}_1(\tilde{x}) + \sum_{i=1}^{m} L_{\tilde{g}_i} L_{\tilde{f}}^{r_1-1}\tilde{h}_1(\tilde{x})u_i \; + L_{\tilde{w}} L_{\tilde{f}}^{r_1-1}\tilde{h}_1(\tilde{x}) \\
&\vdots \\
\dot{\zeta}_1^{(m)} &= \zeta_2^{(m)} \\
&\vdots \\
\dot{\zeta}_{r_m-1}^{(m)} &= \zeta_{r_m}^{(l)} \\
\dot{\zeta}_{r_m}^{(m)} &= L_{\tilde{f}}^{r_m}\tilde{h}_m(\tilde{x}) + \sum_{i=1}^{m} L_{\tilde{g}_i} L_{\tilde{f}}^{r_m-1}\tilde{h}_m(\tilde{x})u_i + L_{\tilde{w}} L_{\tilde{f}}^{r_m-1}\tilde{h}_m(\tilde{x}) \\
\dot{\eta}_1 &= \Psi_1(\zeta, \eta, \theta, \dot{\theta}) \\
&\vdots \\
\dot{\eta}_{(n+N)-\sum_i r_i} &= \Psi_{(n+N)-\sum_i r_i}(\zeta, \eta, \theta, \dot{\theta}) \\
y_{si} &= \zeta_1^{(i)}, \;\; i = 1, \ldots, m
\end{aligned}
\tag{4.15}
$$

where $x_s = T^{-1}(\zeta, \eta, \theta)$, $\zeta = [\zeta^{(1)} \; \cdots \; \zeta^{(m)}]^T \in \mathbb{R}^{\sum_i r_i}$, $\eta = [\eta_1 \; \cdots \; \eta_{(n+N)-\sum_i r_i}]^T \in \mathbb{R}^{(n+N)-\sum_i r_i}$.

Assumption 4.1 includes the matching condition of our robust control methodology. In particular, we consider systems of the form Eq.4.12 for which the time-derivatives of the output y_{si} up to order $r_i - 1$ are independent of the vector of uncertain variables θ. Notice that this condition is different than the standard one which restricts the uncertainty vector θ to enter the system of Eq.4.12 in the same equation with the manipulated input u. The motivation for considering this matching condition is given

by the fact that it is satisfied by a large number of practical applications (note that assumption 4.1 is always satisfied for systems for which $r_i = 1$, for all $i = 1, \ldots, m$.)

Referring to the system of Eq.4.12, we will assume, in order to simplify the presentation of our results, that the matrix:

$$C(\tilde{x}) = \begin{bmatrix} L_{\tilde{g}_1} L_{\tilde{f}}^{r_1 - 1} \tilde{h}_1(\tilde{x}) & \cdots & L_{\tilde{g}_m} L_{\tilde{f}}^{r_1 - 1} \tilde{h}_1(\tilde{x}) \\ \vdots & \cdots & \vdots \\ L_{\tilde{g}_1} L_{\tilde{f}}^{r_m - 1} \tilde{h}_m(\tilde{x}) & \cdots & L_{\tilde{g}_m} L_{\tilde{f}}^{r_m - 1} \tilde{h}_m(\tilde{x}) \end{bmatrix} \tag{4.16}$$

is nonsingular uniformly in $\tilde{x}$. This assumption can be readily relaxed if robust dynamic state feedback, instead of robust state feedback, is used to solve the control problem (see [39] for details).

The next assumption is made to ensure bounded stability of the internal dynamics of the system of Eq.4.12 under a robust state feedback controller of the form of Eq.4.12.

Assumption 4.2: *The dynamical system:*

$$\begin{aligned} \dot{\eta}_1 &= \Psi_1(\zeta, 0, 0, 0) \\ &\vdots \\ \dot{\eta}_{(n+N)-\sum_i r_i} &= \Psi_{(n+N)-\sum_i r_i}(\zeta, 0, 0, 0) \end{aligned} \tag{4.17}$$

is locally exponentially stable.

Finally, we need to assume that there exist a nonlinear time-varying function that captures the size of the uncertain term $[L_{\tilde{w}} L_{\tilde{f}}^{r_1 - 1} \tilde{h}_1(\tilde{x}) \cdots L_{\tilde{w}} L_{\tilde{f}}^{r_m - 1} \tilde{h}_m(\tilde{x})]$. Information of this kind may result from physical considerations, preliminary simulations, experimental data, etc.

Assumption 4.3: *There exists a known function $c(\tilde{x}, t)$ such that the following condition holds:*

$$|[L_{\tilde{w}} L_{\tilde{f}}^{r_1 - 1} \tilde{h}_1(\tilde{x}) \cdots L_{\tilde{w}} L_{\tilde{f}}^{r_m - 1} \tilde{h}_m(\tilde{x})]^T| \leq c(\tilde{x}, t) \tag{4.18}$$

for all $\tilde{x} \in \mathbb{R}^{n+N}$, $\theta \in \mathbb{R}^q$, $t \geq 0$.

Theorem 4.1 that follows provides an explicit formula for the robust controller, conditions that ensure boundedness of the state, and a precise characterization of the ultimate uncertainty attenuation level. To simplify the statement of the theorem, we set $\bar{v}_i = [v_i \; v_i^{(1)} \; \cdots \; v_i^{(r_i)}]^T$ and $\tilde{v} = [\bar{v}_1^T \; \bar{v}_2^T \; \cdots \; \bar{v}_m^T]^T$.

Theorem 4.1: *Suppose that assumptions 4.1, 4.2, and 4.3 hold, and consider the system of Eq.4.1 under the robust state feedback controller:*

$$\begin{aligned} u = a(\tilde{x}, \bar{v}, t) \;\; := \;\; & [C(\tilde{x})]^{-1} \Bigg\{ \sum_{i=1}^{m} \sum_{k=1}^{r_i} \frac{\beta_{ik}}{\beta_{ir_i}} (v_i^{(k)} - L_{\tilde{f}}^k \tilde{h}_i(\tilde{x})) \\ & + \sum_{i=1}^{m} \sum_{k=1}^{r_i} \frac{\beta_{ik}}{\beta_{ir_i}} (v_i^{(k-1)} - L_{\tilde{f}}^{k-1} \tilde{h}_i(\tilde{x})) \\ & - \chi[c(\tilde{x}, t)] \frac{\sum_{i=1}^{l} \sum_{k=1}^{r_i} \frac{\beta_{ik}}{\beta_{ir_i}} (L_{\tilde{f}}^{k-1} \tilde{h}_i(\tilde{x}) - v_i^{(k-1)})}{|\sum_{i=1}^{l} \sum_{k=1}^{r_i} \frac{\beta_{ik}}{\beta_{ir_i}} (L_{\tilde{f}}^{k-1} \tilde{h}_i(\tilde{x}) - v_i^{(k-1)})| + \phi} \Bigg\} \end{aligned} \tag{4.19}$$

where $\frac{\beta_{ik}}{\beta_{ir_i}} = [\frac{\beta_{ik}^1}{\beta_{ir_i}^1} \; \cdots \; \frac{\beta_{ik}^l}{\beta_{ir_i}^l}]^T$ *are column vectors of parameters chosen so that the roots of the equation* $det(B(s)) = 0$, *where* $B(s)$ *is an* $m \times m$ *matrix, whose* (i,j)*-th element is of the form* $\sum_{k=1}^{r_i} \frac{\beta_{jk}^i}{\beta_{jr_i}^i} s^{k-1}$, *lie in the open left-half of the complex plane, and* χ, ϕ *are adjustable parameters with* $\chi > 1$ *and* $\phi > 0$. *Then, there exist positive real numbers* (δ, ϕ^*, d) *such that for each* $\phi \leq \phi^*$, *there exists* $\epsilon^*(\phi)$, *such that if* $\phi \leq \phi^*$, $\epsilon \leq \epsilon^*(\phi)$ *and* $\max\{|x(0)|, |z(0)|, ||\eta(r,0)||_2, ||\theta||, ||\dot{\theta}||, ||\tilde{v}||\} \leq \delta$,

a) the state of the infinite-dimensional closed-loop system is bounded, and

b) the outputs of the infinite-dimensional closed-loop system satisfy:

$$\limsup_{t \to \infty} |y_i - v_i| \leq d, \;\; i = 1, \ldots, l \tag{4.20}$$

Remark 4.7: Regarding the practical application of Theorem 4.1, one has to initially use the method of weighted residuals to derive an ODE system of the form of Eq.4.12,

and then verify assumptions 4.1, 4.2 and 4.3 on the basis of this system. Then, the synthesis formula of Eq.4.19 can be directly used to derive the explicit form of the controller. Moreover, the value of ϵ in the model of Eq.4.1 is typically fixed by the process, say ϵ_p, and thus there is a limit on how small the ultimate bound d can be chosen. For example, one can initially compute, through simulations, a ϕ^* from the desired (δ, d) and, in turn, the value ϵ^* for $\phi \leq \phi^*$. If this ϵ^* is less than ϵ_p, then d may need to be readjusted (increased) so that $\epsilon^* \geq \epsilon_p$. Of course, if ϵ_p is too large, there may be no value of d that works.

Remark 4.8: Referring to the robust nonlinear controller of Eq.4.19, we note that the nonlinear term $-\chi[c(\tilde{x}, t)]$ could have been replaced by a sufficiently large positive constant k. Although this modification would lead to a simplification in the practical implementation of the controller, we select to use the nonlinear term, because the use of a large positive constant results in a controller that computes very large control action, when the discrepancy between y and v (tracking error) is far from being zero. The controller that uses the nonlinear term avoids this problem and does not compute unnecessarily large control action (see the manipulated input profiles for the crystallizer example presented in section 4.4).

Remark 4.9: The on-line implementation of the controller of Eq.4.19 requires that the values of the state variables $\tilde{x}$ are known. Unfortunately, $\tilde{x}$ may not be known in many practical applications. One way to address this problem is to use a nonlinear state observer of the form:

$$\frac{d\omega}{dt} = \tilde{f}(\omega) + \tilde{g}(\omega)u + \tilde{w}(\omega)\theta_n + L(y - \tilde{h}(\omega)) \tag{4.21}$$

where ω denotes the observer state vector (the dimension of the vector ω is equal to the dimension of $\tilde{x}$ in the system of Eq.4.12), $y = [y_1\ y_2\ \cdots y_m]^T$ is the measured

output vector, θ_n denotes a nominal value for $\theta(t)$ and L is a matrix chosen so that the eigenvalues of the matrix $C_L = \frac{\partial \tilde{f}}{\partial \omega}_{(\omega=\omega_s)} - L\frac{\partial \tilde{h}}{\partial \omega}_{(\omega=\omega_s)}$, where ω_s is the operating steady-state, lie in the open left-half of the complex plane, to estimate $\tilde{x}$ from measurements of the controlled outputs y_i. The state observer of Eq.4.21 consists of a replica of the system of Eq.4.12 plus a linear gain multiplying the discrepancy between the actual and the estimated value of the output, and therefore, it is an extended Luenberger-type observer. It can be shown that the bounded stability of the closed-loop system resulting from the application of a robust output feedback controller (resulting from the combination of the controller of Eq.4.19 with the observer of Eq.4.21) to the particulate process model is guaranteed, provided that there exists a matrix L such that $C_L = \frac{1}{\mu}\bar{A}$ where μ is a sufficiently small positive parameter and $\bar{A}$ is a Hurwitz matrix. The reader may refer to the crystallization example of section 4 for an application of this approach for state estimation.

Remark 4.10: We note that the validity of the approach which we followed here to synthesize the nonlinear robust controller of Eq.4.19 relies on the large separation of slow and fast modes of the particulate process model of Eq.4.4. Despite the fact that the model of Eq.4.22 consists of a first-order hyperbolic PDE (population balance) coupled with a nonlinear integro-differential equation (solute mass balance), the approach followed here for the synthesis of robust feedback controllers is not applicable to hyperbolic PDE systems arising in the context of convection-reaction processes. More specifically, the dominant dynamic behavior of the system of Eq.4.1 is characterized by a small number of degrees of freedom (and thus, it can be described by low-order ODE systems which can be used for controller synthesis), while first-order hyperbolic PDE systems involve spatial differential operators whose eigenvalues cluster along vertical or nearly vertical asymptotes in the complex plane and thus, the

controller synthesis problem has to be addressed directly on the basis of the hyperbolic PDE system (see [19]).

4.4 Application to a Continuous Crystallizer with Fines Trap

In this section, we apply the proposed robust control methodology to a continuous crystallizer with fines trap shown in Figure 4.1. The trap is used to remove small

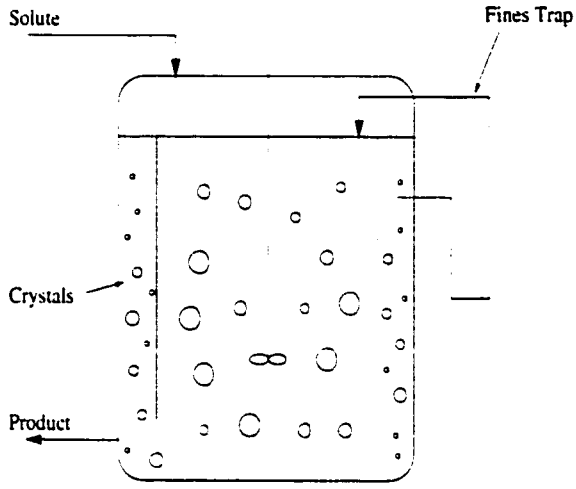

Figure 4.1: A continuous crystallizer with fines trap.

crystals and increase the mean crystal size. In a crystallizer, the precise regulation of the shape of the crystal size distribution is important because the CSD influences significantly the necessary liquid-solid separation and the properties of the product. Therefore, crystallization requires a population balance in order to be accurately described, analyzed and controlled. Under the standard assumptions of constant volume, mixed suspension, mixed product removal and nucleation of crystals of infinitesimal size, application of a population balance to the particulate phase and a mass balance to the continuous phase results in the following dynamic model for the

crystallizer [56]:

$$\begin{aligned} \frac{\partial n}{\partial \bar{t}} &= -\frac{\partial (R(\bar{t})n)}{\partial r} - \frac{n}{\tau} - \bar{h}(r)\frac{n}{\tilde{\tau}} + \delta(r-0)Q(\bar{t}) \\ \frac{dc}{d\bar{t}} &= \frac{(c_0-\rho)}{\bar{\epsilon}\tau} + \frac{(\rho-c)}{\tau} + \frac{(\rho-c)}{\bar{\epsilon}}\frac{d\bar{\epsilon}}{d\bar{t}} \end{aligned} \tag{4.22}$$

where $n(r,\bar{t})$ is the number of crystals of radius $r \in [0,\infty)$ at time $\bar{t}$ per unit volume of suspension, τ is the residence time, c is the solute concentration in the crystallizer, c_0 is the solute concentration in the feed, $\bar{\varepsilon} = 1 - \int_0^\infty n(r,\bar{t})\frac{4}{3}\pi r^3 dr$ is the volume of liquid per unit volume of suspension, $R(\bar{t})$ is the growth rate, $\delta(r-0)$ is the standard Dirac function and $Q(\bar{t})$ is the nucleation rate. $1/\tilde{\tau} = F_0/V$ is the rate at which crystals are circulated through the fines trap (F_0 is the fines recirculation rate and V is the active volume of the crystallizer which is assumed to be constant) and $\bar{h}(r)$ expresses the desired selection curve for fines destruction (classification function). We assume that it is desirable to remove with the fines trap crystals of size r_m and smaller, and thus $\bar{h}(r)$ takes the form:

$$\bar{h}(r) = \left[\begin{array}{ll} 1, & for \;\; r \le r_m \\ 0, & for \;\; r > r_m \end{array} \right] \tag{4.23}$$

In the population balance, the term $\delta(r-0)Q(\bar{t})$ accounts for the production of crystals of infinitesimal (zero) size via nucleation. $R(\bar{t})$ and $Q(\bar{t})$ are assumed to follow McCabe's law and Volmer's nucleation law, respectively:

$$R(\bar{t}) = k_1(c-c_s), \quad Q(\bar{t}) = \bar{\epsilon}k_2 e^{-\frac{k_3}{\left(\frac{c}{c_s}-1\right)^2}} \tag{4.24}$$

where k_1, k_2, k_3 are constants and c_s is the concentration of solute at saturation. Using the expressions for $Q(\bar{t})$ and $R(\bar{t})$, the system of Eq.4.22 can be written as:

$$\begin{aligned} \frac{\partial n}{\partial \bar{t}} &= -k_1(c-c_s)\frac{\partial n}{\partial r} - \frac{n}{\tau} - \bar{h}(r)\frac{n}{\tilde{\tau}} + \delta(r-0)\bar{\epsilon}k_2 e^{-\frac{k_3}{\left(\frac{c}{c_s}-1\right)^2}} \\ \frac{dc}{d\bar{t}} &= \frac{(c_0-\rho)}{\bar{\epsilon}\tau} + \frac{(\rho-c)}{\tau} + \frac{(\rho-c)}{\bar{\epsilon}}\frac{d\bar{\epsilon}}{d\bar{t}} \end{aligned} \tag{4.25}$$

The multivariable control problem is formulated as the one of controlling the crystal concentration and the solute concentration, i.e.:

$$\begin{aligned} y_1(\bar{t}) &= 8\pi\sigma^3 \int_0^\infty n(r,\bar{t})dr = \tilde{x}_0, \\ y_2(\bar{t}) &= \frac{(c(\bar{t}) - c_s)}{(c_0 - c_s)} = \tilde{y}(\bar{t}) \end{aligned} \tag{4.26}$$

by manipulating the flow rate of suspension through the fines trap and the inlet solute concentration, i.e.:

$$\begin{aligned} \bar{u}_1(\bar{t}) &= \frac{1}{\bar{\tau}} - \frac{1}{\bar{\tau}_s}, \\ \bar{u}_2(\bar{t}) &= \frac{c_0 - c_{0_s}}{c_0 - c_s} \end{aligned} \tag{4.27}$$

where $1/\bar{\tau}_s$ and c_{0_s} denote the circulation rate of suspension in the fines trap and the inlet concentration at steady state, respectively. Since both manipulated variables directly enter the equations that describe the dynamics of the CSD and solute concentration, the crystallizer with the crystal concentration and solute concentration as controlled outputs and the flow rate of suspension through the fines trap and solute feed concentration as manipulated inputs is an approximately controllable system (see [72] for a rigorous controllability analysis).

Uncertainties in the form of modeling errors in the pre-exponential factor of the nucleation rate, k_2, and the density of crystals, ρ, are introduced into the system. Specifically:

$$\begin{aligned} k_2 &= k_{2,nom} + 0.5k_{2,nom}sin(0.5t), \\ \rho &= \rho_{nom} + 0.1\rho_{nom} \end{aligned} \tag{4.28}$$

where $k_{2,nom}$ and ρ_{nom} represent the nominal values of the pre-exponential factor and the crystal density respectively. We also consider fast process dynamics arising from unmodeled dynamics of the controlled actuators and the measurement sensors. To

account for the actuator dynamics, we consider the following dynamical system:

$$\begin{aligned} \epsilon_1 \dot{z}_1 &= -z_1 + z_2 \\ \epsilon_1 \dot{z}_2 &= -z_2 + \bar{u}_1 \\ \epsilon_2 \dot{z}_3 &= -z_3 + z_4 \\ \epsilon_2 \dot{z}_4 &= -z_4 + \bar{u}_2 \end{aligned} \tag{4.29}$$

where z_1 and z_3 are the values of $\bar{u}_1$ (flow rate of suspension through the fines trap) and $\bar{u}_2$ (inlet solute concentration) implemented on the process, and ϵ_1, ϵ_2 are small positive parameters. On the other hand, we assume that the sensor dynamics are described by the following dynamical system:

$$\begin{aligned} \epsilon_3 \dot{z}_5 &= -z_5 + z_6 \\ \epsilon_3 \dot{z}_6 &= -z_6 + y_1 \\ \epsilon_4 \dot{z}_7 &= -z_7 + z_8 \\ \epsilon_4 \dot{z}_8 &= -z_8 + y_2 \end{aligned} \tag{4.30}$$

where z_5 and z_7 are the values of y_1 (crystal size concentration) and y_2 (solute concentration) used in the controller, and ϵ_3, ϵ_4 are small positive parameters. The models for the actuator and sensor dynamics of Eqs.4.29-4.30 are coupled with the model of Eq.4.25 leading to the full model that describes the process.

Performing a two-time-scale decomposition to the full process model, one can show that its fast dynamics are stable, and that its slow dynamics are described by the ϵ-independent model of Eq.4.25 which will be used as the basis for controller synthesis. Owing to its distributed parameter nature, Eq.4.25 cannot be directly used for the synthesis of model-based feedback controllers. A model reduction procedure based on a combination of the method of moments and the approximation of the crystal size distribution with a Laguerre series expansion is used to reduce the system of Eq.4.25 into a small set of ordinary differential equations. This model reduction procedure is motivated from the fact that the dominant dynamics of the system of Eq.4.25 are characterized by a small number of degrees of freedom; the reader may refer to [7] for

a detailed analysis of the dynamic behavior of continuous crystallizers. Defining the νth moment of $\eta(r,\bar{t})$ as:

$$\mu_\nu = \int_0^\infty r^\nu n(r,\bar{t})dr, \quad \nu = 0,\ldots, \tag{4.31}$$

multiplying the population balance in Eq.4.25 by r^ν and integrating over all crystal sizes, the following infinite set of ordinary differential equations, which describes the rate of change of all the moments of the crystal size distribution and the solute concentration, is obtained:

$$\begin{aligned}
\frac{d\mu_0}{d\bar{t}} &= -\frac{\mu_0}{\tau} - \int_0^{r_m} \frac{n(r,\bar{t})}{\bar{\tau}}dr + \left(1 - \frac{4}{3}\pi\mu_3\right) k_2 e^{-\frac{k_3}{\left(\frac{c}{c_s}-1\right)^2}} \\
\frac{d\mu_\nu}{d\bar{t}} &= -\frac{\mu_\nu}{\tau} + \nu k_1 (c - c_s)\mu_{\nu-1} - \int_0^{r_m} r^\nu \frac{n(r,\bar{t})}{\bar{\tau}}dr, \quad \nu = 1,2,3,\ldots, \\
\frac{dc}{d\bar{t}} &= \frac{c_0 - c - 4\pi\tau(c - c_s)\mu_2(\rho - c)}{\tau\left(1 - \frac{4}{3}\pi\mu_3\right)}
\end{aligned} \tag{4.32}$$

Referring to the above system, note that it constitutes an unclosed set of moment equations owing to the nature of the classification function of the fines destruction. It is important to point out that when a fines trap is not used (i.e., $h(r) = 0$), then the first four moment equations and the concentration equation consist a closed set of differential equations that accurately describes the dominant dynamics of the crystallizer (see [7] for details).

In order to close the set of moment equations, an approximate analytical expression for $n(r,\bar{t})$ in terms of the moments is needed in order to obtain a closed set of ordinary differential equations. Such an approximation using Laguerre polynomial expansion was suggested in [38] and takes the following form:

$$n(r,\bar{t}) = \frac{\lambda}{a} p^{(\lambda)}\left(\frac{\lambda r}{a}\right) \sum_{n=0}^{\infty} \kappa_n L_n^{(\lambda)}\left(\frac{\lambda r}{a}\right) \tag{4.33}$$

where a and λ are functions of the moments of the crystal size distribution which are

explicit functions of time. $L_n^{(\lambda)}$ are the n^{th} order associated Laguerre polynomials:

$$L_n^{(\lambda)}(z) = \sum_{j=0}^{\infty}(-1)^j \frac{n!(n+\lambda-1)!}{j!(n-j)!(n+\lambda-1-j)!} z^{n-j} \qquad n = 0, 1, 2, \ldots \tag{4.34}$$

which are constructed by orthogonalizing the powers of z with respect to the Γ-distribution weighting function:

$$p^{(\lambda)}(z) = \frac{1}{(\lambda-1)!} z^{\lambda-1} e^{-z} \tag{4.35}$$

and κ_n takes the following form:

$$\kappa_n = \sum_{j=0}^{n}(-1)^j \frac{(\lambda-1)!}{j!(n+\lambda-1-j)!} \frac{(\lambda/a)^{n-j}}{(n-j)!} \mu_{n-j} \tag{4.36}$$

with the leading terms of κ_n being:

$$\begin{aligned} \kappa_0 &= \mu_0 \\ \kappa_1 &= \frac{1}{a}\mu_1 - \mu_0 \\ \kappa_2 &= \frac{1}{2a^2}\frac{\lambda}{\lambda+1}\mu_2 - \frac{1}{a}\mu_1 + \frac{1}{2}\mu_0 \end{aligned} \tag{4.37}$$

If we choose a and λ to be:

$$a = \frac{\mu_1}{\mu_0} \qquad \lambda = \frac{a^2}{\mu_2/\mu_0 - a^2} \tag{4.38}$$

so as to force κ_1 and κ_2 to be 0, Eq.4.33 becomes:

$$n(r,\bar{t}) = \frac{\lambda}{a} p^{(\lambda)}\left(\frac{\lambda r}{a}\right)\left[\mu_0 + \sum_{n=3}^{\infty}\kappa_n L_n^{(\lambda)}\left(\frac{\lambda r}{a}\right)\right] \tag{4.39}$$

Neglecting the terms in Eq.4.39 with $n = 3$ and higher results in the following approximation for the particle size distribution:

$$n(r,\bar{t}) = \frac{\lambda(\bar{t})}{a(\bar{t})} p^{(\lambda(\bar{t}))}\left(\frac{\lambda(\bar{t})r}{a(\bar{t})}\right)\mu_0 \tag{4.40}$$

Substituting Eq.4.40 into Eq.4.32 and introducing the following set of dimensionless variables and parameters:

$$\begin{gathered} t = \frac{\bar{t}}{\tau},\ \tilde{x}_0 = 8\pi\sigma^3\mu_0,\ \tilde{x}_1 = 8\pi\sigma^2\mu_1,\ \tilde{x}_2 = 4\pi\sigma\mu_2, \tilde{x}_3 = \frac{4}{3}\pi\mu_3,\ \ldots, \\ \sigma = k_1\tau(c_0 - c_s), Da = 8\pi\sigma^3 k_2\tau, F = \frac{k_3 c_s^2}{(c_0-c_s)^2},\ \alpha = \frac{(\rho-c_s)}{(c_0-c_s)}, \tilde{y} = \frac{(c-c_s)}{(c_0-c_s)} \end{gathered} \tag{4.41}$$

the following system is obtained:

$$\begin{aligned}
\frac{d\tilde{x}_0}{dt} &= -\tilde{x}_0 + (1-\tilde{x}_3)Da\, e^{\frac{-F}{\tilde{y}^2}} - 8\pi\sigma^3\mu_0\frac{\tau}{\bar{\tau}}\frac{1}{(\lambda-1)!}\left(\frac{\lambda}{a}\right)^{\lambda}\int_0^{r_m} r^{\lambda-1}e^{-\frac{\lambda r}{a}}\,dr \\
\frac{d\tilde{x}_1}{dt} &= -\tilde{x}_1 + \tilde{y}\tilde{x}_0 - 8\pi\sigma^2\mu_0\frac{\tau}{\bar{\tau}}\frac{1}{(\lambda-1)!}\left(\frac{\lambda}{a}\right)^{\lambda}\int_0^{r_m} r^{\lambda}e^{-\frac{\lambda r}{a}}\,dr \\
\frac{d\tilde{x}_2}{dt} &= -\tilde{x}_2 + \tilde{y}\tilde{x}_1 - 4\pi\sigma\mu_0\frac{\tau}{\bar{\tau}}\frac{1}{(\lambda-1)!}\left(\frac{\lambda}{a}\right)^{\lambda}\int_0^{r_m} r^{\lambda+1}e^{-\frac{\lambda r}{a}}\,dr \\
\frac{d\tilde{x}_3}{dt} &= -\tilde{x}_3 + \tilde{y}\tilde{x}_2 - \frac{4}{3}\pi\mu_0\frac{\tau}{\bar{\tau}}\frac{1}{(\lambda-1)!}\left(\frac{\lambda}{a}\right)^{\lambda}\int_0^{r_m} r^{\lambda+2}e^{-\frac{\lambda r}{a}}\,dr \\
&\vdots \\
\frac{d\tilde{y}}{dt} &= \frac{1-\tilde{y}-(\alpha-\tilde{y})\tilde{y}\tilde{x}_2}{1-\tilde{x}_3}
\end{aligned} \tag{4.42}$$

On the basis of the system of Eq.4.42, it is clear that the moments of order four and higher do not affect those of order three and lower, which means that the dominant dynamics of the system of Eq.4.32 can be adequately captured by the first four moment equations and the solute mass balance equation. The expressions of the corresponding dimensionless parameters can be obtained by substituting Eq.4.28 into Eq.4.41 to yield the following:

$$\begin{aligned}
Da &= Da_{nom} + 0.5Da_{nom}sin(0.5t), \\
\alpha &= \alpha_{nom} + \frac{0.1\rho_{nom}}{c_0 - c_s}
\end{aligned} \tag{4.43}$$

where $Da_{nom} = 8\pi\sigma^3 k_{2,nom}\tau$ and $\alpha_{nom} = \dfrac{(\rho_{nom} - c_s)}{(c_0 - c_s)}$. Substituting the formulation of the control problem of Eqs.4.26 and 4.27 into the fifth-order moment model, we obtain a system of the following general form:

$$\begin{aligned}
&\frac{d\tilde{x}}{dt} = \tilde{f}(\tilde{x}) + \tilde{g}_1(\tilde{x})\bar{u}_1 + \tilde{g}_2(\tilde{x})\bar{u}_2 + \tilde{w}_1(\tilde{x})\theta_1 + \tilde{w}_2(\tilde{x})\theta_2 \\
&y_1 = \tilde{h}_1(\tilde{x}) \qquad y_2 = \tilde{h}_2(\tilde{x})
\end{aligned} \tag{4.44}$$

where $\tilde{x}$ denotes the vector $[\tilde{x}_0\ \tilde{x}_1\ \tilde{x}_2\ \tilde{x}_3\ \tilde{y}]^T$, $\tilde{f}(\tilde{x})$, $\tilde{g}_1(\tilde{x})$ and $\tilde{g}_2(\tilde{x})$ are vector functions

and $\tilde{h}_1(\tilde{x})$ and $\tilde{h}_2(\tilde{x})$ are scalar functions whose explicit form is omitted for brevity.

Utilizing the formula of Theorem 4.1, we synthesize a robust nonlinear controller on the basis of the model of Eq.4.44 which has the following form:

$$\begin{aligned}
\bar{u}_1(t) &= [\beta_{12} L_{\tilde{g}_1} \tilde{h}(\omega)]^{-1} \{ v_1 - \beta_{10} y_1 - \beta_{11} L_{\tilde{f}} \tilde{h}_1(\omega) \\
&\quad - \chi_1 \frac{y_1 - v_1}{|y_1 - v_1| + \phi_1} 0.5 Da_{nom} |(1 - \omega_3) e^{\frac{-F}{\omega_4^2}}| \} \\
\bar{u}_2(t) &= [\beta_{22} L_{\tilde{g}_2} \tilde{h}(\omega)]^{-1} \{ v_2 - \beta_{20} y_1 - \beta_{21} L_{\tilde{f}} \tilde{h}_2(\omega) \\
&\quad - \chi_2 \frac{y_2 - v_2}{|y_2 - v_2| + \phi_2} \frac{0.1 \rho_{nom}}{(c_0 - c_s)} |\frac{\omega_4 \omega_2}{1 - \omega_3}| \}
\end{aligned} \tag{4.45}$$

where v_1 and v_2 are the set-points for the two outputs, and β_{10}, β_{11}, β_{12}, β_{20}, β_{21}, β_{22}, Da_{nom}, ρ_{nom}, ϕ_1, ϕ_2, χ_1, χ_2 are parameters which are given in Tables 4.1 and 4.2.

σ	=	$k_1 \tau (c_0 - c_s)$	=	1.0	mm
Da_{nom}	=	$8\pi\sigma^3 k_{2,nom} \tau$	=	200.0	
F	=	$k_3 c_s^2 / (c_0 - c_s)^2$	=	3.0	
α_{nom}	=	$(\rho_{nom} - c_s)/(c_0 - c_s)$	=	40.0	

Table 4.1: Dimensionless parameters.

β_{10}	=	1
β_{11}	=	1.5
β_{12}	=	1.5
β_{20}	=	1
β_{21}	=	1.5
β_{22}	=	1.5
L_1	=	$[1\ 0\ 0\ 0\ 0]^T$
L_2	=	$[0\ 0\ 0\ 0\ 1]^T$
ϕ_1	=	0.0022
ϕ_2	=	0.009
χ_1	=	1.53
χ_2	=	5.48

Table 4.2: Controller parameters.

The practical implementation of the robust nonlinear controller of Eq.4.45 is achieved

by employing the following nonlinear state observer:

$$
\begin{aligned}
\frac{d\omega_0}{dt} &= -\omega_0 + (1-\omega_3)Dae^{\frac{-F}{\bar{y}^2}} - \bar{u}_1(t)8\pi\sigma^3\mu_0\tau\frac{1}{(\lambda-1)!}\left(\frac{\lambda}{a}\right)^{\lambda}\int_0^{r_m} r^{\lambda-1}e^{-\frac{\lambda r}{a}}dr \\
&\quad + L_{10}(\tilde{h}_1(\tilde{x}) - \tilde{h}_1(\omega)) + L_{20}(\tilde{h}_2(\tilde{x}) - \tilde{h}_2(\omega)) \\
\frac{d\omega_1}{dt} &= -\omega_1 + \tilde{y}\omega_0 - \bar{u}_1(t)8\pi\sigma^2\mu_0\tau\frac{1}{(\lambda-1)!}\left(\frac{\lambda}{a}\right)^{\lambda}\int_0^{r_m} r^{\lambda}e^{-\frac{\lambda r}{a}}dr \\
&\quad + L_{11}(\tilde{h}_1(\tilde{x}) - \tilde{h}_1(\omega)) + L_{21}(\tilde{h}_2(\tilde{x}) - \tilde{h}_2(\omega)) \\
\frac{d\omega_2}{dt} &= -\omega_2 + \tilde{y}\omega_1 - \bar{u}_1(t)4\pi\sigma\mu_0\tau\frac{1}{(\lambda-1)!}\left(\frac{\lambda}{a}\right)^{\lambda}\int_0^{r_m} r^{\lambda+1}e^{-\frac{\lambda r}{a}}dr \\
&\quad + L_{12}(\tilde{h}_1(\tilde{x}) - \tilde{h}_1(\omega)) + L_{22}(\tilde{h}_2(\tilde{x}) - \tilde{h}_2(\omega)) \\
\frac{d\omega_3}{dt} &= -\omega_3 + \tilde{y}\omega_2 - \bar{u}_1(t)\frac{4}{3}\pi\mu_0\tau\frac{1}{(\lambda-1)!}\left(\frac{\lambda}{a}\right)^{\lambda}\int_0^{r_m} r^{\lambda+2}e^{-\frac{\lambda r}{a}}dr \\
&\quad + L_{13}(\tilde{h}_1(\tilde{x}) - \tilde{h}_1(\omega)) + L_{23}(\tilde{h}_2(\tilde{x}) - \tilde{h}_2(\omega)) \\
\frac{d\omega_4}{dt} &= \frac{1-\omega_4-(\alpha-\omega_4)\omega_4\omega_2}{1-\omega_3} + \frac{1}{1-\tilde{\omega}_3}\bar{u}_2(t) + L_{14}(\tilde{h}_1(\tilde{x}) - \tilde{h}_1(\omega)) \\
&\quad + L_{24}(\tilde{h}_2(\tilde{x}) - \tilde{h}_2(\omega))
\end{aligned}
\tag{4.46}
$$

where ω denotes the observer state vector whose dimension is equal to that of $\tilde{x}$, and $\tilde{h}_1(\tilde{x})$ and $\tilde{h}_2(\tilde{x})$ are the measured outputs. The state observer of Eq.4.46 consists of a replica of the system of Eq.4.44 plus two linear gain vectors $L_1 = [L_{10}\ L_{11}\ L_{12}\ L_{13}\ L_{14}]$ and $L_2 = [L_{20}\ L_{21}\ L_{22}\ L_{23}\ L_{24}]$ multiplying the discrepancy between the actual and the estimated values of the outputs. The values of the gains L_1 and L_2 are given in Table 4.3. The practical implementation of the nonlinear robust output feedback controller of Eqs.4.45-4.46 requires on-line measurements of the controlled outputs, $\tilde{x}_0$ (crystal concentration) and $\tilde{y}$ (solute concentration); in practice, measurements of $\tilde{x}_0$ can be obtained by using, for example, light scattering (see [5, 66] for details), and measurements of $\tilde{y}$ can be obtained by using a mass spectrometer.

The performance of the nonlinear robust output feedback controller of Eqs.4.45-4.46 was tested through numerical simulations. The values of the system parameters and the ones in their corresponding dimensionless forms (Eq.4.41) are shown in Tables 4.3 and 4.1 respectively. In all simulation runs, the following initial condition:

c_0	=	1000.0	$kg\ m^{-3}$
c_s	=	980.2	$kg\ m^{-3}$
ρ_{nom}	=	1770.0	$kg\ m^{-3}$
τ	=	1.0	hr
$1/\tilde{\tau}_s$	=	0.0	hr^{-1}
k_1	=	5.065×10^{-2}	$mm\ m^3\ kg^{-1}\ hr^{-1}$
$k_{2,nom}$	=	7.958	$mm^{-3}\ hr^{-1}$
k_3	=	1.217×10^{-3}	
r_m	=	1	mm

Table 4.3: Process parameters.

$$\begin{aligned} n(r,0) &= (2.189 \times 10^3) e^{-1.168r} mm^{-4}, \\ c(0) &= 992.1\ kg\ m^{-3} \end{aligned} \tag{4.47}$$

was used for the process model of Eq.4.25 and the finite difference method with 1000 discretization points was used for the simulations. The initial conditions for the observer states were computed numerically by using the initial conditions of Eq.4.47. We note that even though the number of discretization points, 1000, used to solve the system of Eq.4.22 is very large (owing to the poor convergence properties of the finite-difference scheme), the computation of an accurate (i.e., independent of the discretization) solution is critical for the thorough evaluation of the performance of a nonlinear feedback controller synthesized on the basis of a low-order approximation of the distributed parameter system of Eq.4.22. The adequacy of 1000 discretization points to yield an accurate solution was established through extensive simulations of the open- and closed-loop systems.

In the first set of simulation runs, we implemented the nonlinear robust multi-

variable controller on the crystallizer model of Eq.4.25 with the actuator dynamics of Eq.4.29 in the presence of parametric uncertainty in the pre-exponential factor of the nucleation rate, k_2, and the density of crystals, ρ. A 0.03 decrease in the value of the set-point from the initial conditions was applied to the first controlled output, $\tilde{x}_0$ ($v_1 = 0.015$), while the set-point for the second output, $\tilde{y}$, was set to be the same as the initial conditions ($v_2 = 0.5996$). The closed-loop output profiles are shown in Figure 4.2 (solid lines) with $\epsilon_1 = 0.1$ for the first manipulated input (flowrate of suspension

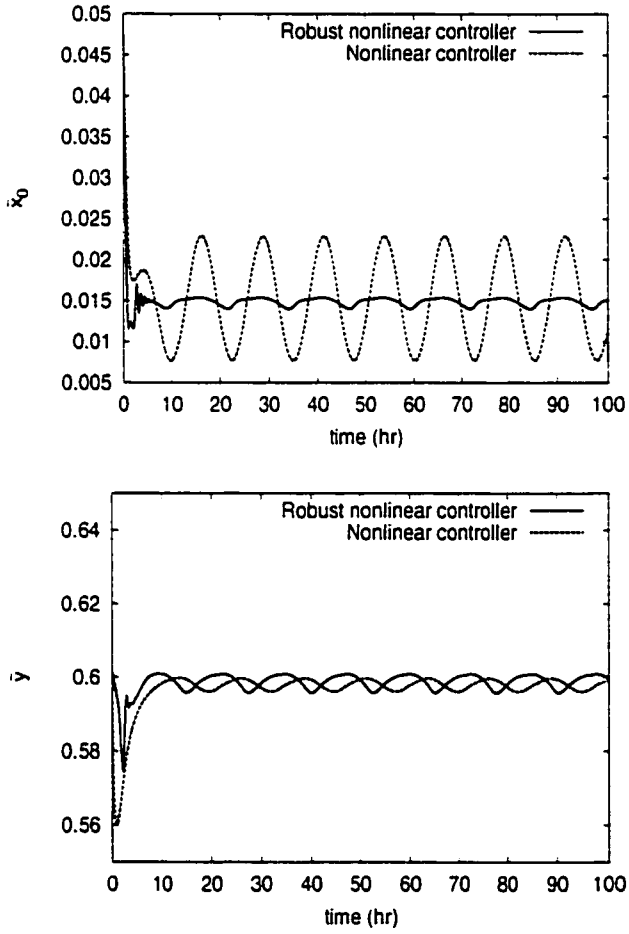

Figure 4.2: Closed-loop output profiles for $\tilde{x}_0$ (top plot) and $\tilde{y}$ (bottom plot) under robust nonlinear controller (solid line) and nonlinear controller which does not account for uncertainty (dashed line) - actuator dynamics are included in the process model.

through fines trap) and $\epsilon_2 = 0.02$ for the second manipulated input (inlet solute concentration); these are the largest values for ϵ_1, ϵ_2 for which an acceptable closed-loop output response is achieved with stability. Clearly the controller regulates the outputs to the set-point values attenuating the effect of the time-varying uncertainty on the process outputs and being robust to unmodeled actuator dynamics. Figure 4.3 shows

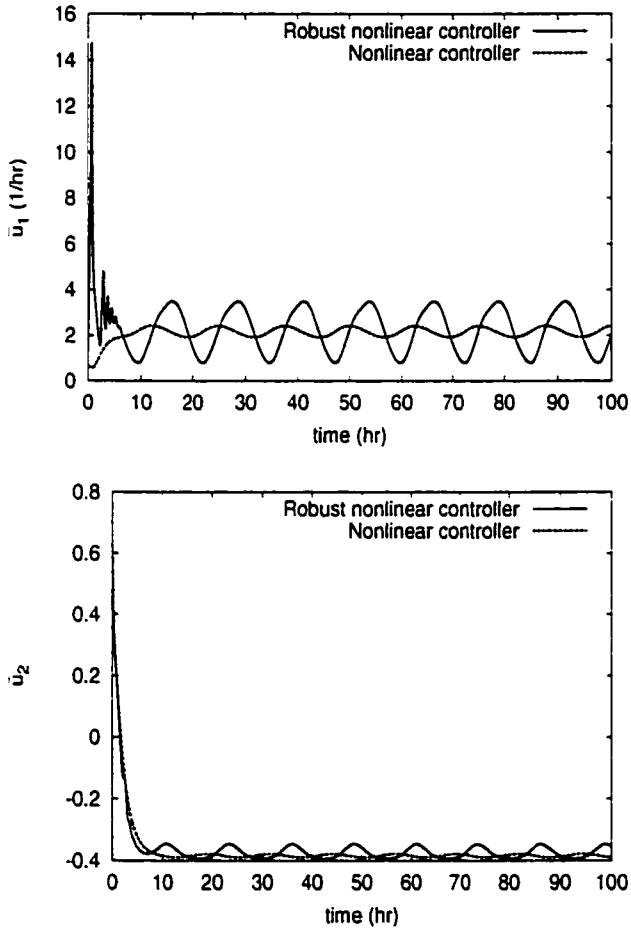

Figure 4.3: Manipulated input profiles for $1/\bar{\tau}$ (top plot) and c_0 (bottom plot) under robust nonlinear controller (solid line) and nonlinear controller which does not account for uncertainty (dashed line) - actuator dynamics are included in the process model.

the profiles of the manipulated inputs (solid lines). It is observed that the control action computed by the robust controller exhibits an oscillatory behavior in order to

compensate for the time-variation of the parameter Da. For the sake of comparison, we also implemented the nonlinear multivariable controller of Eq.4.45 with $\chi = 0$ (i.e., no uncertainty compensation is included in the controller). Figure 4.2 displays the closed-loop output profiles (dashed lines) and Figure 4.3 displays the corresponding manipulated input profiles (dashed lines). Clearly, this controller cannot compensate for the effect of the time-varying uncertainty leading to very poor closed-loop performance. Finally, to evaluate the ability of the controller in attenuating the effect of the time-varying uncertain variables in the entire CSD, the closed-loop profile of the evolution of the CSD under robust nonlinear control is shown in Figure 4.4 (bottom plot) and compared to the one of the open-loop process (top plot). It is obvious that fluctuations in the CSD are effectively damped by the use of robust nonlinear control.

In the second set of simulation runs, we implemented the nonlinear robust multivariable controller on the crystallizer model of Eq.4.25 with the actuator dynamics of Eq.4.29 and the sensor dynamics of Eq.4.30 in the presence of the same parametric uncertainty considered in the first set of simulation runs. Again, a 0.03 decrease in the value of the set-point from the initial conditions was applied to the first controlled output, $\tilde{x}_0$ ($v_1 = 0.015$), while the set-point for the second controlled output, $\tilde{y}$, was set to be $v_2 = 0.5996$. The closed-loop output profiles are shown in Figure 4.5 (solid lines) with $\epsilon_1 = 0.1$ for the first manipulated input (flowrate of suspension through fines trap), $\epsilon_2 = 0.02$ for the second manipulated input (inlet solute concentration), $\epsilon_3 = 0.01$ for the first measured output (crystal concentration), $\epsilon_4 = 0.01$ for the second measured output (solute concentration); these are the largest values for $\epsilon_1, \epsilon_2, \epsilon_3, \epsilon_4$ for which an acceptable closed-loop output response is achieved with stability. Clearly the controller regulates the outputs to the set-point values minimizing the effect of the time-varying uncertainty. We also implemented the nonlinear

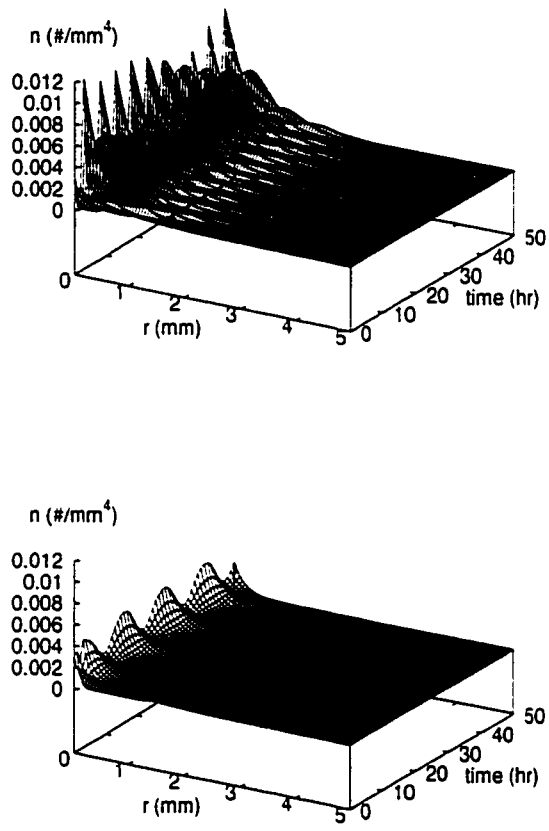

Figure 4.4: Profile of evolution of crystal size distribution, open-loop (top plot) and closed-loop under robust nonlinear controller (bottom plot) - actuator dynamics are included in the process model.

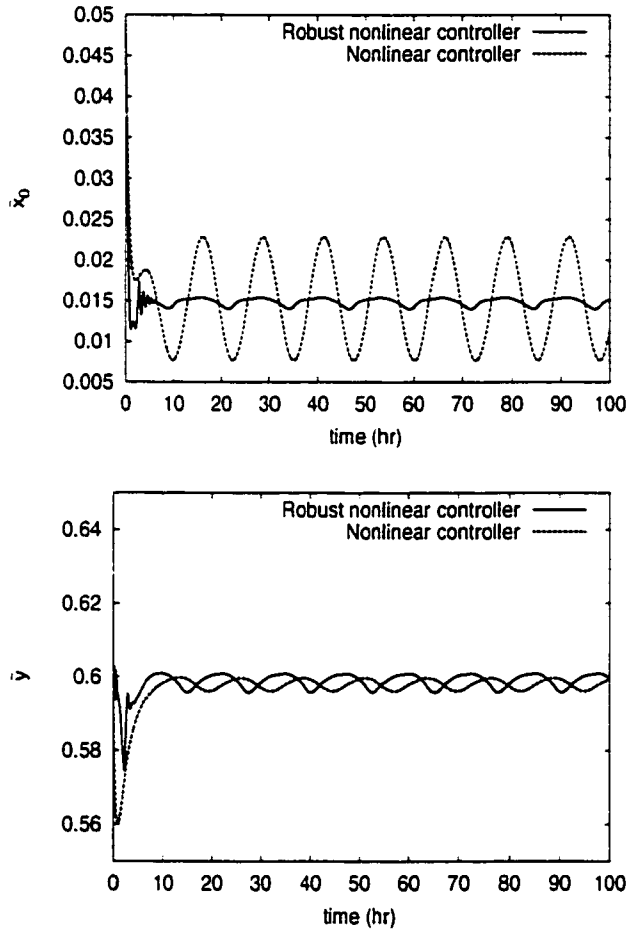

Figure 4.5: Closed-loop output profiles for $\bar{x}_0$ (top plot) and $\bar{y}$ (bottom plot) under robust nonlinear controller (solid line) and nonlinear controller which does not account for uncertainty (dashed line) - actuator and sensor dynamics are included in the process model.

multivariable controller of Eq.4.45 with $\chi = 0$ (i.e., no uncertainty compensation is included in the controller). Figure 4.5 shows the closed-loop output profiles (dashed lines). It is clear that this controller cannot attenuate the effect of the uncertainty on the outputs leading to poor performance. Figure 4.6 shows the profiles of the

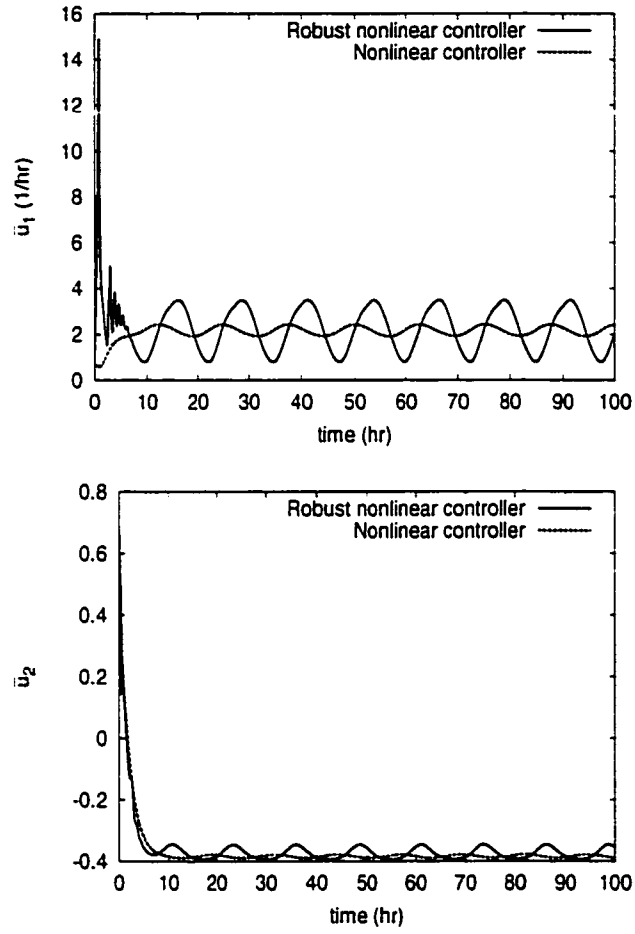

Figure 4.6: Manipulated input profiles for $1/\bar{\tau}$ (top plot) and c_0 (bottom plot) under robust nonlinear controller (solid line) and nonlinear controller which does not account for uncertainty (dashed line) - actuator and sensor dynamics are included in the process model.

manipulated inputs of the robust controller (solid lines) and the ones of the nonlinear controller which does not compensate for uncertainty (dashed lines). Again, the control actions computed by the robust controller exhibit oscillatory behavior to

compensate for the time-varying uncertainty. Finally, the ability of the robust nonlinear controller to attenuate the uncertainty can be also seen in Figure 4.7 (bottom

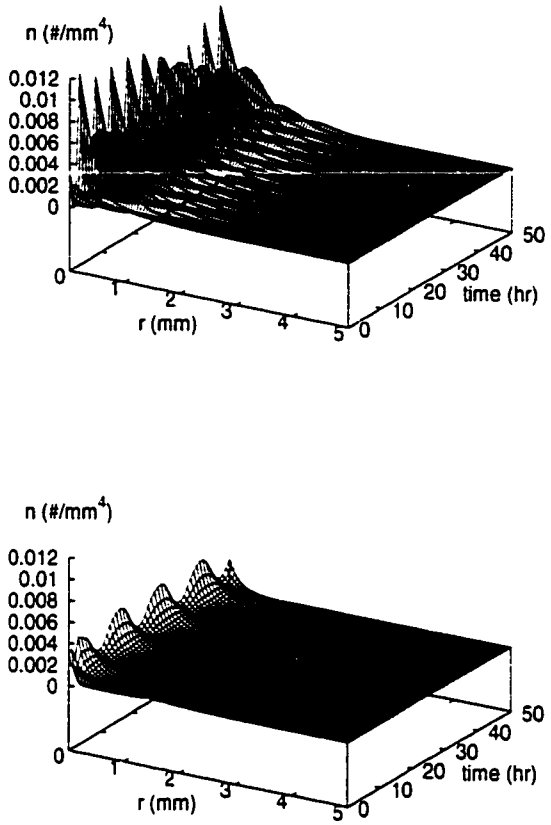

Figure 4.7: Profile of evolution of crystal size distribution, open-loop (top plot) and closed-loop under robust nonlinear controller (bottom plot) - actuator and sensor dynamics are included in the process model.

plot) where the evolution of the CSD under robust nonlinear control is shown and compared with the open-loop profile (top plot).

Remark 4.11: It is important to note that we have also performed simulations of the process under proportional-integral control and obtained a very poor closed-loop performance (worst than the performance obtained under nonlinear control without

uncertainty compensation). This is expected because proportional-integral control cannot effectively deal with the presence of time-varying uncertainty and significant nonlinearities in the process model. These simulations are not included in the manuscript for reasons of brevity.

4.5 Conclusions

A general method was developed for the synthesis of practically-implementable robust nonlinear controllers for a broad class of particulate processes described by population balances that explicitly handle time-varying uncertain variables (e.g., unknown process parameters and disturbances) and unmodeled dynamics (e.g., fast actuator and sensor dynamics not included in the process model). The robust controllers are synthesized on the basis of the uncertain population balances via Lyapunov's direct method and enforce stability in the closed-loop system, attenuation of the effect of uncertain variables and achieve particle size distributions with desired characteristics. The robustness of the proposed controllers with respect to stable and sufficiently fast unmodeled dynamics was established through a singular perturbation analysis. The controllers were applied to a continuous crystallizer with fines trap in which the nucleation rate and the crystal density change with time and the actuator and sensor dynamics are not included in the model used for the synthesis of the controller. Simulation runs of the closed-loop system clearly demonstrated the ability of the controllers to attenuate the uncertainty and achieve a crystal size distribution with desired characteristics, and documented their superiority over nonlinear controllers that do not account for the presence of uncertainty.

Chapter 5

Analysis and Control of Particulate Processes with Input Constraints

5.1 Introduction

This chapter focuses on the development and application of a general methodology for the analysis and control of constrained spatially-homogeneous particulate processes modeled by population balance equations. Initially, a nonlinear model reduction procedure based on the method of weighted residuals is presented for the construction of finite-dimensional ODE systems that accurately reproduce the dominant dynamics of the particulate process. These ODE systems are then used to analyze the limitations imposed by input constraints on the ability to modify the dynamics of the particulate process, leading to an explicit characterization of the set of admissible set-points that can be achieved in the presence of constraints. This information together with the derived ODE systems are then used as the basis for the synthesis of practically-implementable nonlinear bounded output feedback controllers that enforce

exponential stability in the closed-loop system and achieve particle size distributions with desired characteristics in the presence of active input constraints. Precise closed-loop stability conditions are given and controller implementation issues are addressed. The proposed methodology is successfully applied to a continuous crystallizer. The results of this chapter were first presented in [11, 12, 26].

5.2 Preliminaries

5.2.1 Particulate Process Model with Input Constraints

We focus on spatially homogeneous (well-mixed) particulate processes with simultaneous particle growth, nucleation, agglomeration and breakage and consider the case of a single internal particle coordinate, which is assumed to be the particle size. Applying a population balance to the particle phase as well as material and energy balances to the continuous phase, we obtain the following general nonlinear system of partial integro-differential equations

$$\begin{aligned} \frac{\partial n}{\partial t} &= -\frac{\partial (G(x,r)n)}{\partial r} + w(n,x,r), \quad n(0,t) = b(x(t)) \\ \dot{x} &= f(x) + g(x)sat(u(t)) + A\int_0^{r_{max}} a(n,r,x)dr \end{aligned} \tag{5.1}$$

where $n(r,t) \in [L_2[0,r_{max}), \mathbb{R}]$ is the size distribution function which is assumed to be a continuous and sufficiently smooth function of its arguments (we use the symbol $L_2[0,r_{max})$ to denote a Hilbert space of continuous functions defined on the interval $[0,r_{max}))$, $r \in [0,r_{max})$ is the particle size (r_{max} is the maximum particle size, which may be infinity), t is the time, $x \in \mathbb{R}^n$ is the vector of state variables which describe properties of the continuous phase (e.g., solute concentration, temperature and pH in a crystallizer), $u(t) = [u_1(t)\ u_2(t)\ \cdots\ u_m(t)]^T \in \mathbb{R}^m$ is the vector of manipulated

inputs, and *sat* refers to the saturation function defined by

$$sat(u_i) = \left\{ \begin{array}{ccc} u_{i,min} & if & u_i < u_{i,min} \\ u_i & if & u_{i,min} \leq u_i \leq u_{i,max} \\ u_{i,max} & if & u_i > u_{i,max} \end{array} \right\} \tag{5.2}$$

where $u_i \in \mathbb{R}$ and for a vector $u \in \mathbb{R}^m$, $sat(u) = [sat(u_1)\ sat(u_2)\ \cdots\ sat(u_m)]^T$. The presence of the *sat* operator in Eq.5.1 signifies the presence of hard constraints on the manipulated input. Such constraints may arise naturally due to inherent limitations on the capacity of control actuators used to regulate particulate processes or may be imposed for economic or safety reasons.

In Eq.5.1, the n-equation is the population balance where $G(x,r)$ is the growth rate that accounts for particle growth through condensation, and $w(n,x,r)$ is a term that accounts for the net rate of introduction of new particles into the system (it includes all the means by which particles appear or disappear within the system including particle agglomeration, breakage, nucleation, feed and removal). The x-subsystem of Eq.5.1 is derived by applying material and energy balances to the continuous phase. In this subsystem, $f(x)$, $a(n,r,x)$ are smooth nonlinear vector functions, $g(x)$ is a nonlinear matrix function, and A is a constant matrix. The term $A\int_0^{r_{max}} a(n,r,x)dr$ represents mass and heat transfer from the continuous phase to all the particles in the population.

We define a vector of controlled outputs to express the various control objectives (e.g. regulation of total number of particles, mean particle size, temperature, pH, etc.) as:

$$y_i(t) = h_i(\int_0^{r_{max}} c_\kappa(r)n(r,t)dr, x),\ \ i = 1,\ldots,m,\ \ \kappa = 1,\ldots,l \tag{5.3}$$

where $y_i(t)$ is the ith controlled output, $h_i(\int_0^{r_{max}} c_\kappa(r)n(r,t)dr, x)$ is a nonlinear scalar smooth function of its arguments and $c_\kappa(r)$ is a known smooth function of r which

depends on the desired performance specifications. To simplify the notation of our theoretical development, we will not consider measured outputs separately from controlled outputs, which means that we need to assume the availability of on-line measurements of the controlled output $y_i(t)$.

Throughout the chapter, we will use the inner product and norm in $L_2[0, r_{max})$, which are defined, respectively, as:

$$(\phi_1, \phi_2) = \int_0^{r_{max}} \phi_1(z)\phi_2(z)dz, \quad ||\phi_1||_2 = (\phi_1, \phi_1)^{\frac{1}{2}} \tag{5.4}$$

where ϕ_1, ϕ_2 are two elements of $L_2[0, r_{max})$. Furthermore, the order of magnitude and Lie derivative notations will be needed in our development. In particular, $\delta(\epsilon) = O(\epsilon)$ if there exist positive real numbers $\bar{k}_1$ and $\bar{k}_2$ such that: $|\delta(\epsilon)| \leq \bar{k}_1|\epsilon|$, $\forall\ |\epsilon| < \bar{k}_2$, and $L_f\bar{h}$ denotes the standard Lie derivative of a scalar function $\bar{h}(x)$ with respect to the vector function $f(x)$, $L_f^k\bar{h}$ denotes the k-th order Lie derivative and $L_gL_f^{k-1}\bar{h}$ denotes the mixed Lie derivative where $g(x)$ is a vector function.

5.2.2 Motivating Example: a Continuous Crystallizer

Crystallization is a particulate process that is widely used in industry and requires a population balance to be accurately described, analyzed, and controlled. Crystallizers typically exhibit highly oscillatory behavior which suggests the use of feedback control to ensure stable operation and attain a crystal size distribution with desired characteristics. However, one of the biggest problems that hinder the effective implementation of conventional feedback controller design methods is the presence of hard constraints on the manipulated input which limits our ability to modify the dynamics of the process in the desired manner. To illustrate some of the detrimental effects of constraints on the closed-loop stability and performance of particulate processes under conventional controller design methods, we consider in this subsection the isothermal

continuous crystallizer example studied in Chapter 2. The mathematical model for this crystallizer is given by

$$\begin{aligned} \frac{\partial n}{\partial \bar{t}} &= -k_1(c-c_s)\frac{\partial n}{\partial r} - \frac{n}{\tau} + \delta(r-0)\bar{\epsilon}k_2 e^{-\frac{k_3}{\left(\frac{c}{c_s}-1\right)^2}} \\ \frac{dc}{d\bar{t}} &= \frac{(c_0-\rho)}{\bar{\epsilon}\tau} + \frac{(\rho-c)}{\tau} + \frac{(\rho-c)}{\bar{\epsilon}}\frac{d\bar{\epsilon}}{d\bar{t}} \end{aligned} \tag{5.5}$$

where $n(r,\bar{t})$ is the number of crystals of radius $r \in [0,\infty)$ at time $\bar{t}$ per unit volume of suspension, τ is the residence time, c is the solute concentration in the crystallizer, c_0 is the solute concentration in the feed, $\bar{\epsilon} = 1 - \int_0^\infty n(r,\bar{t})\frac{4}{3}\pi r^3 dr$ is the volume of liquid per unit volume of suspension, c_s is the concentration of solute at saturation, k_1, k_2, and k_3 are constants, and $\delta(r-0)$ is the standard Dirac function. The term containing the Dirac function in Eq.5.5 accounts for the production of crystals of infinitesimal (zero) size via nucleation. The parameters used for this crystallizer process model can be found in Chapter 2 where it was shown that the crystallizer exhibits highly oscillatory behavior resulting from the interplay between the growth and nucleation terms in the population balance (unstable steady-state surrounded by a stable limit cycle.)

The control objective is to stabilize the crystallizer and achieve a crystal-size distribution with desired mass by manipulating the solute feed concentration. The manipulated input is therefore taken to be $u(t) = \frac{c_0 - c_{0s}}{c_0 - c_s}$, where c_{0s} is the steady-state solute feed concentration, and the controlled output is defined as

$$y(\bar{t}) = 8\pi\sigma^3 \int_0^\infty n(r,\bar{t})dr = \tilde{x}_0 \tag{5.6}$$

where $\sigma = k_1\tau(c_0 - c_s)$. Note that both are in dimensionless form. To achieve the desired control objective, we implement a conventional proportional-integral (PI)

control scheme

$$\begin{aligned} \frac{d\eta}{dt} &= e \\ u &= K_c[e + \frac{1}{\tau_I}\eta] \end{aligned} \tag{5.7}$$

on the crystallizer process model of Eq.5.5, where $e = y_{sp} - y$ and u is the controller output. If there are no limits on the maximum solute feed concentration that can be used to achieve the desired control objectives, then the controller output and process input are the same. However, suppose that there are limitations on the maximum solute feed concentration, i.e, $|u| \leq u_{max}$. In this case, if the solute feed concentration calculated by the controller is, for example, higher than u_{max}, then the actual solute concentration fed to the crystallizer will be just u_{max} leading to a mismatch between the controller output and actual crystallizer input.

Closed-loop simulation runs were performed to test the ability of the PI controller to achieve the desired control objective in the presence of limitations (constraints) on the maximum solute feed concentration. Figure 5.1 depicts the dimensionless crystal concentration ($\tilde{x}_0$) and dimensionless solute feed concentration (u) profiles for a 0.4 increase in the set-point in the absence of any constraints on the manipulated input (i.e., $|u| < \infty$.) It is evident from the figure that the PI manages eventually to drive the output to its new set-point. By contrast, Figure 5.2 depicts the closed-loop response to the same 0.4 increase in the set-point in the presence of input constraints $u \in [0, 2]$. As can be seen from this figure, the controller fails (regardless of the PI tuning parameters) to stabilize the crystallizer in the presence of the imposed constraints leading to sustained oscillations.

The above example highlights two important issues that need to be addressed for the effective control of constrained particulate processes. The first issue pertains to the need for a general framework that explicitly characterizes the limitations imposed

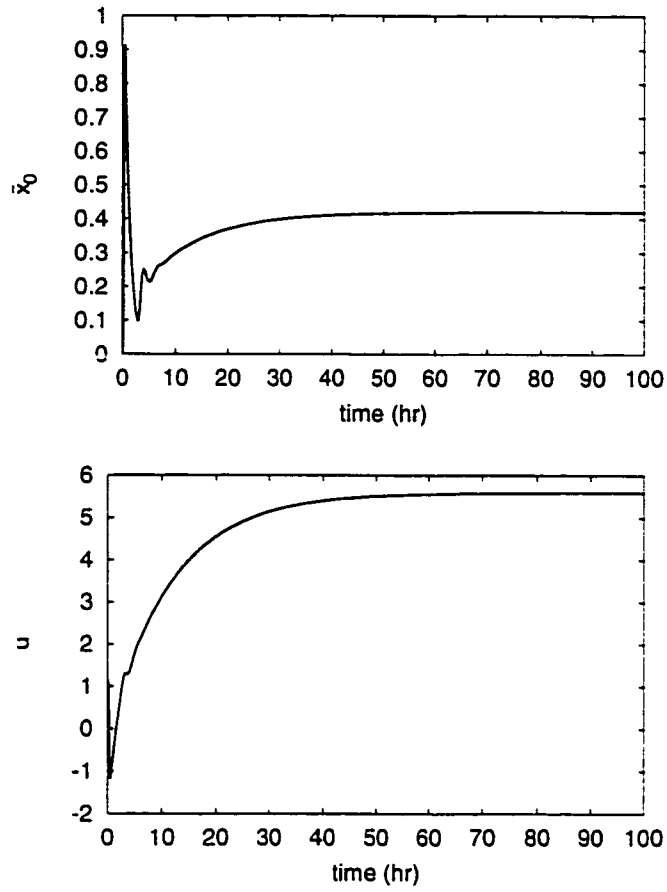

Figure 5.1: Controlled output and manipulated input profiles under PI control in the absence of input constraints.

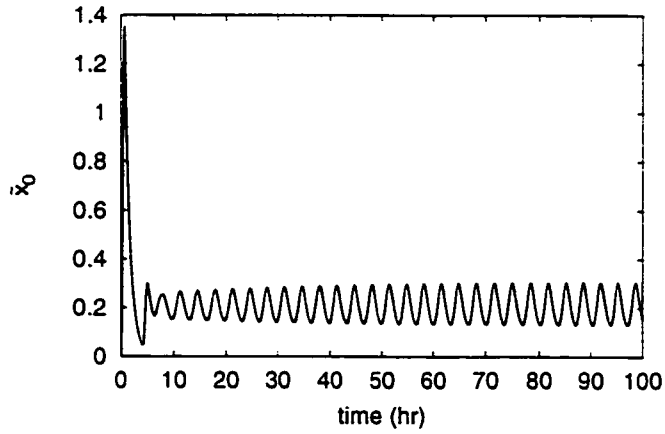

Figure 5.2: Closed-loop profile of crystal concentration under PI control for $u \in [0, 2]$.

by input constraints on our ability to steer the particulate process in a desired direction. Such a frameowrk is needed to provide process operators with the necessary knowledge of which control objectives (e.g., set-point changes) are possible and can be achieved in the presence of known constraints on the manipulated input, *independent of the specific control scheme to be used.* Recall from Figure 5.2 that the saturation-induced instability of the crystallizer was a direct consequence of the fact that the requested set-point change demanded larger control action than was available and permitted by the given constraints on the solute feed concentration. The set-point change was therefore infeasible under the specified constraints. Relaxing these constraints, as we will see later on, consequently allows the PI to eventually achieve the requested set-point change. The a priori availability of this kind of feasibility information is a pre-requisite for any effective controller design method that can successfully address the problems caused by input constraints on the operation of the process.

The second issue that the crystallizer example highlights is that of the choice of the specific controller design method to achieve the desired control objectives in the presence of input constraints. Since conventional control schemes (such as the PI controller used in the above example) are not designed to explicitly handle the presence of input constraints, there is clearly a need for alternative, effective and direct control strategies that can handle the presence of input constraints explicitly in the controller design and provide, simultaneously, an explicit characterization of the regions of guaranteed closed-loop stability starting from where the requested stability and performance of the particulate process can be guaranteed in the presence of input constraints.

Motivated by the above discussion, the development of a rigorous, yet practical,

framework for the analysis and control of constrained particulate processes is the subject of this thesis. We begin in the next section with an outline of the proposed framework, which will serve as the road map for our development throughout the manuscript.

5.3 Methodological Framework for Analysis and Control of Constrained Particulate Processes

Owing to its distributed parameter nature, the system of Eq.5.1 cannot be used directly as the basis for either the analysis of the limitations imposed by input constraints on the particulate process dynamics or the synthesis of practically implementable (low-order) nonlinear controllers that cope effectively with the problem of constraints. This fact, together with the realization that the dominant dynamics of particulate processes are characterized by a small number of degrees of freedom (see, e.g., Chapter 2), motivate employing the following methodology for the analysis and control of constrained particulate processes of the form of Eq.5.1:

1. Initially, the method of weighted residuals is used to derive a nonlinear, possibly high-order, ODE system that accurately reproduces the solutions and dynamics of the system of Eq.5.1. Then, a procedure based on the concept of approximate inertial manifold is employed for the construction of low-order ODE systems that accurately reproduce the dominant dynamics of the large scale ODE system obtained by the method of weighted residuals.

2. Next, the low-order ODE approximation of the system of Eq.5.1 is used as the basis for analyzing the limitations imposed by input constraints on our ability to modify the dynamics of the particulate process and identifying the set of feasible

set-points that can be attained in the presence of the given input constraints.

3. Then, given the set of feasible control objectives permitted by the constraints, the low-order ODE approximation of the system of Eq.5.1 is used as the basis for the direct synthesis, via Lyapunov techniques, of practically implementable bounded nonlinear output feedback controllers that cope effectively with the presence of input constraints by: a) enforcing stability and set-point tracking in the constrained closed-loop ODE system , and b) providing an explicit characterization of the set of operating conditions starting from where the constrained closed-loop system stability is guaranteed.

4. Finally, the resulting closed-loop system (particulate process model of Eq.5.1 and controller) is analyzed to derive conditions that guarantee that the desired stability and set-point tracking properties are enforced in the infinite-dimensional closed-loop system.

5.4 Model Reduction

We initially use the method of weighted residuals to derive a set of nonlinear ODEs that accurately reproduce the solutions and the dominant dynamics of the distributed parameter system of Eq.5.1. The central idea of the method of weighted residuals is to approximate the exact solution of $n(r,t)$ by an infinite series of orthogonal basis functions defined on the interval $[0, r_{max})$ with time-varying coefficients, substitute the series expansion into Eq.5.1, and then take the inner product with respect to a complete set of weighted functions, to compute a set of ODEs which describes the rate of change of the time-varying coefficients of the series expansion of the solution. Specifically, we expand the solution of $n(r,t)$ in an infinite series in terms of an orthogonal and complete set of basis functions, $\phi_k(r)$, where $r \in [0, r_{max})$, $k = 1, \ldots, \infty$,

as follows:

$$n(r,t) = \sum_{k=1}^{\infty} a_k(t)\phi_k(r) \tag{5.8}$$

where $a_k(t)$ are time-varying coefficients. Substituting the above expansion into the particulate process model of Eq.5.1, we obtain:

$$\begin{aligned} \sum_{k=1}^{\infty}\phi_k(r)\frac{\partial a_k(t)}{\partial t} &= -\sum_{k=1}^{\infty}a_k(t)\frac{\partial(G(x,r)\phi_k(r))}{\partial r} + w(\sum_{k=1}^{\infty}a_k(t)\phi_k(r),x,r) \\ \dot{x} &= f(x) + g(x)sat(u(t)) + A\int_0^{r_{max}} a_2(\sum_{k=1}^{\infty}a_k(t)\phi_k(r),r,x)dr) \end{aligned} \tag{5.9}$$

Multiplying the population balance with the weighting functions, $\psi_\nu(r)$, and integrating over the entire particle size spectrum (i.e., taking inner product in $L_2[0,r_{max})$ with the weighting functions), the following infinite set of nonlinear ODEs is obtained:

$$\begin{aligned} \int_0^{r_{max}}\psi_\nu(r)\sum_{k=1}^{\infty}\phi_k(r)\frac{\partial a_k(t)}{\partial t}dr &= -\sum_{k=1}^{\infty}a_k(t)\int_0^{r_{max}}\psi_\nu(r)\frac{\partial(G(x,r)\phi_k(r))}{\partial r}dr \\ &\quad +\int_0^{r_{max}}\psi_\nu(r)w(\sum_{k=1}^{\infty}a_k(t)\phi_k(r),x,r)dr, \\ &\quad \nu = 1,\ldots,\infty \\ \dot{x} &= f(x) + g(x)sat(u(t)) \\ &\quad +A\int_0^{r_{max}} a_2(\sum_{k=1}^{\infty}a_k(t)\phi_k(r),r,x)dr) \end{aligned} \tag{5.10}$$

Eq.5.10 is an infinite set of ODEs which describe the rate of change of the time varying coefficients, $a_k(t)$, where $k = 1,\ldots,\infty$, of the series expansion of the solution. An accurate approximation of Eq.5.10 is obtained by truncating the series expansion of $n(r,t)$ up to order N and keeping the first N equations (i.e., $\nu = 1,\ldots,N$). The

infinite-dimensional system of Eq.5.10 reduces to the following finite set of ODEs:

$$\begin{aligned}\int_0^{r_{max}} \psi_\nu(r)\sum_{k=1}^{N}\phi_k(r)\frac{\partial a_{kN}(t)}{\partial t}dr &= -\sum_{k=1}^{N}a_{kN}(t)\int_0^{r_{max}}\psi_\nu(r)\frac{\partial(G(x_N,r)\phi_k(r))}{\partial r}dr \\ &\quad +\int_0^{r_{max}}\psi_\nu(r)w(\sum_{k=1}^{N}a_{kN}(t)\phi_k(r),x_N,r)dr, \\ &\quad \nu = 1,\ldots,N \\ \dot{x}_N &= f(x_N)+g(x_N)sat(u(t)) \\ &\quad +A\int_0^{r_{max}}a_2(\sum_{k=1}^{N}a_{kN}(t)\phi_k(r),r,x_N)dr)\end{aligned} \tag{5.11}$$

where x_N and a_{kN} are the approximations of x and a_k obtained by an N-th order truncation. Introducing the vector notation $a_N = [a_{1N}\ \cdots\ a_{NN}]$, and after some rearrangements, Eq.5.11 can be represented in the following general form:

$$\begin{aligned}\dot{a}_N &= f^*(a_N,x_N) \\ \dot{x}_N &= f(x_N)+g(x_N)sat(u(t))+A\int_0^{r_{max}}a_2(\sum_{k=1}^{N}a_{kN}(t)\phi_k(r),r,x_N)dr)\end{aligned} \tag{5.12}$$

where the explicit expression of $f^*(a_N,x_N)$ is omitted for brevity. Setting $\tilde{x} = [a_N^T\ x_N^T]^T$, we obtain the following multi-input multi-output finite-dimensional ODE system:

$$\begin{aligned}\dot{\tilde{x}} &= \tilde{f}(\tilde{x})+\sum_{i=1}^{m}\tilde{g}_i(\tilde{x})sat(u_i) \\ y_{si} &= \tilde{h}_i(\tilde{x}),\ \ i=1,\ldots,m\end{aligned} \tag{5.13}$$

where $\tilde{f}(\tilde{x}),\tilde{g}_i(\tilde{x}),\tilde{w}(\tilde{x})$ are nonlinear vector functions whose explicit form is omitted brevity. Using results from singular perturbation theory, the asymptotic validity of the ODE approximation was established in Proposition 2.1.

Remark 5.1: In the series expansion of Eq.5.8, the basis, $\{\phi_k\}$, $j = 1,\ldots,\infty$, of $L_2[0,r_{max})$ can be chosen from standard basis functions sets (for example, when $r_{max}=\infty$, $\{\phi_k\}$ can be chosen to be Laguerre polynomials in which case the method of weighted residuals reduces to the method of moments when the weighting functions

are chosen as $\psi_\nu = r^\nu$), or it can be computed by applying Karhunen-Loève expansion on an appropriately chosen ensemble of solutions of the system of Eq.5.1 (see [36] for details on Karhunen-Loève expansion).

Remark 5.2: When an arbitrary set of basis functions is used in the expansion of Eq.5.8,the ODE system of Eq.5.12 may be of very high order in order to accurately describe the dominant dynamics of the system of Eq.5.1, and therefore, to be suitable for the synthesis of a high-performance nonlinear controller. Unfortunately, high dimensionality of the system of Eq.5.12 leads to complex design and high-order controllers, which cannot be readily implemented in practice. An approach to overcome this problem is to reduce the dimension of the system of Eq.5.12 further by utilizing the concept of approximate inertial manifolds for particulate process models proposed in Chapter 2.

5.5 Computation of Admissible Set-points

Having obtained a low-order approximate ODE system that accurately reproduces the solution and dominant dynamics of the particulate process, we are now in a position to analyze the limitations imposed by constraints on our ability to modify the dynamics of particulate processes, on the basis of the constrained ODE system of Eq.5.13. Particulate processes typically operate at constant set-points corresponding to equilibrium points of the closed-loop system (e.g., a desired total number of particles, mean particle size, temperature). However, it may not be feasible to steer the closed-loop system to the desired operating point, in the presence of constraints, irrespectively of the choice of the control strategy. Thus, even before designing a control policy, it becomes important to investigate the feasibility of controlling the particulate process at a desired set-point in the presence of constraints. Addressing

this problem, in its full generality, entails two main tasks. The first task is that of identifying the set of admissible set-points that the particulate process can be steered to in the presence of constraints. The second task is that of characterizing the set of admissible initial conditions, starting from where, a given admissible set-point can be reached in the presence of constraints. In this section, we will focus on the first task and defer discussion of the second task to the next section.

To accomplish our goal of identifying the set of admissible set-points permitted by input constraints, it is useful to view the constrained ODE system of Eq.5.13 as a dynamical system where the control input u_i is viewed as a parameter that takes values in the set of admissible control inputs, i.e. the interval $U_i = [u_{i,min}, u_{i,max}]$. In other words, we consider the following unforced system

$$\dot{\tilde{x}} = \tilde{f}(\tilde{x}) + \sum_{i=1}^{m} \tilde{g}_i(\tilde{x}) u_i^0, \quad i = 1, \ldots, m \tag{5.14}$$

obtained from the system of Eq.5.13 for a constant value of u_i denoted by $u_i^0 \in U_i$. An immediate consequence of this view is the realization that the presence of constraints on the values that the parameter u_i^0 in the system of Eq.5.14 can take leads to natural limitations on the steady-states or equilibrium states and, consequently the set-points, that the ODE system can attain. Exploiting this fact, the problem of characterizing the limitations imposed by input constraints is equivalent to that of explicitly characterizing the dependence of the equilibrium states of the constrained ODE system of Eq.5.14 on the admissible values of u_i^0 dictated by the given input constraints. For a given value of the control input $u_i^0 \in U_i$, one can obtain the admissible equilibrium states of the system of Eq.5.13 by solving the following set of algebraic equations

$$0 = \tilde{f}(\tilde{x}_s) + \sum_{i=1}^{m} \tilde{g}_i(\tilde{x}_s) u_i^0, \quad i = 1, \ldots, m \tag{5.15}$$

where $\tilde{x}_s$ represents the admissible steady-state for the above ODE system. As the

value of u_i^0 is varied smoothly over the set of admissible control inputs U_i, we obtain the set of all admissible equilibrium points of the constrained ODE system of Eq.5.13 that can be attained in the presence of constraints. Finally, the admissible set-points can be computed directly from the following relation:

$$v_i \;=\; \tilde{h}_i(\tilde{x}_s), \;\; i = 1, \ldots, m \tag{5.16}$$

Remark 5.3: The above analysis provides a systematic and practical method for computing the approximate admissible set-points of the constrained particulate process of Eq.5.1 on the basis of the ODE system of Eq.5.13. The only task involved in this method is the solution of a small (due to the low-dimensional nature) set of algebraic equations of the form of Eq.5.15 as u_i^0 takes values in the set of admissible control inputs. Note that this analysis is independent of the specific control strategy that one may wish to implement. Note also that this analysis does not provide any information regarding where, in state-space, a particular admissible set-point can be reached from. In other words, given an admissible equilibrium point $\tilde{x}_s$ obtained by solving Eq.5.15, the above analysis does not say if this point will actually be achieved under a given controller and starting from a given initial condition. The task of providing such information will be addressed in the controller design step of our methodology. What the above analysis allows us to conclude, however, is whether the given input constraints place any fundamental limitations on our ability to reach a particular set-point, and can therefore be used by process operators to identify a priori (before controller design) admissible control objectives permitted by input constraints.

Remark 5.4: Recent research on the dynamical analysis of nonlinear control systems with input constraints (see, for example, [21, 22]) has provided a system-theoretic

characterization of the regions of controllability under constraints, the so-called control sets, where *any* two points in state-space can be reached from each other with the available control action. As the range of manipulated input is varied smoothly over a sufficiently small finite range, these control sets emerge and evolve around the equilibrium points of the nominal system of Eq.5.14. Although control sets provide a more detailed characterization of the limitations imposed by input constraints on the system dynamics, such characterization remains largely theoretical and not very useful from a computational standpoint. The construction of control sets is actually a very cumbersome task even for low-dimensional systems (see, for example, [45].) On the other hand, computation of the set of admissible set-points, contained within a control set, is a relatively straightforward task that is computationally feasible and provides at the same time a valuable piece of information.

Let us now apply our feasibility analysis to the continuous crystallizer example considered earlier in the preliminaries section. It was shown in Chapter 2 that upon application of the method of moments to the continuous crystallizer process of Eq.5.5 and neglecting moments of order four and higher, one can derive the following dimensionless ODE system that accurately reproduces the dynamics of the distributed process model of Eq.5.5:

$$\begin{aligned}
\dot{\tilde{x}}_0 &= -\tilde{x}_0 + (1-\tilde{x}_3) Da\, e^{\frac{-F}{\tilde{y}^2}} \\
\dot{\tilde{x}}_1 &= -\tilde{x}_1 + \tilde{y}\tilde{x}_0 \\
\dot{\tilde{x}}_2 &= -\tilde{x}_2 + \tilde{y}\tilde{x}_1 \\
\dot{\tilde{x}}_3 &= -\tilde{x}_3 + \tilde{y}\tilde{x}_2 \\
\dot{\tilde{y}} &= \frac{1-\tilde{y}-(\alpha-\tilde{y})\tilde{y}\tilde{x}_2}{1-\tilde{x}_3} + \frac{u}{1-\tilde{x}_3}
\end{aligned} \tag{5.17}$$

where

$$t = \frac{\bar{t}}{\tau},\ \tilde{x}_0 = 8\pi\sigma^3\mu_0,\ \tilde{x}_1 = 8\pi\sigma^2\mu_1,\ \tilde{x}_2 = 4\pi\sigma\mu_2,\ \tilde{x}_3 = \frac{4}{3}\pi\mu_3,\ \ldots,$$

$$\sigma = k_1\tau(c_0 - c_s),\ Da = 8\pi\sigma^3 k_2\tau,\ F = \frac{k_3 c_s^2}{(c_0 - c_s)^2},\ \alpha = \frac{(\rho - c_s)}{(c_0 - c_s)},\ \tilde{y} = \frac{(c - c_s)}{(c_0 - c_s)},$$

$$u = \frac{(c_0 - c_{0s})}{(c_0 - c_s)} \tag{5.18}$$

μ_i is the $i-$th moment, $\tilde{x}_0$ is a dimensionless crystal concentration and u is a dimensionless solute feed concentration (for definitions of the remaining variables and values of the model parameters, the reader is referred to Chapter 2). To compute the admissible set-points for the above system, we take the set of admissible control inputs to be $U = [0, 6]$. Setting the left hand side of Eq.5.17 equal to zero, we obtain a set of algebraic equations that can be solved for each value of $u \in U$. Figure 5.3 illustrates

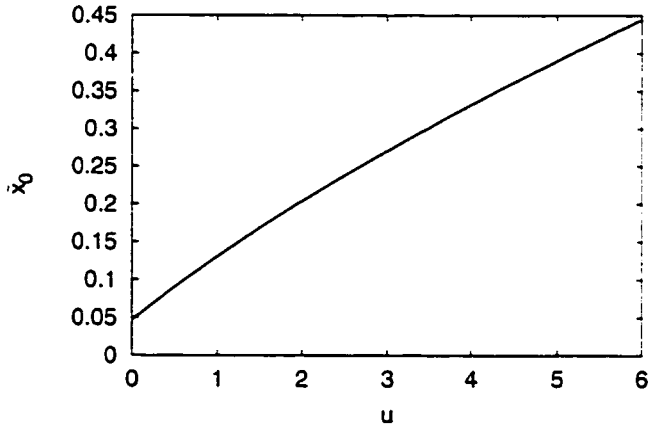

Figure 5.3: Admissible set-points for crystal concentration for $u \in [0, 6]$.

the admissible set-points for the crystal concentration which can be achieved with the available control inputs. From this figure, the reason for the PI controller's failure to stabilize the crystallizer in section 5.2.2 and achieve the requested 0.4 change in the set point is evident. Allowing the control inputs to vary only in the set $[0, 2]$ renders the requested set-point $\tilde{x}_0 = 0.4$ infeasible.

5.6 Bounded Nonlinear Control of Particulate Processes

Having obtained a low-order ODE system that captures the dominant dynamics of the particulate process and identified the set of feasible control objectives that can be achieved in the presence of constraints, we are now motivated to proceed with the third step of our proposed methodology. In this section, we use the constrained low-order ODE system of Eq.5.13 as the basis for developing an effective control strategy that handles explicitly the problem of constraints. The key components of this strategy involve: a) the synthesis of a practically implementable bounded nonlinear output feedback controller that enforces stability and set-point tracking in the closed-loop system in the presence of active input constraints and b) the explicit characterization of the state-space region of guaranteed closed-loop stability obtained under the designed controller. The output feedback controller is constructed through a standard combination of a bounded state feedback controller with a state observer. The state feedback controller is synthesized via Lyapunov-based control methods and the state observer is an extended Luenberger-type observer. Before we proceed with the controller design , we begin in the next subsection with some preliminaries that will be used to state the controller synthesis result.

5.6.1 Preliminaries

Referring to the system of Eq.5.13, we define the relative order of the output y_{s_i} with respect to the vector of manipulated inputs u as the smallest integer r_i for which

$$\left[L_{\tilde{g}_1} L_{\tilde{f}}^{r_i-1} \tilde{h}_i(\tilde{x}) \ \cdots \ L_{\tilde{g}_m} L_{\tilde{f}}^{r_i-1} \tilde{h}_i(\tilde{x})\right] \not\equiv [0 \ \cdots \ 0] \tag{5.19}$$

or $r_i = \infty$ if such an integer does not exist. We also define the characteristic matrix

$$C(\tilde{x}) = \begin{bmatrix} L_{\tilde{g}_1} L_{\tilde{f}}^{r_1-1} \tilde{h}_1(\tilde{x}) & \cdots & L_{\tilde{g}_m} L_{\tilde{f}}^{r_1-1} \tilde{h}_1(\tilde{x}) \\ L_{\tilde{g}_1} L_{\tilde{f}}^{r_2-1} \tilde{h}_2(\tilde{x}) & \cdots & L_{\tilde{g}_m} L_{\tilde{f}}^{r_2-1} \tilde{h}_2(\tilde{x}) \\ \vdots & \cdots & \vdots \\ L_{\tilde{g}_1} L_{\tilde{f}}^{r_m-1} \tilde{h}_m(\tilde{x}) & \cdots & L_{\tilde{g}_m} L_{\tilde{f}}^{r_m-1} \tilde{h}_m(\tilde{x}) \end{bmatrix} \tag{5.20}$$

To proceed with the controller synthesis and under the assumption that the relative degree is well-defined, we transform the system of Eq.5.13 into the following partially linear form

$$\begin{aligned} \dot{\zeta}_1^{(i)} &= \zeta_2^{(i)} \\ &\vdots \\ \dot{\zeta}_{r_i-1}^{(i)} &= \zeta_{r_i}^{(i)} \\ \dot{\zeta}_{r_i}^{(i)} &= L_{\tilde{f}}^{r_i} \tilde{h}_i(\tilde{x}) + \sum_{k=1}^{m} L_{\tilde{g}_k} L_{\tilde{f}}^{r_i-1} \tilde{h}_i(\tilde{x}) u_k \\ \dot{\eta}_1 &= \Psi_1(\zeta, \eta) \\ &\vdots \\ \dot{\eta}_{(n+N)-\sum_i r_i} &= \Psi_{(n+N)-\sum_i r_i}(\zeta, \eta) \\ y_{s_i} &= \zeta_1^{(i)}, \quad i = 1, \ldots, m \end{aligned} \tag{5.21}$$

where $\tilde{x} = T^{-1}(\zeta, \eta)$, $\zeta = [\zeta^{(1)^T} \ \cdots \ \zeta^{(m)^T}]^T$, $\eta = [\eta_1 \ \cdots \ \eta_{(n+N)-\sum_i r_i}]^T$. This transformation is standard in all general nonlinear process control methods whose objective is to force the process output to follow the reference input. Defining the tracking error $e_k^{(i)} = \zeta_k^{(i)} - v_i^{(k-1)}$ and introducing the vector notation $e^{(i)} = [e_1^{(i)} \ e_2^{(i)} \ \cdots \ e_{r_i}^{(i)}]^T$, $e = [e^{(1)^T} \ e^{(2)^T} \ \cdots \ e^{(m)^T}]^T$, where $i = 1, \cdots, m$, $k = 1, \cdots, r_i$, the ζ-subsystem of Eq.5.21 can be further transformed into the following more compact form

$$\dot{e} = Ae + B\left[l_1(e, \eta, \bar{v}) + C(\tilde{x})u\right] \tag{5.22}$$

where A, B, are constant matrices of dimensions $(\sum_{i=1}^m r_i) \times (\sum_{i=1}^m r_i)$ and $(\sum_{i=1}^m r_i) \times m$, respectively, $l_1(e, \eta, \bar{v})$ is a $(\sum_{i=1}^m r_i) \times 1$ continuous nonlinear vector function, and $\bar{v}$ is a vector of the form $\bar{v} = \mathcal{V}(v_i, v_i^{(1)}, \ldots, v_i^{(r_i)})$ where $\mathcal{V}(v_i, v_i^{(1)}, \ldots, v_i^{(r_i)})$ is a smooth vector function, $v_i^{(k)}$ is the k^{th} time derivative of the external reference input v_i (which

is assumed to be a smooth function of time.) The specific forms of these functions are omitted for brevity. Finally, we define the function $\bar{f}(e,\eta,\bar{v}) = Ae + Bl_1(\tilde{x})$, and denote by $\bar{g}_i(e,\eta,\bar{v})$ the $i-$th column of the matrix function $BC(\tilde{x}), \quad i = 1,\cdots m$.

5.6.2 Controller Synthesis

Towards the end goal of synthesizing the necessary bounded nonlinear output feedback controller, we use the nonlinear system of Eq.5.21 first to synthesize, via Lyapunov-based control methods, a bounded nonlinear state feedback controller of the general form

$$u \;=\; p(\tilde{x},\bar{v}) \tag{5.23}$$

where $p(\tilde{x},\bar{v})$ is a bounded vector function, i.e. $|u| \leq u_{max}$ where $|\cdot|$ is the Euclidean norm, that: a) enforces exponential stability and reference input tracking in the closed-loop system in the presence of active input constraints and b) provides an explicit characterization of the region in state-space where the aforementioned properties are guaranteed to hold in the closed-loop system.

To construct the desired stabilizing state feedback controller for the system of Eq.5.13, we use Lyapunov-based control methods. The basic idea behind any Lyapunov-based controller design is the selection of an appropriate Lyapunov function whose time-derivative can be rendered negative definite, via feedback, along the trajectories of the closed-loop system. A natural choice for our system, suggested by the partially linear form of Eq.5.22, is the quadratic Lyapunov function $V = e^T P e$ where P is a positive definite matrix chosen to satisfy the following Riccati matrix inequality

$$A^T P + PA - PBB^T P \;<\; 0 \tag{5.24}$$

and consequently guarantee the negative definiteness of $\dot{V}$. Using this Lyapunov

function, we design a bounded nonlinear state feedback controller of the form

$$u = -\frac{1}{2}R^{-1}(\tilde{x})I\,(L_{\tilde{g}}V)^T \tag{5.25}$$

where $R^{-1}(\tilde{x})$ is a strictly positive nonlinear scalar function whose specific expression is given in Theorem 5.1 below, I is the identity matrix and $L_{\tilde{g}}V$ is a row vector given by $L_{\tilde{g}}V = [L_{\tilde{g}_1}V \cdots L_{\tilde{g}_m}V]$. As we will discuss shortly, the bounded nature of the state feedback controller will assist in addressing the problem of constraints by providing an explicit characterization of the set of feasible initial states, starting from where, the desired closed-loop properties are guaranteed.

Under the hypothesis that the system of Eq.5.13 is locally observable (i.e., its linearization around the desired operating steady-state is observable), the practical implementation of a nonlinear state feedback controller of the form of Eq.5.25 will be achieved by employing the following nonlinear state observer:

$$\frac{d\omega}{dt} = \tilde{f}(\omega) + \tilde{g}(\omega)sat(u) + L(y - \tilde{h}(\omega)) \tag{5.26}$$

where ω denotes the observer state vector (the dimension of the vector ω is equal to the dimension of $\tilde{x}$ in the system of Eq.5.13), $y = [y_1\ y_2\ \cdots y_l]^T$ is the measured output vector and L is a matrix chosen so that the eigenvalues of the matrix $C_L = \frac{\partial \tilde{f}}{\partial \omega}_{(\omega=\omega_s)} - L\frac{\partial \tilde{h}}{\partial \omega}_{(\omega=\omega_s)}$, where ω_s is the operating steady-state, lie in the open left-half of the complex plane. The state observer of Eq.5.26 consists of a replica of the system of Eq.5.13 plus a linear gain multiplying the discrepancy between the actual and the estimated value of the output, and therefore, it is an extended Luenberger-type observer. Finally, the state feedback control law of Eq.5.25 and the state observer of Eq.5.26 can be combined to yield the desired bounded nonlinear output feedback control law.

We are now in a position to state the main result of this subsection. Theorem 5.1 below provides the explicit synthesis formula for the desired bounded output feedback

control law and states precise conditions that guarantee closed-loop stability and asymptotic output tracking in the presence of input constraints in the closed-loop ODE system (the proof can be found in the appendix.)

Theorem 5.1: *Consider the system of Eq.5.13 and assume that:* 1) *it is locally observable in the sense that there exists a matrix L such that $C_L = \frac{1}{\mu}\bar{A}$ where μ is a small positive parameter and $\bar{A}$ is a Hurwitz matrix,* 2) *its characteristic matrix, $C(\tilde{x})$, is nonsingular $\forall\, \tilde{x} \in D \subset \mathbb{R}^{n+N}$, and* 3) *its inverse dynamics are input-to-state stable and exponentially stable when $\zeta = 0$. Now consider the system of Eq.5.13 under the nonlinear output feedback controller*

$$\begin{aligned} \frac{d\omega}{dt} &= \tilde{f}(\omega) - \frac{1}{2}\tilde{g}(\omega)R^{-1}(\omega)I\left(L_{\tilde{g}}V(\omega)\right)^T + L(y - \tilde{h}(\omega)) \\ u &= -\frac{1}{2}R^{-1}(\omega)I\left(L_{\tilde{g}}V(\omega)\right)^T \end{aligned} \tag{5.27}$$

where

$$\frac{1}{2}R^{-1}(\omega) = \frac{L_{\tilde{f}}^{*}V + \sqrt{(L_{\tilde{f}}^{*}V)^2 + \left(u_{max}^2(L_{\tilde{g}}V)(L_{\tilde{g}}V)^T\right)^2}}{(L_{\tilde{g}}V)(L_{\tilde{g}}V)^T\left[1 + \sqrt{1 + u_{max}^2(L_{\tilde{g}}V)(L_{\tilde{g}}V)^T}\right]} \tag{5.28}$$

and $L_{\tilde{f}}^{*}V = L_{\tilde{f}}V + \rho|e|^2$, $\rho > 0$. Then, given any positive real number δ_x such that

$$L_{\tilde{f}}^{*}V \leq u_{max}|(L_{\tilde{g}}V)^T| \tag{5.29}$$

for $|x| \leq \delta_x$, there exists $\mu^* > 0$ such that if $\mu \in (0, \mu^*]$, $|x(0)| \leq \delta_x$, $|\omega(0)| \leq \delta_x$, the following holds in the presence of input constraints:

(1) The closed-loop system is exponentially stable.

(2) The output of the closed-loop ODE system satisfies a relation of the form

$$\lim_{t\to\infty} |y_{ri} - v_i| = 0. \tag{5.30}$$

where v_i is the set-point for the ith controlled output.

Remark 5.5: The inequality of Eq.5.29 describes explicitly the set of feasible initial conditions, starting from where, the desired stability and set-point tracking proper-

ties are guaranteed in the constrained closed-loop ODE system under the bounded *state* feedback controller of Eq.5.25. As such it characterizes the region of guaranteed closed-loop stability. Depending on the value of u_{max}, this is in general an open unbounded region in the state-space. According to Theorem 5.1, starting from *any* compact subset of this region (the size of this subset is determined by δ_x which can be selected arbitrarily large), there always exists $\mu > 0$ such that the desired closed-loop properties are guaranteed under the dynamic *output* feedback controller of Eq.5.27. Therefore, although combination of the bounded state feedback controller with an observer results in some loss in the size of the region, this loss can be made arbitrarily small by selecting μ to be sufficiently small. The region of guaranteed closed-loop stability therefore remains practically preserved under the controller-observer combination.

Remark 5.6: The inequality of Eq.5.29 displays the intuitive dependence of the size of the region of guaranteed closed-loop stability on input constraints. According to this inequality, the tighter the input constraints are made (i.e., smaller u_{max}), for example, the smaller the resulting closed-loop stability region. This is in consistent with one's intuition, since under such conditions (tighter constraints), fewer initial conditions will satisfy the inequality of Eq.5.29 resulting in a smaller closed-loop stability region. Finally note that, according to the inequality of Eq.5.29, the largest region of closed-loop stability under the control law of Eq.5.27 is obtained, as expected, in the absence of constraints (i.e., as $u_{max} \to \infty$).

Remark 5.7: Although the inequality of Eq.5.29 can be used to compute the region of guaranteed closed-loop stability, the actual construction of this region is not necessary to conclude whether the desired closed-loop properties can be guaranteed for a given initial condition. Instead, one can directly substitute the desired initial

condition into Eq.5.29 and check before implementing the controller whether the inequality is satisfied. If so, then both stability and set-point tracking are guaranteed in the presence of input constraints. This aspect of the controller design has important practical implications because it provides process operators with a systematic and easily implementable guide to identify a priori (that is before implementing the controller) feasible initial operating conditions form which to operate and steer the process safely and reliably under input constraints while at the same time satisfying the requested control objectives.

Remark 5.8: Note that the state feedback component of the controller of Eq.5.27 (with $\omega = \tilde{x}$) uses directly the available information on input constraints to achieve the requested closed-loop stability and performance properties (note the explicit dependence of the expression in Eq.5.28 on u_{max}.) Note also that, whenever Eq.5.29 holds, the control action is bounded by u_{max}. Both the explicit incorporation of constraints in the controller design and the explicit characterization of the region of guaranteed closed-loop stability follow directly from the boundedness property of the state feedback component of Eq.5.27.

Remark 5.9: The control law of Eq.5.27 has two desirable properties not present in other conventional or nonlinear controller designs based on the concept of input/output linearization (see [39] for details.) The first property is the fact that the controller of Eq.5.27 recognizes the beneficial effect of the term $L_f V$ when $L_f V < 0$ and prevents its unnecessary cancellation. In this case, the term $L_f V$ is a beneficial (stabilizing) nonlinearity whose cancellation may generate unnecessarily large control action, and in some cases generate positive feedback and destabilize the process. Under such circumstances, the controller design of Eq.5.27 guards against the wasteful cancellation of such nonlinearities and avoids the expenditure of unnecessarily large

control effort. This property is particularly important in the presence of constraints that limit the available control action. The ability of the controller to use reasonably small control action to enforce the desired control objectives makes the controller design proposed in Theorem 5.1 better equipped to handle the problem of constraints. The second property that the controller of Eq.5.27 possesses is the fact that it dominates the term $L_f V$, instead of cancelling it, when $L_f V > 0$. This situation arises, for example, when the process is open-loop unstable. In this case, the term $L_f V$ is a destabilizing one that must be eliminated. The controller of Eq.5.27, however, eliminates the term by domination rather than by cancellation. This property guards against the non-robustness of cancellation designs which increases the risk of instability due to the presence of other uncertainties not taken into account in the controller design. This means that input perturbations (or equivalently, an error in implementing the control law) will be tolerated in the sense that the trajectories will remain bounded.

Remark 5.10: The fact that the state feedback controller of Eq.5.25 uses small control action to accomplish the desired closed-loop properties is characteristic of certain optimality properties that this controller possesses. In fact, one can rigorously prove, through the inverse optimal control approach (see, for example, [30, 74, 27],) that this controller is optimal with respect to an infinite-time meaningful quadratic cost functional of the form

$$J = \int_0^\infty (e^T Q(\tilde{x}) e + u^T R(\tilde{x}) I u) dt \tag{5.31}$$

which imposes penalty on both the tracking error and control action. In the above performance index, $Q(\tilde{x})$ is a positive definite matrix that can be found directly from the steady-state Hamilton-Jacobi-Bellman (HJB) equation (which is the optimality condition for the stabilization problem) associated with the system of Eq.5.13 and

cost functional of Eq.5.31

$$0 \equiv e^T Q(\tilde{x})e + L_{\tilde{f}}V - \frac{1}{4}(L_{\tilde{g}}V)R^{-1}(\tilde{x})I\,(L_{\tilde{g}}V)^T \tag{5.32}$$

The inverse optimal approach provides a rigorous framework for associating meaningful optimality (i.e. meaningful performance indices) with certain stabilizing controllers (such as those of Eq.5.25) and therefore helps explain the basis for their optimality properties. The key idea of this approach is to first design a stabilizing controller and then show that it minimizes a meaningful performance index of the form of Eq.5.31 by establishing that the resulting weights Q, R are positive definite matrices, which, in turn, renders the penalties imposed in the cost functional physically sensible. This approach has been used in the literature for the design of nonlinear optimal controllers without recourse to the unwieldy task of solving the HJB equation . For additional details on controller design using this approach as well as some of the history and motivation behind it, the reader is referred to [27, 74, 43]. Finally, one can easily show that the minimum cost achieved by the state feedback controller is $V(e(0))$.

Remark 5.11: Note that the controller-observer combination of Eq.5.27 practically preserves the optimality properties of the state feedback controller explained in the previous remark. The output feedback controller design of Eq.5.27 is near-optimal in the sense that the cost incurred by implementing this controller on the system of Eq.5.13 tends to the optimal (minimal) cost achieved by implementing the bounded optimal state feedback controller (i.e., u of Eq.5.27 with $\omega = \tilde{x}$) when μ is selected to be sufficiently small. Using standard singular perturbation argument, one can actually show that cost associated with the output feedback controller is $O(\mu)$ close to the optimal cost associated with the state feedback controller (i.e. $J_{min} = V(e(0))+O(\mu)$.) The reason for this near-optimality is the fact that by choosing μ to be sufficiently

small, the observer states can be made to converge quickly to the process states. This fact can be exploited to make the performance of the output feedback controller arbitrarily close to that of the optimal state feedback controller.

Remark 5.12: The requirement that the observer states start within the region of guaranteed closed-loop stability ($|\omega(0)| \leq \delta_x$) is motivated by the fact that the process states themselves should start inside this region in order to guarantee stability of the constrained closed-loop system; and therefore, one must initiate the observer within the same region to guarantee convergence of the observer states to the process states. Note, however, that no restriction is placed on where, inside the stability region, the observer states can start (that is we allow for initialization errors) since they can be made to converge sufficiently fast to the actual states by selecting μ to be sufficiently small.

Remark 5.13: Regarding the practical application of Theorem 5.1, one has to initially use the method of weighted residuals to derive an ODE system of the form of Eq.5.13, and then verify assumptions 1, 2 and 3 on the basis of this system. Then, given the available input constraints u_{max} and the desired initial condition, one should check if the inequality of Eq.5.29 is satisfied. If this is case, then the desired closed -loop properties are guaranteed and the synthesis formula of Eq.5.27 can be directly used to derive the explicit form of the controller and implement it.

5.6.3 Application to the Crystallizer Moment Model

The objective of this subsection is to illustrate the application of the results of Theorem 5.1 to the fifth-order moment model of Eq.5.17 which describes the dominant dynamics of the continuous crystallizer of Eq.5.5. The control problem here is the same as that considered in the motivating example which involves regulating the crystal

concentration by manipulating the solute feed concentration in the presence of constraints on the manipulated input. Utilizing the dimensionless variables of Eq.5.18, the system of Eq.5.17 can be recast in the form of Eq.5.13 with $\tilde{x} = [\tilde{x}_0\ \tilde{x}_1\ \tilde{x}_2\ \tilde{x}_3\ \tilde{y}]^T$ and

$$\tilde{f}(\tilde{x}) = \begin{bmatrix} -\tilde{x}_0 + (1-\tilde{x}_3)Dae^{\frac{-F}{\tilde{y}^2}} \\ -\tilde{x}_1 + \tilde{y}\tilde{x}_0 \\ -\tilde{x}_2 + \tilde{y}\tilde{x}_1 \\ -\tilde{x}_3 + \tilde{y}\tilde{x}_2 \\ \dfrac{1-\tilde{y}-(\alpha-\tilde{y})\tilde{y}\tilde{x}_2}{1-\tilde{x}_3} \end{bmatrix}, \quad \tilde{g}(\tilde{x}) = \begin{bmatrix} 0 \\ 0 \\ 0 \\ 0 \\ \dfrac{1}{1-\tilde{x}_3} \end{bmatrix}$$

On the basis of this system, one can easily verify that assumptions 1, 2 and 3 of Theorem 5.1 are satisfied. A direct application of the synthesis formula of Eq.5.27 then yields the following bounded nonlinear output feedback controller

$$\begin{aligned} \dot{\omega}_0 &= -\omega_0 + (1-\omega_3)Dae^{\frac{-F}{\omega_4^2}} + L_0[\tilde{x}_0 - \omega_0] \\ \dot{\omega}_1 &= -\omega_1 + \omega_4\omega_0 + L_1[\tilde{x}_0 - \omega_0] \\ \dot{\omega}_2 &= -\omega_2 + \omega_4\omega_1 + L_2[\tilde{x}_0 - \omega_0] \\ \dot{\omega}_3 &= -\omega_3 + \omega_4\omega_2 + L_3[\tilde{x}_0 - \omega_0] \\ \dot{\omega}_4 &= \frac{1-\omega_4-(\alpha-\omega_4)\omega_4\omega_2}{1-\omega_3} - \frac{1}{2}\frac{R^{-1}(\omega)L_{\tilde{g}}V(\omega)}{1-\omega_3} + L_4[\tilde{x}_0 - \omega_0] \\ u &= -\frac{1}{2}R^{-1}(\omega)L_{\tilde{g}}V(\omega) \end{aligned} \tag{5.33}$$

where

$$V = e^T P e, \quad P = \begin{bmatrix} 1 & c \\ c & 1 \end{bmatrix}, \quad c \in (0,1) \tag{5.34}$$

Guided by the information provided in Figure 5.3, we constrain the admissible values of the manipulated input to vary in the range $0 \leq u \leq 6$ to achieve the requested set-point of $\tilde{x}_0 = 0.4$. Two closed-loop simulation runs were performed to evaluate the set-point tracking capability of the bounded nonlinear output feedback controller of Eq.5.33 in the presence of constraints. The initial conditions for the states of the moment model, the states of the observer, and the values of the nonlinear controller

parameters are all given in Table 5.1 for both runs. Note that in both cases, the initial

	First run	Second run
$\tilde{x}(0)$	$[0.059\ 0.035\ 0.022\ 0.014\ 0.60]^T$	$[0.44\ 0.61\ 0.85\ 1.14\ 0.60]^T$
$\omega(0)$	$[0.047\ 0.028\ 0.017\ 0.010\ 0.60]^T$	$[0.42\ 0.59\ 0.80\ 1.07\ 0.60]^T$
L	$[1.0\ 0.0\ 0.0\ 0.0\ 1.0]^T$	$[1.0\ 0.0\ 0.0\ 0.0\ 1.0]^T$
c	0.90	0.90
ρ	0.001	0.001

Table 5.1: Initial conditions and controller parameters for crystallizer moment model.

observer states do not match those of the moment model to study the performance of the controller in the presence of initialization errors.

In the first simulation run, we considered achieving the set-point of $\tilde{x}_0 = 0.4$ starting from an initial condition that lies inside the region of guaranteed closed-loop stability (i.e. satisfies the inequality of Eq.5.29). Figure 5.4 shows the closed-loop output (top plot) and manipulated input (bottom plot) profiles for this case. It is clear from the figure that, starting from this initial condition, the bounded output feedback controller successfully achieves the requested set-point in the presence of input constraints. In the second simulation run, the same set-point was considered starting from an initial condition that lies outside the region of guaranteed stability (note that the initial condition for the second run given in Table 5.1 does not satisfy Eq.5.29). The closed-loop output and manipulated input profiles for this run are depicted in Figure 5.5, which shows that, in this case, the controller fails to achieve the requested set-point in the presence of constraints. These simulation findings verify the prediction of Theorem 5.1 which guarantees the desired properties in the constrained closed-loop ODE system under the bounded output feedback controller of Eq.5.33 for initial conditions that satisfy Eq.5.29.

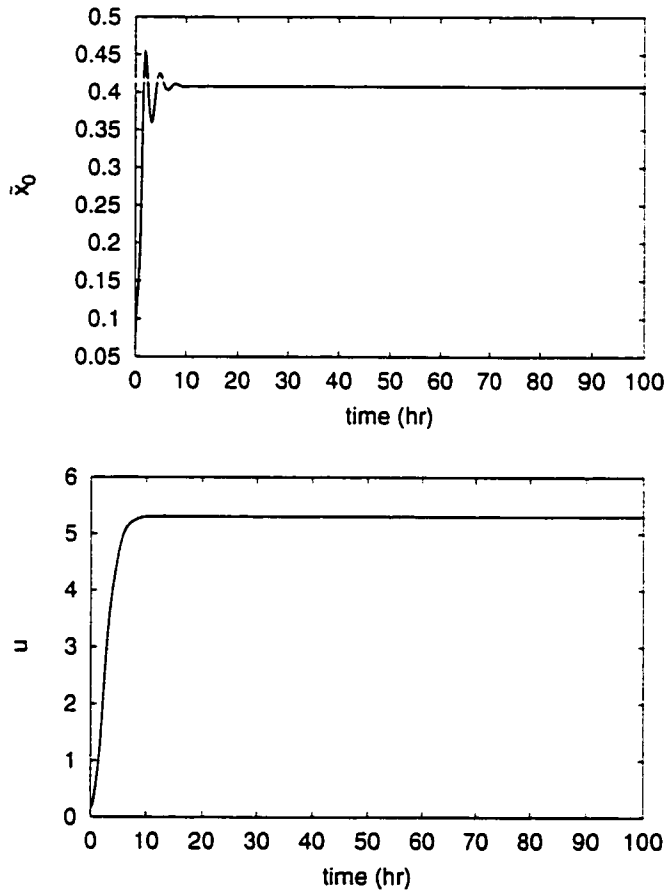

Figure 5.4: Controlled output and manipulated input profiles for the crystallizer moment model under bounded nonlinear controller for $u \in [0, 6]$ and initial condition satisfying Eq.5.29.

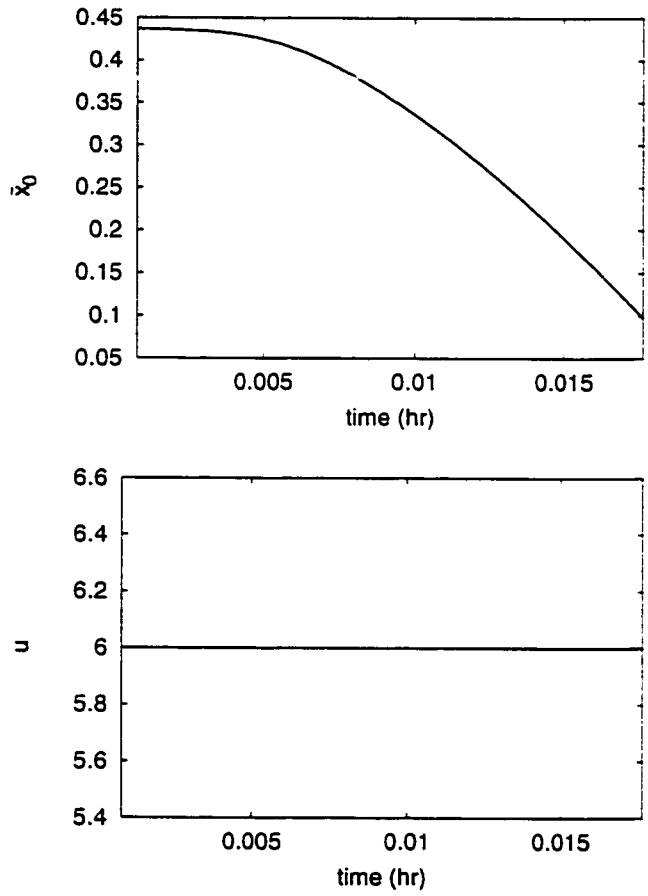

Figure 5.5: Controlled output and manipulated input profiles for the crystallizer moment model under bounded nonlinear controller for $u \in [0, 6]$ and initial condition violating Eq.5.29.

5.6.4 Controller Implementation on the Infinite-dimensional Particulate Process Model

In the previous two subsections, we designed, on the basis of the ODE system of Eq.5.13, a bounded nonlinear output feedback controller with well characterized stability properties in the presence of constraints and illustrated its application to the constrained low-dimensional ODE system of Eq.5.13 which captures the dominant dynamics of the particulate process. In this subsection, we proceed with the final step of our methodology and implement the bounded output feedback controller of Eq.5.27 on the infinite dimensional particulate process model of Eq.5.1. Theorem 5.2 below states precise conditions that guarantee closed-loop stability and asymptotic output tracking in the presence of constraints. The proof of this theorem can be found in the appendix.

Theorem 5.2: *Consider the system of Eq.5.13, for which assumptions 1, 2, and 3 of Theorem 5.1 hold. Consider also the particulate process model of Eq.5.1 under the nonlinear output feedback controller of Eq.5.27. Then, for sufficiently large N, there exist positive real numbers $\delta_n, \bar{\delta}_x, \delta_\omega, \bar{\mu}^*$ such that if $\mu \in (0, \bar{\mu}^*]$, $||n(r,0)||_2 < \delta_n$, $|x(0)| < \bar{\delta}_x$, $|\omega(0)| < \delta_\omega$:*

(1) The closed-loop system (particulate process model and controller of Eq.5.27) is exponentially stable.

(2) $\lim_{t\to\infty} |y_i - v_i| = O(\epsilon(N))$, *where v_i is the set-point for the ith controlled output and $\epsilon(N)$ is a small positive real number that depends on N and satisfies* $\lim_{N\to\infty} \epsilon(N) = 0$.

Remark 5.14: Theorem 5.2 establishes that a bounded nonlinear output feedback controller which guarantees exponential stability and output tracking in the con-

strained finite-dimensional closed-loop system (Eqs.5.13-5.27), continues to enforce the same properties locally in the constrained infinite-dimensional closed-loop system (Eqs.5.1-5.27). This result is intuitively expected because for sufficiently large N: a) the dynamics of the modes of the particulate process model which are not taken into account in the controller design (i.e., not included in the ODE model of Eq.5.13) are locally exponentially stable, and b) the control action, $u(t)$, does not influence the dynamics of the modes which are not taken into account in the controller design.

Remark 5.15: It was pointed out in Remark 5.5 that the inequality of Eq.5.29 represents the set of feasible initial conditions starting from where the constrained finite-dimensional closed-loop system (Eqs.5.13-5.27) is guaranteed to be stable. Note that owing to the infinite-dimensional nature of the particulate process model of Eq.5.1, this inequality cannot be used directly to check the feasible initial conditions for the infinite-dimensional system (this is because the amplitude of the residual modes not included in the controller design may not, in general, be negligible). Furthermore, the local nature of the result of Theorem 5.2 implies that the initial conditions, for the infinite-dimensional system, must be selected sufficiently small to guarantee exponential stability of the closed-loop system. However, the inequality of Eq.5.29 continues to provide a useful guide for the selection of the feasible initial observer states that guarantee stability of the constrained infinite-dimensional closed-loop system (Eqs.5.1-5.27). To see why this is the case, recall from Theorem 5.1 that selection of the initial observer states within the region described by Eq.5.29 guarantees stability of the constrained finite-dimensional closed-loop system (and consequently local exponential stability of the infinite-dimensional system according to Theorem 5.2). Guided by this result, we conclude that in order to guarantee stability of the constrained infinite-dimensional closed-loop system the initial observer states should, at

least, not be chosen outside this region. The region of Eq.5.29 therefore provides a reasonable initial guess for where to initiate the observer.

Remark 5.16: The exponential stability of the closed-loop system guarantees that in the presence of small initialization errors of the observer states (i.e., $\omega(0) \neq \tilde{x}(0)$), uncertainty in the process parameters and disturbances, the states of the closed-loop system will remain bounded. Furthermore, since the number of manipulated inputs and controlled outputs is finite, it is possible to implement a linear error feedback controller (for example, a proportional integral (PI) controller for single-input single-output processes) around the $(y_i - v_i)$, $i = 1, \ldots, l$, loops to ensure asymptotic offsetless output tracking in the closed-loop system, in the presence of such uncertainty.

5.7 Application to a Continuous Crystallizer with Input Constraints

In this section, the proposed nonlinear control method is used to stabilize the continuous crystallizer introduced in subsection 5.2.2 in the presence of input constraints. Motivated by the fact that the crystallizer with the crystal size distribution as controlled output and the solute feed concentration as manipulated input is an approximately controllable system (see [72] for a rigorous controllability analysis), we consider the control problem of manipulating the solute feed concentration to achieve a crystal size distribution with desired mass, i.e., the controlled output is defined as:

$$y(\bar{t}) \;=\; 8\pi\sigma^3 \int_0^\infty n(r,\bar{t})dr = \tilde{x}_0; \tag{5.35}$$

The reader may refer to [56, 63, 25, 66] for the use of other manipulated variables including fines destruction rate and crystallizer temperature for the stabilization of

crystallizers (note that the proposed control method can be used for the synthesis of nonlinear controllers when such manipulated inputs are considered).

Following the proposed methodology outlined in section 5.3, the design of the necessary bounded nonlinear output feedback controller is carried out on the basis of the low-dimensional ODE model (moment model) of Eq.5.17 which captures the dominant dynamics of the crystallizer. The controller design procedure as well as the explicit controller formula are given in section 5.6.3 of this manuscript where the controller was implemented first on the constrained ODE moment model. In this section, we implement the same controller on the constrained infinite-dimensional crystallizer model of Eq.5.5. The practical implementation of the nonlinear controllers of Eq.5.33 requires on-line measurements of the controlled output, $\tilde{x}_0$; in practice, such measurements can be obtained by using, for example, light scattering (see [5, 66] for details).

Several simulation runs were performed to evaluate the performance, robustness, and constraint-handling properties of the bounded nonlinear controller of Eq.5.33 and compare them with those of a PI controller. The values of the nonlinear controller parameters and the PI controller parameters K_c, τ_I, which were used in the simulations, are given in Table 5.2 (K_c, τ_I were computed through extensive trial and error). In all the simulation runs, the initial condition:

	Nominal conditions	with parametric uncertainty
K_c	0.5	0.5
τ_I	1.5	1.0
c	0.90	0.90
ρ	0.001	0.001
τ_i'	–	1.0

Table 5.2: Controller parameters for infinite-dimensional crystallizer model.

$$n(r,0) = 0.0,\ c(0) = 990.0\ kg/m^3$$

was used for the process model of Eq.5.5 and the finite difference method with 1000 discretization points was used for its simulation. The initial conditions for the dynamic system included in the controller of Eq.5.33 were set to be: $\omega_0 = 0.047$, $\omega_1 = 0.028$, $\omega_2 = 0.017$, $\omega_3 = 0.01$ and $\omega_4 = 0.5996$ (note that they do not correspond to the initial conditions used for the distributed parameter model in order to study the performance of the controller in the presence of significant initialization errors).

In the first set of simulation runs, the set-point tracking capability of the nonlinear controller in the presence of input constraints ($0 \leq u \leq 6$) was evaluated under nominal conditions for a 0.4 increase in the value of the set-point ($v = 0.4$). Figure 5.6 shows the closed-loop output (top plot) and manipulated input (middle plot) profiles obtained by using the bounded nonlinear controller (solid lines) of Eq.5.33. For the sake of comparison, the corresponding profiles under PI control are also included (dashed lines). Clearly, the bounded nonlinear controller drives the controlled output to its new set-point value in a significantly shorter time than the one required by the PI controller (note that both controlled outputs exhibit the same overshoot). Note also the superior transient behavior of the closed-loop output under the bounded nonlinear controller compared to the oscillatory response obtained under PI control. For the same simulation run, the evolution of the closed-loop profile of the crystal size distribution is shown in Figure 5.6 (bottom plot.) An exponentially-decaying crystal size distribution is obtained at the steady-state.

Next, the robustness properties of the bounded nonlinear controller in the presence of parametric uncertainties were investigated, for a 0.4 increase in the value of the set-point. To ensure offsetless tracking in the presence of constant uncertainty in

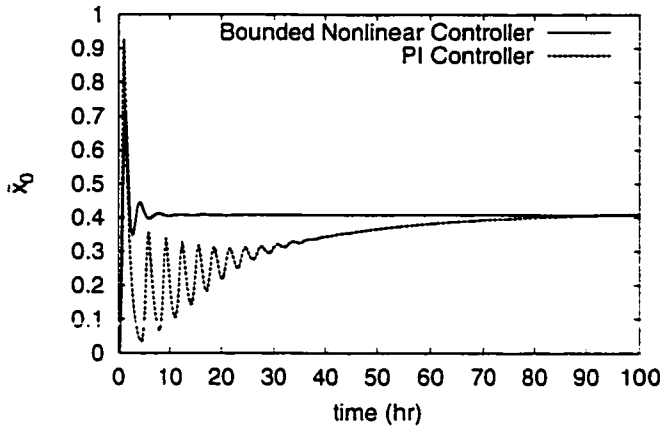

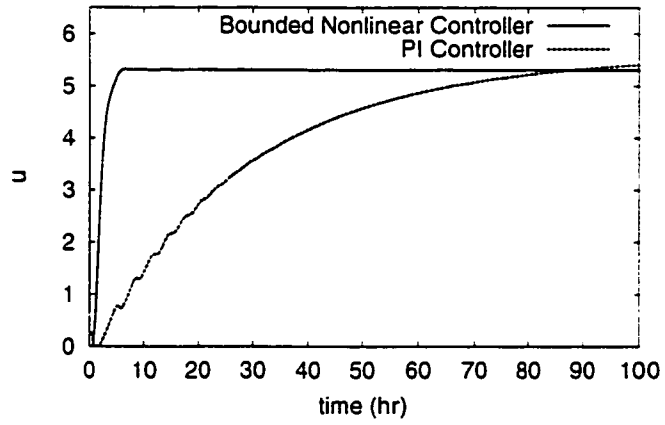

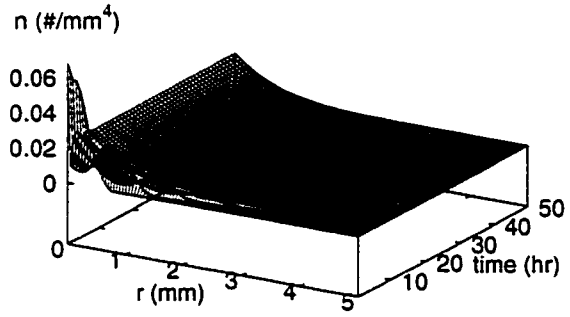

Figure 5.6: Controlled output, manipulated input, and crystal size distribution profiles for the crystallizer process model of Eq.5 under bounded nonlinear controller (solid line) and PI controller (dashed line) for 0.4 increase in the set-point and $u \in [0, 6]$.

process parameters, the bounded nonlinear controller of Eq.5.33 was complemented with integral action (i.e., the term $v - \bar{h}(\omega)$ was substituted by $v - y + \frac{1}{\tau_i'}\xi$, where $\dot{\xi} = v - y$, $\xi(0) = 0$ and τ_i' is the integral time constant). Figure 5.7 shows the closed-loop output (top plot), manipulated input (middle plot), and evolution of the crystal size distribution (bottom plot) profiles under the bounded nonlinear controller (solid lines) in the presence of 5% error in both F and τ. The corresponding output and input profiles under PI control are also included (dashed lines). We observe that the bounded nonlinear controller exhibits very good robustness properties, driving the output quickly to its new set-point.

Finally, we tested the robustness of the bounded nonlinear controller in the presence of unmodeled actuator and sensor dynamics. To account for the actuator and sensor dynamics, the process model of Eq.5.5 was augmented with the dynamical system $\epsilon_a \dot{z}_1 = -z_1 + z_2$, $\epsilon_a \dot{z}_2 = -z_2 + u$ and the dynamical system $\epsilon_s \dot{z}_3 = -z_3 + z_4$, $\epsilon_s \dot{z}_4 = -z_4 + y$, where $z_1, z_2 \in \mathbb{R}$ are the actuator states, $z_3, z_4 \in \mathbb{R}$ are the sensor states, z_1 is the actuator output, z_3 is the sensor output, and ϵ_a, ϵ_s are small parameters characterizing how fast the actuator and sensor dynamics are, respectively. In this case, the bounded nonlinear controller was also found to be robust with respect to unmodeled dynamics for $\epsilon_a = \epsilon_s = 0.05$. The corresponding closed-loop output (top plot), manipulated input (middle plot), and evolution of crystal size distribution (bottom plot) profiles are depicted in Figure 5.8.

5.8 Conclusions

In this chapter, we considered spatially-homogeneous particulate processes with input constraints and developed a rigorous and general methodology for the analysis and control of such processes. Initially, a model reduction procedure based on the

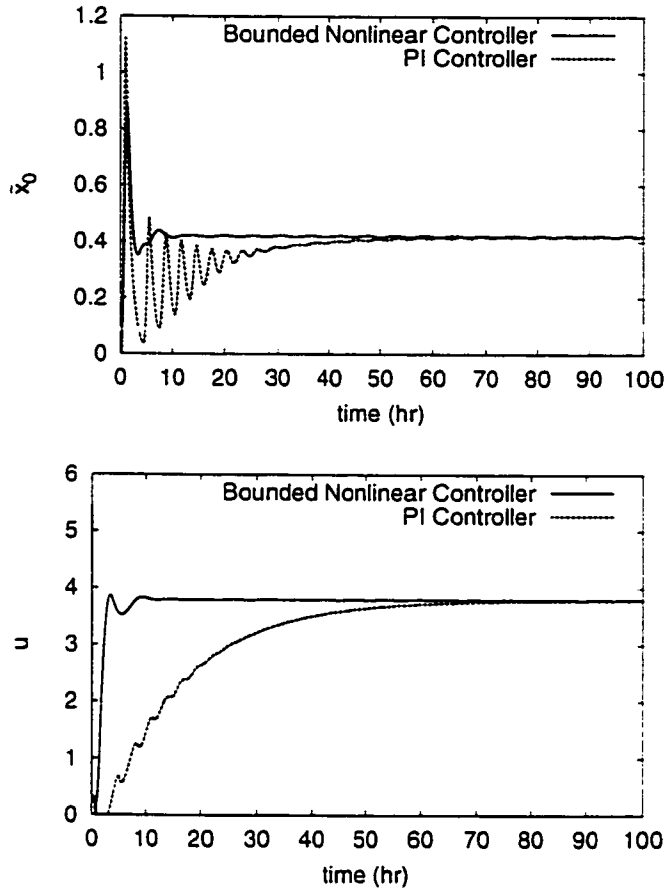

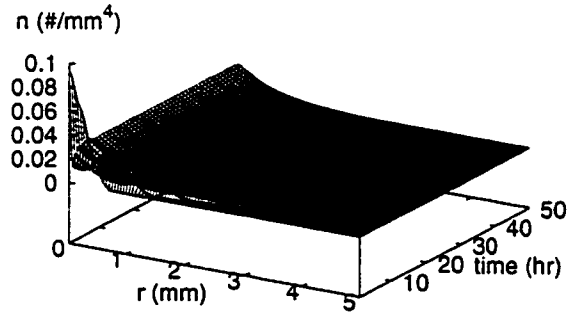

Figure 5.7: Controlled output, manipulated input, and crystal size distribution evolution profiles for the crystallizer process model of Eq.5 under bounded nonlinear controller for 0.4 increase in the set-point in the presence of 5% modeling error in both F and τ and $u \in [0, 6]$.

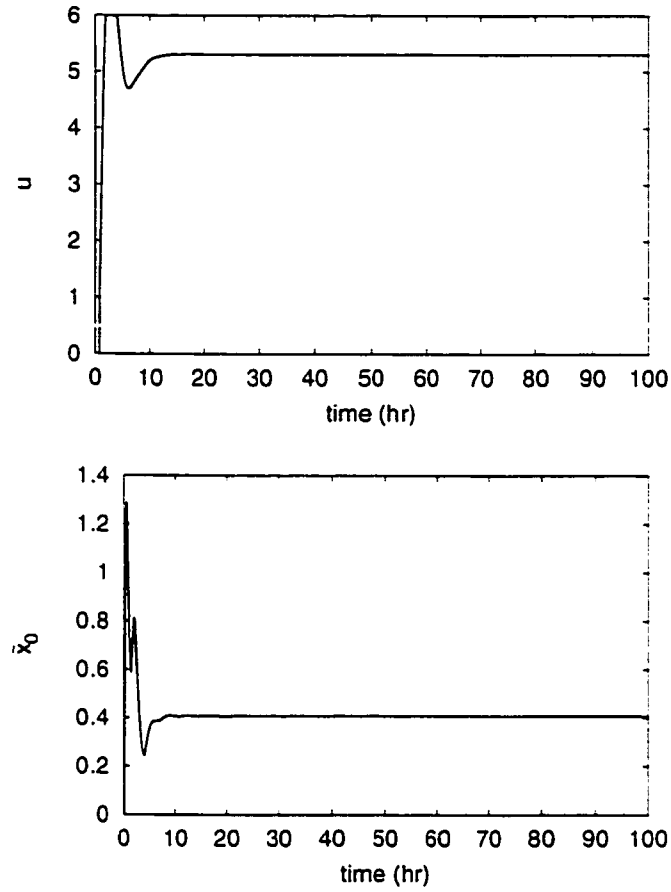

Figure 5.8: Controlled output, manipulated input, and crystal size distribution evolution profiles for the crystallizer process model of Eq.5 under bounded nonlinear controller for 0.4 increase in the set-point in the presence of actuator and sensor unmodeled dynamics and $u \in [0, 6]$.

method of weighted residuals was presented for the construction of finite-dimensional ODE systems that accurately reproduce the dynamics of the particulate process. These ODE systems were then used to identify the set of feasible control objectives (set-points) that can be achieved in the presence of constraints. This information together with the derived ODE systems was then used as the basis for the synthesis of practically-implementable nonlinear bounded output feedback controllers that enforce exponential stability in the closed-loop system and achieve particle size distributions with desired characteristics, in the presence of active input constraints. Precise closed-loop stability conditions were given and controller implementation issues were addressed. The proposed methodology was successfully applied to a continuous crystallizer, which exhibits open-loop unstable (oscillatory) behavior, and shown to cope effectively with the problem of constraints.

Chapter 6

Conlusions

The present doctoral thesis has focused on the development of a general and practical framework, for the synthesis of nonlinear control systems for particulate processes based on population balance models that systematically addresses the problems of modification of the input/output behavior, attenuation of the effect unmeasured disturbances and unknown parameters, and handling of hard constraints in the capacity of the control actuators. The proposed control algorithms were succesfully applied to crystallization processes. Specifically, the main contributions of this dissertation can be summarized as follows:

1. **Nonlinear control of particulate processes.** A general method was developed for the synthesis of practically implementable nonlinear model-based feedback controllers that enforce the desired stability and performance specifications (such as PSDs with desired total mass and mean particle size) in the closed-loop system. A a model reduction procedure based on a combination of the method of weighted residuals and the concept of approximate inertial manifold was proposed and used for the construction of low-order ODE systems that accurately reproduce the dominant dynamics of the particulate process. These

ODE systems were subsequently used for the synthesis of nonlinear low-order output feedback controllers that enforce exponential stability in the closed-loop system and achieve a desired particle size distribution. Precise closed-loop stability conditions are given and controller implementation issues are addressed.

2. **Robust control of particulate processes.** A general method was proposed for the synthesis of practically-implementable robust nonlinear controllers that explicitly handle time-varying uncertain variables (e.g., unknown process parameters and disturbances) and unmodeled dynamics (e.g., fast actuator and sensor dynamics not included in the process model). The robust nonlinear controllers were synthesized via Lyapunov's direct method and were shown to enforce stability in the closed-loop system and attenuation of the effect of uncertain variables on the outputs, and achieve particle size distributions with desired characteristics.

3. **Constrained control of particulate processes.** We developed a general methodology for the analysis and control of constrained particulate processes modeled by population balance equations. Using finite-dimensional ODE approximations of the population balances, we characterized the limitations imposed by input constraints on our ability to modify the dynamics of the particulate process and provided an explicit characterization of the set of admissible set-points that can be achieved in the presence of constraints. This information together with the derived ODE systems was then used as the basis for the synthesis of practically-implementable nonlinear bounded output feedback controllers that enforce exponential stability in the closed-loop system and achieve particle size distributions with desired characteristics in the presence of active input constraints.

4. **Application to crystallization processes.** The developed control methods were successfully applied to a batch crystallization process, and to continuous crystallizers with and without fines dissolver.

Appendix A

Proofs of Chapter 2

Proof of Proposition 2.1: To simplify the notation of the proof, we assume that the growth rate $G(x,r)$ is independent of r. Furthermore, since the nonlinear terms $w(n,x,r), a(n,r,x)$ are smooth functions of their arguments, they can be exactly expanded in an infinite series as follows:

$$\begin{aligned} w(n,x,r) &= \sum_{k=1}^{\infty} b_k(x,a_k,t)\phi_k(r) \\ a(n,r,x) &= \sum_{k=1}^{\infty} c_k(x,a_k,t)\phi_k(r) \end{aligned} \tag{A.1}$$

where $b_k(x,a_k,t), c_k(x,a_k,t)$ are coefficients and $\phi_k(r)$, $k=1,\ldots,\infty$ is the complete set of basis functions used to expand $n(r,t)$ in Eq.5.8. Using that $G(x,r)$ is independent of r and the expansions of Eq.A.1, the infinite dimensional system of Eq.5.10 can be written as:

$$\begin{aligned} \int_0^{r_{max}} \psi_\nu(r)\sum_{k=1}^{\infty}\phi_k(r)\frac{\partial a_k(t)}{\partial t}dr &= -G(x)\sum_{k=1}^{\infty}a_k(t)\int_0^{r_{max}}\psi_\nu(r)\frac{\partial \phi_k(r)}{\partial r}dr \\ &\quad + \int_0^{r_{max}}\psi_\nu(r)\sum_{k=1}^{\infty}b_k(x,a_k,t)\phi_k(r)dr, \quad \nu=1,\ldots,\infty \\ \dot{x} &= f(x) + A\int_0^{r_{max}}\sum_{k=1}^{\infty}c_k(x,a_k,t)\phi_k(r)dr \end{aligned} \tag{A.2}$$

while the truncated system of Eq.2.20 takes the form:

$$\begin{aligned}\int_0^{r_{max}} \psi_\nu(r)\sum_{k=1}^{N}\phi_k(r)\frac{\partial a_{kN}(t)}{\partial t}dr &= -G(x_N)\sum_{k=1}^{N}a_{kN}(t)\int_0^{r_{max}}\psi_\nu(r)\frac{\partial \phi_k(r)}{\partial r}dr \\ &\quad +\int_0^{r_{max}}\psi_\nu(r)\sum_{k=1}^{N}b_k(x_N,a_{kN},t)\phi_k(r)dr, \\ \nu &= 1,\ldots,N \\ \dot{x}_N &= f(x_N)+A\int_0^{r_{max}}\sum_{k=1}^{N}c_k(x_N,a_{kN},t)\phi_k(r)dr\end{aligned} \tag{A.3}$$

Defining the error variables $e_n = n(r,t) - n_N(r,t) = \sum_{k=1}^{\infty}a_k(t)\phi_k(r) - \sum_{k=1}^{N}a_{kN}(t)\phi_k(r)$ and $e_x = x(t) - x_N(t)$ and computing the difference between Eq.A.2 and Eq.A.3, we get:

$$\begin{aligned}\int_0^{r_{max}}\psi_\nu(r)\frac{\partial e_n}{\partial t}dr &= -G(x)\int_0^{r_{max}}\psi_\nu(r)\frac{\partial n}{\partial r}dr + G(x_N)\int_0^{r_{max}}\psi_\nu(r)\frac{\partial n_N}{\partial r}dr \\ &\quad +\int_0^{r_{max}}\psi_\nu(r)\sum_{k=1}^{\infty}b_k(x,a_k,t)\phi_k(r)dr \\ &\quad -\int_0^{r_{max}}\psi_\nu(r)\sum_{k=1}^{N}b_k(x_N,a_{kN},t)\phi_k(r)dr \\ \dot{e}_x &= f(x)-f(x_N)+A\int_0^{r_{max}}\sum_{k=1}^{\infty}c_k(x,a_k,t)\phi_k(r)dr \\ &\quad -A\int_0^{r_{max}}\sum_{k=1}^{N}c_k(x_N,a_{kN},t)\phi_k(r)dr\end{aligned} \tag{A.4}$$

The above error system is locally exponentially stable (this follows from the assumption that the system of Eq.2.20 is locally exponentially stable for any N), and thus, applying standard results from perturbation theory [47], we obtain the following bound for $e_n(r,t), e_x(t)$ for all $t \geq 0$:

$$\begin{aligned}e_n(r,t) &= O(\epsilon(N)) \\ e_x(t) &= O(\epsilon(N))\end{aligned} \tag{A.5}$$

From the above result, the estimates of Eq.2.21 follow directly. $\triangle$

Proof of Proposition 2.2: To prove that local exponential stability of the system of Eq.5.13 ensures local exponential stability of the system of Eq.2.20, we need to show that the off manifold transients decay exponentially. To this end, we define $e_m = a_{fN} - \tilde{\Sigma}_{l+1}(\tilde{x}) = a_{fN} - \tilde{a}_{fN}$ and compute $\dot{a}_{fN}$:

$$\dot{e}_m = \tilde{A}a_{fN} + \tilde{f}_q(a_{fN}, \tilde{x}) - \dot{\tilde{a}}_{fN} \tag{A.6}$$

From the definition of the approximate inertial manifold $\dot{\tilde{a}}_{fN} \equiv \hat{0} = \tilde{A}\tilde{a}_{fN} + \tilde{f}_q(\tilde{a}_{fN}, \tilde{x})$, and thus, the system of Eq.A.6 can be written as:

$$\begin{aligned} \dot{e}_m &= \tilde{A}a_{fN} + \tilde{f}_q(a_{fN}, \tilde{x}) - \tilde{A}\tilde{a}_{fN} - \tilde{f}_q(\tilde{a}_{fN}, \tilde{x}) \\ &= \tilde{A}e_m + \tilde{f}_q(a_{fN}, \tilde{x}) - \tilde{f}_q(\tilde{a}_{fN}, \tilde{x}) \end{aligned} \tag{A.7}$$

Since $\tilde{A}$ is Hurwitz, the terms $\tilde{f}_q(a_{fN}, \tilde{x}), \tilde{f}_q(\tilde{a}_{fN}, \tilde{x})$ do not include linear terms and the system of Eq.5.13 is locally exponentially stable, one can show that the linearization of the system of Eq.2.26 is exponentially stable, and thus, the nonlinear system is locally exponentially stable.

To establish the closeness of solutions result, we exploit the fact that the local exponential stability implies [47] $a_{kN}(t) = \tilde{a}_{kN}(t) + \bar{\epsilon}(\bar{l})$, and also that $\Sigma(\tilde{x}) = \tilde{\Sigma}_{l+1}(\tilde{x}) + \bar{\epsilon}(\bar{l})$, as $t \to \infty$. Computing the discrepancy $\lim_{t\to\infty} ||n_N - \bar{n}_N||_2$, using the above estimates, it can be shown that $\lim_{t\to\infty} ||n_N - \bar{n}_N||_2 = O(\bar{\epsilon}(\bar{l}))$. $\triangle$

Proof of Theorem 2.1: Under the controller of Eq.2.39, the closed-loop system takes the form:

$$\begin{aligned} \frac{d\omega}{dt} &= \tilde{f}(\omega) + L(y - \tilde{h}(\omega)) + \tilde{g}(\omega)\left\{[\beta_{1r_1} \cdots \beta_{mr_m}]C(\omega)\right\}^{-1}\left\{v - \sum_{i=1}^{m}\sum_{k=0}^{r_i}\beta_{ik}L_{\tilde{f}}^{k}\tilde{h}_i(\omega)\right\} \\ \frac{\partial n}{\partial t} &= -\frac{\partial(G(x,r)n)}{\partial r} + w(n,x,r) \\ \dot{x} &= f(x) + A\int_0^{r_{max}} a(n,r,x)dr \\ &\quad + g(x)\left\{[\beta_{1r_1} \cdots \beta_{mr_m}]C(\omega)\right\}^{-1}\left\{v - \sum_{i=1}^{m}\sum_{k=0}^{r_i}\beta_{ik}L_{\tilde{f}}^{k}\tilde{h}_i(\omega)\right\} \end{aligned} \tag{A.8}$$

Applying the method of weighted residuals to the above system, we obtain the following approximate ODE system:

$$\begin{aligned}
\frac{d\omega}{dt} &= \bar{f}(\omega) + L(y - \bar{h}(\omega)) \\
&\quad + \bar{g}(\omega)\left\{[\beta_{1r_1}\cdots\beta_{mr_m}]C(\omega)\right\}^{-1} \\
&\quad \times \left\{v - \sum_{i=1}^{m}\sum_{k=0}^{r_i}\beta_{ik}L_{\bar{f}}^{k}\bar{h}_i(\omega)\right\} \\
\int_0^{r_{max}}\psi_\nu(r)\sum_{k=1}^{N}\phi_k(r)\frac{\partial a_{kN}(t)}{\partial t}dr &= -\sum_{k=1}^{N}a_{kN}(t)\int_0^{r_{max}}\psi_\nu(r)\frac{\partial(G(x_N,r)\phi_k(r))}{\partial r}dr \\
&\quad + \int_0^{r_{max}}\psi_\nu(r)w(\sum_{k=1}^{N}a_{kN}(t)\phi_k(r), x_N, r)dr, \\
&\quad \nu = 1,\ldots,N \\
\dot{x}_N &= f(x_N) + A\int_0^{r_{max}}a(\sum_{k=1}^{N}a_{kN}(t)\phi_k(r), r, x_N)dr \\
&\quad + g(x_N)\left\{[\beta_{1r_1}\cdots\beta_{mr_m}]C(\omega)\right\}^{-1} \\
&\quad \times \left\{v - \sum_{i=1}^{m}\sum_{k=0}^{r_i}\beta_{ik}L_{\bar{f}}^{k}\bar{h}_i(\omega)\right\}
\end{aligned} \tag{A.9}$$

Using the vector notation $a_N = [a_{1N}\ \cdots\ a_{NN}]^T$, the above system can be written as:

$$\begin{aligned}
\frac{d\omega}{dt} &= \bar{f}(\omega) + L(y - \bar{h}(\omega)) + \bar{g}(\omega)\left\{[\beta_{1r_1}\cdots\beta_{mr_m}]C(\omega)\right\}^{-1}\left\{v - \sum_{i=1}^{m}\sum_{k=0}^{r_i}\beta_{ik}L_{\bar{f}}^{k}\bar{h}_i(\omega)\right\} \\
\dot{a}_N &= \bar{f}(a_N, x_N) \\
\dot{x}_N &= f(x_N) + A\int_0^{r_{max}}a(\sum_{k=1}^{N}a_{kN}(t)\phi_k(r), x_N, r)dr \\
&\quad + g(x_N)\left\{[\beta_{1r_1}\cdots\beta_{mr_m}]C(\omega)\right\}^{-1}\left\{v - \sum_{i=1}^{m}\sum_{k=0}^{r_i}\beta_{ik}L_{\bar{f}}^{k}\bar{h}_i(\omega)\right\}
\end{aligned} \tag{A.10}$$

where the explicit form of the nonlinear function $\bar{f}(a_N, x_N)$ is omitted for brevity. Exploiting the orthogonality of the basis functions $\phi_k(r)$ and using the expression for

n_N of Eq.2.24, we can write the system of Eq.A.10 as:

$$\begin{aligned}
\frac{d\omega}{dt} &= \bar{f}(\omega) + L(y - \bar{h}(\omega)) + \bar{g}(\omega)\left\{[\beta_{1r_1}\cdots\beta_{mr_m}]C(\omega)\right\}^{-1}\left\{v - \sum_{i=1}^{m}\sum_{k=0}^{r_i}\beta_{ik}L_{\bar{f}}^{k}\bar{h}_i(\omega)\right\} \\
\dot{a}_{sN} &= \bar{f}_p(a_{sN}, a_{fN}, x_N) \\
\dot{a}_{fN} &= \bar{f}_q(a_{sN}, a_{fN}, x_N) \\
\dot{x}_N &= f(x_N) + A\int_0^{r_{max}} a(n_p + n_q, x_N, r)dr \\
&\quad + g(x_N)\left\{[\beta_{1r_1}\cdots\beta_{mr_m}]C(\omega)\right\}^{-1}\left\{v - \sum_{i=1}^{m}\sum_{k=0}^{r_i}\beta_{ik}L_{\bar{f}}^{k}\bar{h}_i(\omega)\right\}
\end{aligned} \tag{A.11}$$

where $\bar{f} = [\bar{f}_p^T \ \bar{f}_q^T]^T$, $a_{sN} = [a_{1N} \ \cdots a_{pN}]^T$, and $a_{fN} = [a_{(p+1)N} \ \cdots a_{NN}]^T$. Defining the observer error vector $e_o = \omega - \tilde{x}$, using the assumption $C_L = \frac{1}{\mu}\bar{A}$ where $\bar{A}$ is a Hurwitz matrix, and multiplying the $\dot{e}_o$-subsystem by μ, the system of Eq.A.11 can be written as:

$$\begin{aligned}
\mu\frac{de_o}{dt} &= \bar{A}e_o + \mu\hat{f}(\omega, \tilde{x}, v) \\
\dot{a}_{sN} &= \bar{f}_p(a_{sN}, a_{fN}, x_N) \\
\dot{a}_{fN} &= \bar{f}_q(a_{sN}, a_{fN}, x_N) \\
\dot{x}_N &= f(x_N) + A\int_0^{r_{max}} a(n_p + n_q, x_N, r)dr \\
&\quad + g(x_N)\left\{[\beta_{1r_1}\cdots\beta_{mr_m}]C(\omega)\right\}^{-1}\left\{v - \sum_{i=1}^{m}\sum_{k=0}^{r_i}\beta_{ik}L_{\bar{f}}^{k}\bar{h}_i(\omega)\right\}
\end{aligned} \tag{A.12}$$

where $\hat{f}(\omega, \tilde{x}, v)$ is a nonlinear vector function. The above system is in singularly perturbed form (see [47] for details) and possesses an exponentially stable fast subsystem: $\frac{de_o}{d\tau} = \bar{A}e_o$, where $\tau = t/\mu$, and a slow subsystem that has the form:

$$\begin{aligned}
\dot{a}_{sN} &= \bar{f}_p(a_{sN}, a_{fN}, x_N) \\
\dot{a}_{fN} &= \bar{f}_q(a_{sN}, a_{fN}, x_N) \\
\dot{x}_N &= f(x_N) + A\int_0^{r_{max}} a(n_p + n_q, x_N, r)dr \\
&\quad + g(x_N)\left\{[\beta_{1r_1}\cdots\beta_{mr_m}]C(\tilde{x})\right\}^{-1}\left\{v - \sum_{i=1}^{m}\sum_{k=0}^{r_i}\beta_{ik}L_{\bar{f}}^{k}\bar{h}_i(\tilde{x})\right\}
\end{aligned} \tag{A.13}$$

Setting $a_{fN} = \bar{\Sigma}_{l+1}(a_{sN}, x_N)$ (model reduction based on the concept of approximate

inertial manifold) and using the notation of subsection 2.3.4, we finally obtain:

$$\begin{aligned} \dot{\tilde{x}} &= \tilde{f}(\tilde{x}) + \tilde{g}(\tilde{x})\{[\beta_{1r_1}\cdots\beta_{mr_m}]C(\tilde{x})\}^{-1}\left\{v - \sum_{i=1}^{m}\sum_{k=0}^{r_i}\beta_{ik}L_{\tilde{f}}^{k}\tilde{h}_i(\tilde{x})\right\} \\ y_{si} &= \tilde{h}_i(\tilde{x}),\ \ i = 1,\ldots,m \end{aligned} \tag{A.14}$$

Using assumptions 2 and 3 of the theorem, one can show that the above system is locally exponentially stable and $\lim_{t\to\infty}|y_{si} - v_i| = 0$. From the assumption that $\bar{l}$ is sufficiently large and Proposition 2.2, we have that the systems of Eq.A.13 and Eq.A.14 possess the same stability properties, and thus, the slow subsystem of Eq.A.13 is also locally exponentially stable. The local exponential stability of the fast and slow subsystems implies [47] that there exists a μ^* such that if $\mu \in (0, \mu^*]$, then the closed-loop system of Eq.A.11 is locally exponentially stable. From the closeness of solutions results of Propositions 2.1 and 2.2, the asymptotic output tracking result $\lim_{t\to\infty}|y_i - v_i| = O(\hat{\epsilon}(N + \bar{l}))$ then follows. $\triangle$

Appendix B

Proof of Chapter 4

Proof of Theorem 4.1 : Substituting the controller of Eq.4.19 into the particulate process model of Eq.5.1, we obtain:

$$\begin{aligned}
\frac{\partial n}{\partial t} &= -\frac{\partial (G(x,r)n)}{\partial r} + \bar{w}(n,x,r,z,\theta(t)) + \bar{g}_1(n,x,r)a(\tilde{x},\bar{v},t), \quad n(0,t) = b(x(t)) \\
\dot{x} &= \bar{f}(x) + Q_1(x)z + \bar{g}_2(x)a(\tilde{x},\bar{v},t) + \bar{g}_3(x,\theta(t),\int_0^{r_{max}} a_2(n,r,x)dr) \\
\epsilon\dot{z} &= \bar{f}(x) + Q_2(x)z + \bar{g}_2(x)a(\tilde{x},\bar{v},t) + \bar{g}_3(x,\theta(t),\int_0^{r_{max}} a_2(n,r,x)dr)
\end{aligned} \tag{B.1}$$

Performing a decomposition of the above system into the fast and slow time-scales, we obtain the following system that describes the fast dynamics of the closed-loop system:

$$\frac{dz}{d\tau} = \bar{f}(x) + Q_2(x)z + \bar{g}_2(x)a(\tilde{x},\bar{v},t) + \bar{g}_3(x,\theta(t),\int_0^{r_{max}} a_2(n,r,x)dr) \tag{B.2}$$

Since the feedback law $a(\tilde{x},\bar{v},t)$ does not use feedback of the fast state z, the above system is exponentially stable. Setting $\epsilon = 0$, the system that describes the slow dynamics of the closed-loop system is obtained:

$$\begin{aligned}
\frac{\partial n}{\partial t} &= -\frac{\partial (G(x,r)n)}{\partial r} + w(n,x,r,\theta(t)) + g_1(n,x,r)a(\tilde{x},\bar{v},t), \quad n(0,t) = b(x(t)) \\
\dot{x} &= f(x) + g_2(x)a(\tilde{x},\bar{v},t) + g_3(x,\theta(t),\int_0^{r_{max}} a_2(n,r,x)dr)
\end{aligned} \tag{B.3}$$

Applying the method of weighted residuals to the above system, we obtain:

$$\begin{aligned}
\int_0^{r_{max}} \psi_\nu(r) \sum_{k=1}^{N} \phi_k(r) \frac{\partial a_{kN}(t)}{\partial t} dr &= -\sum_{k=1}^{N} a_{kN}(t) \int_0^{r_{max}} \psi_\nu(r) \frac{\partial (G(x_N, r)\phi_k(r))}{\partial r} dr \\
&\quad + \int_0^{r_{max}} \psi_\nu(r) w(\sum_{k=1}^{N} a_{kN}(t)\phi_k(r), x_N, r, \theta(t)) dr \\
&\quad + \int_0^{r_{max}} \psi_\nu(r) g_1(\sum_{k=1}^{N} a_{kN}(t)\phi_k(r), x_N, r) a(\tilde{x}, \bar{v}, t) dr, \\
&\quad \nu = 1, \ldots, N \\
\dot{x}_N &= f(x_N) + g_2(x_N) a(\tilde{x}, \bar{v}, t) \\
&\quad + g_3(x_N, \theta(t), \int_0^{r_{max}} a_2(\sum_{k=1}^{N} a_{kN}(t)\phi_k(r), r, x_N) dr) \\
y_{si}(t) &= h_i(\int_0^{r_{max}} c_\kappa \sum_{k=1}^{N} a_{kN}(t)\phi_k(r) dr, x_N), \\
&\quad i = 1, \ldots, m, \quad \kappa = 1, \ldots, l
\end{aligned} \tag{B.4}$$

or using the vector notation:

$$\begin{aligned}
\dot{\tilde{x}} &= \tilde{f}(\tilde{x}) + \sum_{i=1}^{m} \tilde{g}_i(\tilde{x}) a_i(\tilde{x}, \bar{v}, t) + \tilde{w}(\tilde{x}, \theta) \\
y_{si} &= \tilde{h}_i(\tilde{x}), \quad i = 1, \ldots, m
\end{aligned} \tag{B.5}$$

For the above system we have shown in [14] that there exists a $\phi \in (0, \phi^*]$ such that if

$\max\{|\tilde{x}(0)|, ||\theta||, ||\dot{\theta}||, ||\bar{v}||\} \leq \delta$, then its state is bounded and its outputs satisfy $\limsup_{t\to\infty} |y_{si}(t) - v_i| \leq O(\phi)$, $i = 1, \ldots, l$. Finally, since the fast subsystem of Eq.B.2 is exponentially stable, we can use standard stability results for singularly perturbed systems to obtain that if $\max\{|x(0)|, ||\eta(0)||_2, ||\theta||, ||\dot{\theta}||, ||\bar{v}||\} \leq \delta$, then the state of the closed-loop system is bounded and that its outputs satisfy the relation of Eq.4.20. $\triangle$

Appendix C

Proofs of Chapter 5

Proof of Theorem 5.1 : Consider the representation of the system of Eq.5.13 in the form of Eqs.5.21-5.22. Under the controller of Eq.5.27, the closed-loop system takes the following form

$$\begin{aligned}
\frac{d\omega}{dt} &= \tilde{f}(\omega) - \frac{1}{2}\tilde{g}(\omega)R^{-1}(\omega)I\left(L_{\tilde{g}}V(\omega)\right)^T + L(y - \tilde{h}(\omega)) \\
\dot{e} &= Ae + B\left[l_1(e,\eta,\bar{v}) - \frac{1}{2}C(\tilde{x})R^{-1}(\omega)I\left(L_{\tilde{g}}V(\omega)\right)^T\right] \\
\dot{\eta}_1 &= \Psi_1(\zeta,\eta) \\
&\vdots \\
\dot{\eta}_{(n+N)-\sum_i r_i} &= \Psi_{(n+N)-\sum_i r_i}(\zeta,\eta) \\
y_{s_i} &= \zeta_1^{(i)}, \quad i = 1,\ldots,m
\end{aligned} \tag{C.1}$$

Defining the observer error vector $e_o = \omega - \tilde{x}$, using the assumption $C_L = \frac{1}{\mu}\bar{A}$ where $\bar{A}$ is a Hurwitz matrix, and multiplying the $\dot{e}_o$-subsystem by μ, the system of Eq.C.1

can be written as:

$$\begin{aligned}
\mu\frac{de_o}{dt} &= \bar{A}e_o + \mu\hat{f}(\omega,\tilde{x},v) \\
\dot{e} &= Ae + B\left[l_1(e,\eta,\bar{v}) - \frac{1}{2}C(\tilde{x})R^{-1}(\omega)I\left(L_{\bar{g}}V(\omega)\right)^T\right] \\
\dot{\eta}_1 &= \Psi_1(\zeta,\eta) \\
&\vdots \\
\dot{\eta}_{(n+N)-\sum_i r_i} &= \Psi_{(n+N)-\sum_i r_i}(\zeta,\eta) \\
y_{s_i} &= \zeta_1^{(i)},\ \ i=1,\ldots,m
\end{aligned} \tag{C.2}$$

where $\hat{f}(\omega,\tilde{x},v)$ is a nonlinear vector function. The above system is in singularly perturbed form (see [47] for details) and possesses an exponentially stable fast subsystem: $\frac{de_o}{d\tau} = \bar{A}e_o$, where $\tau = t/\mu$, and a slow subsystem that has the form:

$$\begin{aligned}
\dot{e} &= Ae + B\left[l_1(e,\eta,\bar{v}) - \frac{1}{2}C(\tilde{x})R^{-1}(\tilde{x})I\left(L_{\bar{g}}V(\tilde{x})\right)^T\right] \\
\dot{\eta}_1 &= \Psi_1(\zeta,\eta) \\
&\vdots \\
\dot{\eta}_{(n+N)-\sum_i r_i} &= \Psi_{(n+N)-\sum_i r_i}(\zeta,\eta) \\
y_{s_i} &= \zeta_1^{(i)},\ \ i=1,\ldots,m
\end{aligned} \tag{C.3}$$

Consider now the Lyapunov function candidate $V = e^TPe$ introduced in theorem 5.1. Evaluating the time-derivative of this function along the trajectories of the closed-loop slow e-subsystem in Eq.C.3, we obtain

$$\begin{aligned}
\dot{V} &= L_{\bar{f}}V + L_{\bar{g}}Vu \\
&= L_{\bar{f}}V - L_{\bar{g}}V\frac{L_{\bar{f}}^*V + \sqrt{(L_{\bar{f}}^*V)^2 + \left(u_{max}^2(L_{\bar{g}}V)(L_{\bar{g}}V)^T\right)^2}}{(L_{\bar{g}}V)(L_{\bar{g}}V)^T\left[1+\sqrt{1+u_{max}^2(L_{\bar{g}}V)(L_{\bar{g}}V)^T}\right]}(L_{\bar{g}}V)^T \\
&= \frac{-\rho|e|^2 + L_{\bar{f}}V\sqrt{1+u_{max}^2(L_{\bar{g}}V)(L_{\bar{g}}V)^T} - \sqrt{(L_{\bar{f}}^*V)^2 + \left(u_{max}^2(L_{\bar{g}}V)(L_{\bar{g}}V)^T\right)^2}}{\left[1+\sqrt{1+u_{max}^2(L_{\bar{g}}V)(L_{\bar{g}}V)^T}\right]}
\end{aligned} \tag{C.4}$$

It is clear from the above equation and the fact that $\rho > 0$ that whenever $L_{\bar{f}}^*V \leq 0$,

we have $L_{\bar{f}}V \leq 0$ and the time-derivative of V satisfies

$$\dot{V} \leq \frac{-\rho|e|^2}{\left[1+\sqrt{1+u_{max}^2(L_{\bar{g}}V)(L_{\bar{g}}V)^T}\right]} < 0 \quad \forall \ e \neq 0 \tag{C.5}$$

Furthermore, whenever $0 < L_{\bar{f}}^*V \leq u_{max}|L_{\bar{g}}V|$, we have $\sqrt{(L_{\bar{f}}^*V)^2 + (u_{max}^2(L_{\bar{g}}V)(L_{\bar{g}}V)^T)^2} \geq L_{\bar{f}}V\sqrt{1+u_{max}^2(L_{\bar{g}}V)(L_{\bar{g}}V)^T}$ and $\dot{V}$ satisfies Eq.C.5. Summarizing, we have that whenever $L_{\bar{f}}^*V \leq u_{max}|L_{\bar{g}}V|$, the closed-loop slow e-subsystem is asymptotically stable. Therefore, given any positive real number δ_x such that $|\tilde{x}(0)| \leq \delta_x$ (and Eq.5.29 holds for all $|\tilde{x}| \leq \delta_x$), there exists a positive real number M such that $|\tilde{x}(t)| \leq M \ \forall \ t \geq 0$ (i.e. the closed-loop trajectories are bounded) and, consequently, the denominator expression in Eq.C.5 is bounded. It follows then that there exists a positive real number k_1 such that $\dot{V} \leq -k_1|e|^2$ and the origin of the closed-loop slow e-subsystem is exponentially stable. Therefore, the following inequality holds for the e-states of the closed-loop slow system

$$|e(t)| \leq K_e|e(0)|e^{-a_1 t} \quad \forall \ t \geq 0 \tag{C.6}$$

for some $K_e \geq 1, a_1 > 0$. From assumption 2, we have that the η states of the closed-loop slow system satisfy the following inequality

$$|\eta(t)| \leq K_\eta|\eta(0)|e^{-at} + \gamma_\eta(||e||) \quad \forall \ t \geq 0 \tag{C.7}$$

for some $K_\eta \geq 1, a > 0$, where γ_η is a class K function . At this point, one can show, using the results in [20], that the inequalities of Eqs.C.6-C.7 continue to hold, for the states of the closed-loop singularly perturbed system of Eq.C.2, up to an arbitrarily small offset, d, for initial conditions in arbitrarily large compact subsets of the region described by Eq.5.29, provided that the singular perturbation parameter μ is sufficiently small. This offset can be selected to be sufficiently small such that, after a sufficiently large time (when the exponential terms in Eqs.C.6-C.7 die out), the states of the closed-loop system are confined within a small ball centered around the

origin. Direct application then of the result of theorem 9.3 in [47] yields that there exists a μ^* such that if $\mu \leq \mu^*$, the closed-loop system of Eq.C.2 is exponentially stable (A somewhat similar argument was used in the proof of theorem 1 in [28], see this reference for mathematical details.) It follows then that

$$|e(t)| \leq \alpha |e(0)| e^{-\beta t} \quad \forall \ t \geq 0 \tag{C.8}$$

for some $\alpha \geq 1$ and $\beta > 0$. The asymptotic output tracking result can be easily obtained by taking the limit of both sides of Eq.C.8 as $t \to \infty$

$$\lim_{t \to \infty} |e_i(t)| = \lim_{t \to \infty} |y_{si}(t) - v_i(t)| = 0, \quad i = 1, \cdots, m \tag{C.9}$$

$\triangle$

Proof of Theorem 5.2 : Under the controller of Eq.5.27, the infinite-dimensional closed-loop system takes the form:

$$\begin{aligned} \frac{d\omega}{dt} &= \tilde{f}(\omega) - \frac{1}{2}\tilde{g}(\omega) R^{-1}(\omega) I(L_{\tilde{g}} V(\omega))^T + L(y - \tilde{h}(\omega)) \\ \frac{\partial n}{\partial t} &= -\frac{\partial (G(x,r)n)}{\partial r} + w(n,x,r) \\ \dot{x} &= f(x) - \frac{1}{2} g(x) R^{-1}(\omega) I(L_{\tilde{g}} V(\omega))^T + A \int_0^{r_{max}} a(n,r,x) dr \end{aligned} \tag{C.10}$$

Applying the method of weighted residuals to the above system, we obtain the fol-

lowing approximate ODE system:

$$\begin{aligned}
\frac{d\omega}{dt} &= \tilde{f}(\omega) - \frac{1}{2}\tilde{g}(\omega)R^{-1}(\omega)I(L_{\tilde{g}}V(\omega))^T + L(y - \tilde{h}(\omega)) \\
\int_0^{r_{max}} \psi_\nu(r)\sum_{k=1}^{N}\phi_k(r)\frac{\partial a_{kN}(t)}{\partial t}dr &= -\sum_{k=1}^{N} a_{kN}(t)\int_0^{r_{max}} \psi_\nu(r)\frac{\partial(G(x_N,r)\phi_k(r))}{\partial r}dr \\
&\quad + \int_0^{r_{max}} \psi_\nu(r) w(\sum_{k=1}^{N} a_{kN}(t)\phi_k(r), x_N, r)dr, \\
&\quad \nu = 1, \ldots, N \\
\dot{x}_N &= f(x_N) - \frac{1}{2}g(x_N)R^{-1}(\omega)I(L_{\tilde{g}}V(\omega))^T \\
&\quad + A\int_0^{r_{max}} a(\sum_{k=1}^{N} a_{kN}(t)\phi_k(r), r, x_N)dr
\end{aligned} \tag{C.11}$$

Using the vector notation $a_N = [a_{1N} \cdots a_{NN}]$, and after some rearrangements, the above system can be written as:

$$\begin{aligned}
\frac{d\omega}{dt} &= \tilde{f}(\omega) - \frac{1}{2}\tilde{g}(\omega)R^{-1}(\omega)I(L_{\tilde{g}}V(\omega))^T + L(y - \tilde{h}(\omega)) \\
\dot{a}_N &= f^*(a_N, x_N) \\
\dot{x}_N &= f(x_N) - \frac{1}{2}g(x_N)R^{-1}(\omega)I(L_{\tilde{g}}V(\omega))^T + A\int_0^{r_{max}} a_2(\sum_{k=1}^{N} a_{kN}(t)\phi_k(r), r, x_N)dr)
\end{aligned} \tag{C.12}$$

where the explicit expression of the nonlinear function $f^*(a_N, x_N)$ is omitted for brevity. Setting $\tilde{x} = [a_N^T\ x_N^T]^T$, we finally obtain the following closed-loop system:

$$\begin{aligned}
\frac{d\omega}{dt} &= \tilde{f}(\omega) - \frac{1}{2}\tilde{g}(\omega)R^{-1}(\omega)I(L_{\tilde{g}}V(\omega))^T + L(y - \tilde{h}(\omega)) \\
\dot{\tilde{x}} &= \tilde{f}(\tilde{x}) - \frac{1}{2}\sum_{i=1}^{m}\tilde{g}_i(\tilde{x})R^{-1}(\omega)L_{\tilde{g}_i}V(\omega),\ \ i = 1, \ldots, m
\end{aligned} \tag{C.13}$$

Under assumptions 1, 2, and 3 stated in theorem 5.1, we have already shown in the proof of theorem 5.1 above that there exists $\mu^* > 0$ such that if $\mu \in (0, \mu^*]$, the above system is locally exponentially stable and $\lim_{t\to\infty} |y_{si} - v_i| = 0$. Using the results of

proposition 2.1, we have that, for sufficiently large N, the following estimates hold

$$\begin{aligned} n(r,t) &= n_N(r,t) + O(\epsilon(N)) \\ x(t) &= x_N(t) + O(\epsilon(N)) \end{aligned} \tag{C.14}$$

where $\epsilon(N)$ is a small positive real number that depends on N and satisfies $\lim_{N\to\infty} \epsilon(N) = 0$, and $n_N(r,t) = \sum_{k=1}^{N} a_{kN}(t)\phi_k(r)$ is the approximation of $n(r,t)$. It follows then that, for sufficiently large N, there exist positive real numbers $\delta_n, \bar{\delta}_x, \delta_\omega, \bar{\mu}^*$ such that if $\mu \in (0, \bar{\mu}^*]$, $||n(r,0)||_2 < \delta_n$, $|x(0)| < \bar{\delta}_x$, $|\omega(0)| < \delta_\omega$, the closed-loop system of Eq.C.10 is exponentially stable and $\lim_{t\to\infty} |y_i - v_i| = O(\epsilon(N))$.

△

Bibliography

[1] J. Alvarez, J. J. Alvarez, M. A. Barron, and R. Suraez. The global stabilization of a two-input three-state polymerization reactor with saturated feedback. In *Proceedings of the American Control Conference*, pages 2917–2921, San Francisco, CA, 1993.

[2] J. Alvarez, J. J. Alvarez, and R. Suraez. Nonlinear bounded control for a class of continuous agitated tank reactors. *Chem. Eng. Sci.*, 46:3235–3249, 1991.

[3] C. Antoniades and P. D. Christofides. Feedback control of nonlinear differential difference equation systems. *Chem. Eng. Sci.*, 54:5677–5709, 1999.

[4] M. J. Balas. Finite-dimensional direct adaptive control for discrete-time infinite-dimensional linear systems. *J. Math. Anal. Appl.*, 196:153–171, 1995.

[5] C. F. Bohren and D. R. Huffman. *Absorption and Scattering of Light by Small Particles.* Wiley, New York, 1983.

[6] C. I. Byrnes. Adaptive stabilization of infinite dimensional linear systems. In *Proceedings of 26th IEEE Conference on Decision and Control*, pages 1435–1440, Los Angeles, CA, 1987.

[7] T. Chiu and P. D. Christofides. Nonlinear control of particulate processes. *AIChE J.*, 45:1279–1297, 1999.

[8] T. Chiu and P. D. Christofides. Robust nonlinear control of a continuous crystallizer. *Comp. & Chem. Eng.*, 23(s):249–252, 1999.

[9] T. Chiu and P. D. Christofides. Robust control of particulate processes using uncertain population balances. *AIChE J.*, 46:266–280, 2000.

[10] T. Y. Chiu and P. D. Christofides. Control of particulate processes based on uncertain population balance models. In *AIChE Annual Meeting, paper 246g, Miami Beach, FL*, 1998.

[11] T. Y. Chiu and P. D. Christofides. Dynamics and control of constrained particulate processes. In *AIChE Annual Meeting, paper 146b, Dallas, TX*, 1999.

[12] T. Y. Chiu, N. H. El-Farra, and P. D. Christofides. Nonlinear control of particulate processes with input constraints. In *Proceedings of American Control Conference*, pages 1752–1759, Chicago, IL, 2000.

[13] D. Chmielewski and V. Manousiouthakis. Constrained infinite-time nonlinear quadratic-optimal control with application to chemical reactors. In *Proceedings of Conference on Control Applications*, Honolulu, HA, 1998.

[14] P. D. Christofides. Robust control of parabolic PDE systems. *Chem. Eng. Sci.*, 53:2949–2965, 1998.

[15] P. D. Christofides. *Nonlinear and Robust Control of PDE Systems: Methods and Applications to Transport-Reaction Processes.* Birkhäuser, Boston, 2000.

[16] P. D. Christofides and T. Chiu. Nonlinear control of particulate processes. In *AIChE Annual Meeting, paper 196a, Los Angeles, CA*, 1997.

[17] P. D. Christofides and P. Daoutidis. Feedback control of hyperbolic PDE systems. *AIChE J.*, 42:3063–3086, 1996.

[18] P. D. Christofides and P. Daoutidis. Nonlinear control of diffusion-convection-reaction processes. *Comp. Chem. Engng.*, 20(s):1071–1076, 1996.

[19] P. D. Christofides and P. Daoutidis. Robust control of hyperbolic PDE systems. *Chem. Eng. Sci.*, 53:85–105, 1998.

[20] P. D. Christofides and A. R. Teel. Singular perturbations and input-to-state stability. *IEEE Trans. Autom. Contr.*, 41:1645–1650, 1996.

[21] F. Colonius and W. Kliemann. On control sets and feedback for nonlinear systems. In *Proceedings of IFAC Nonlinear Control System Design Symposium*, pages 49–54, M. Fliess Ed., Bordeaux., 1992.

[22] F. Colonius and W. Kliemann. Some aspects of control of systems as dynamical systems. *J. Dynamics and Differential Equations*, 5:469–479, 1993.

[23] M. A. Demetriou. Model reference adaptive control of slowly time-varying parabolic systems. In *Proceedings of 33rd IEEE Conference on Decision and Control*, pages 775–780, Orlando, FL, 1994.

[24] J. Dimitratos, G. Elicabe, and C. Georgakis. Control of emulsion polymerization reactors. *AIChE J.*, 40:1993–2021, 1994.

[25] J. W. Eaton and J. B. Rawlings. Feedback control of chemical processes using on-line optimization techniques. *Comp. Chem. Eng.*, 14:469–479, 1990.

[26] N. H. El-Farra, T. Y. Chiu, and P. D. Christofides. Analysis and control of particulate processes with input constraints. *AIChE J.*, submitted, 2000.

[27] N. H. El-Farra and P. D. Christofides. Robust optimal control of nonlinear systems. In *Proceedings of American Control Conference*, pages 124–128, San Diego, CA, 1999.

[28] N. H. El-Farra and P. D. Christofides. Robust near-optimal output feedback control of nonlinear systems. *Intr. J. Contr.* to appear, 2000.

[29] C. Foias and R. Témam. Algebraic approximation of attractors: The finite dimensional case. *Physica D*, 32:163–182, 1988.

[30] R. A. Freeman and P. V. Kokotovic. *Robust Nonlinear Control Design: State-Space and Lyapunov Techniques.* Birkhauser, Boston, 1996.

[31] S. K. Friedlander. *Smoke, Dust, and Haze: Fundamentals of Aerosol Behavior.* Wiley, New York, 1977.

[32] K. Fukunaga. *Introduction to statistical pattern recognition.* Academic Press, New York, 1990.

[33] F. Gelbard and J. H. Seinfeld. Numerical solution of the dynamic equation for particulate processes. *J. Comp. Phys.*, 28:357–375, 1978.

[34] F. Gelbard, Y. Tambour, and J. H. Seinfield. Sectional representation of simulating aerosol dynamics. *J. Coll. Inter. Sci.*, 68:363–382, 1980.

[35] P. J. Hill and K. M. Ng. New discretization procedure for the agglomeration equation. *AIChE J.*, 42:727–741, 1996.

[36] P. Holmes, J. L. Lumley, and G. Berkooz. *Turbulence, Coherent Structures, Dynamical Systems and Symmetry.* Cambridge University Press, New York, 1996.

[37] M. J. Hounslow. A discretized population balance for continuous systems at steady-state. *AIChE J.*, 36:106–116, 1990.

[38] H. M. Hulburt and S. Katz. Some problems in particle technology: A statistical mechanical formulation. *Chem. Eng. Sci.*, 19:555–574, 1964.

[39] A. Isidori. *Nonlinear Control Systems: An Introduction.* Springer-Verlag, Berlin-Heidelberg, third edition, 1995.

[40] G. R. Jerauld, Y. Vasatis, and M. F. Doherty. Simple conditions for the appearance of sustained oscillations in continuous crystallizers. *Chem. Eng. Sci.*, 38:1675–1681, 1983.

[41] A. G. Jones. Optimal operation of a batch cooling crystallizer. *Chem. Eng. Sci.*, 29:1075–1087, 1974.

[42] A. G. Jones and J. W. Mullin. Programmed cooling crystallization of potassium sulphate solutions. *Chem. Eng. Sci.*, 29:105–118, 1974.

[43] R. E. Kalman. When is a control system optimal? *J. Basic Eng.*, 86:51–60, 1964.

[44] N. Kapoor and P. Daoutidis. An observer-based anti-windup scheme for nonlinear systems with input constraints. *Int. J. Control*, 72:18–29, 1999.

[45] N. Kapoor and P. Daoutidis. On the dynamics of nonlinear systems with input constraints. *Chaos*, 9:88–94, 1999.

[46] T. A. Kendi and F. J. Doyle. An anti-windup scheme for input-output linearization. In *Proceedings of 3rd European Control Conference*, pages 2653–2658, Rome, Italy, 1995.

[47] H. K. Khalil. *Nonlinear Systems.* Macmillan Publishing Company, New York, second edition, 1996.

[48] P. V. Kokotovic, H. K. Khalil, and J. O'Reilly. *Singular Perturbations in Control: Analysis and Design.* Academic Press, London, 1986.

[49] M. V. Kothare, P. J. Campo, M. Morari, and C. N. Nett. A unified framework for the study of anti-windup designs. *Automatica*, 30:1869–1883, 1994.

[50] A. Kumar, P. D. Christofides, and P. Daoutidis. Singular perturbation modeling and control of nonlinear two-time-scale processes with non-explicit time-scale multiplicity. *Chem. Eng. Sci.*, 53:1491–1504, 1998.

[51] S. Kumar and D. Ramkrishna. On the solution of population balance equations by discretization-I. a fixed pivot technique. *Chem. Eng. Sci.*, 51:1311–1332, 1996.

[52] S. Kumar and D. Ramkrishna. On the solution of population balance equations by discretization-II. a moving pivot technique. *Chem. Eng. Sci.*, 51:1333–1342, 1996.

[53] M. J. Kurtz and M. A. Henson. Linear model predictive control of input-output linearized processes with constraints. In *Proceedings of 5th International Conference on Chemical Process Control.* in press, Tahoe City, CA, 1997.

[54] M. J. Kurtz, G-Y. Zhu, A. Zamamiri, M. A. Henson, and M. A. Hjortso. Control of oscillating microbial cultures described by population balance models. *Ind. Eng. Chem. Res.*, 37:4059–4070, 1998.

[55] J. D. Landgrebe and S. E. Pratsinis. A discrete sectional model for particulate production by gas phase chemical reaction and aerosol coagulation in the free molecular regime. *J. Coll. Inter. Sci.*, 139:63–86, 1990.

[56] S. J. Lei, R. Shinnar, and S. Katz. The stability and dynamic behavior of a continuous crystallizer with a fines trap. *AIChE J.*, 17:1459–1470, 1971.

[57] S. M. Miller and J. B. Rawlings. Model identification and control strategies for batch cooling crystallizers. *AIChE J.*, 40:1312–1327, 1994.

[58] S. L. Oliveira, V. Nevistic, and M. Morari. Control of nonlinear systems subject to input constraints. In *Proc. of Symposium on Nonlinear Control Systems Design'95*, pages 913–918, Tahoe City, CA, 1995.

[59] S. Palanki, C. Kravaris, and H. Y. Wang. Synthesis of state feedback laws for end-point optimization in batch processes. *Chem. Eng. Sci.*, 48:135–152, 1993.

[60] S. Palanki, C. Kravaris, and H. Y. Wang. Optimal feedback control of batch reactors with a state inequality constraint and free terminal time. *Chem. Eng. Sci.*, 49:85–97, 1994.

[61] S. E. Pratsinis. Simultaneous nucleation, condensation, and coagulation in aerosol reactors. *J. Coll. Inter. Sci.*, 124:416–426, 1988.

[62] D. Ramkrishna. The status of population balances. *Rev. Chem. Eng.*, 3:49–95, 1985.

[63] A. D. Randolph, L. Chen, and A. Tavana. Feedback control of CSD in a KCl crystallizer with a fines dissolver. *AIChE J.*, 33:583–591, 1987.

[64] A. D. Randolph and M. A. Larson. *Theory of Particulate Processes.* Academic press, Second edition, San Diego, 1988.

[65] C. V. Rao and J. B. Rawlings. Steady states and constraints in model predictive control. *AIChE J.*, 45:1266–1278, 1999.

[66] J. B. Rawlings, S. M. Miller, and W. R. Witkowski. Model identification and control of solution crystallization processes. *I & EC Res.*, 32:1275–1296, 1993.

[67] J. B. Rawlings and W. H. Ray. Emulsion polymerization reactor stability: simplified model analysis. *AIChE J.*, 33:1663–1667, 1987.

[68] J. B. Rawlings and W. H. Ray. Stability of continuous emulsion polymerization reactors: a detailed model analysis. *Chem. Eng. Sci.*, 42:2767–2777, 1987.

[69] S. Rohani and J. R. Bourne. Self-tuning control of crystal size distribution in a cooling batch crystallizer. *Chem. Eng. Sci.*, 12:3457–3466, 1990.

[70] A. T. Schwarm and M. Nikolaou. Chance-constrained model predictive control. *AIChE J.*, 45:1743–1752, 1999.

[71] P. O. M. Scokaert and J. B. Rawlings. Feasibility issues in linear model predictive control. *AIChE J.*, 45:1649–1259, 1999.

[72] D. Semino and W. H. Ray. Control of systems described by population balance equations-I. controllability analysis. *Chem. Eng. Sci.*, 50:1805–1824, 1995.

[73] D. Semino and W. H. Ray. Control of systems described by population balance equations-II. emulsion polymerization with constrained control action. *Chem. Eng. Sci.*, 50:1825–1839, 1995.

[74] R. Sepulchre, M. Jankovic, and P. Kokotovic. *Constructive Nonlinear Control.* Springer-Verlag, Berlin-Heidelberg, 1997.

[75] S. Y. Shvartsman and I. G. Kevrekidis. Nonlinear model reduction for control of distributed parameter systems: A computer assisted study. *AIChE J.*, 44:1579–1595, 1998.

[76] R. Temam. *Infinite-Dimensional Dynamical Systems in Mechanics and Physics.* Springer-Verlag, New York, 1988.

[77] S. Valluri and M. Soroush. Analytical control of SISO nonlinear processes with input constraints. *AIChE J.*, 44:116–130, 1998.

[78] J. T. Wen and M. J. Balas. Robust adaptive control in hilbert space. *J. Math. Anal. Appl.*, 143:1–26, 1989.

[79] M. M. R. Williams and S. K. Loyalka. *Aerosol Science: Theory & Practice.* Pergamon Press, Oxford, England, 1991.

[80] E. B. Ydstie and A. A. Alonso. Process systems and passivity via the Clausius-Planck inequality. *Syst. & Contr. Lett.*, 30:253–264, 1997.

[81] E. B. Ydstie and P. V. Krishnan. From thermodynamics to a macroscopic theory for process control. In *AIChE Ann. Mtg., paper 228a, San Francisco, CA*, 1994.